

# **Brittle-Matrix Composite Structures**

Rostislav Chudoba

25th June 2019



# Contents

<b>List of Figures</b>	<b>4</b>
<b>1 Introduction</b>	<b>8</b>
1.1 What is this course about? . . . . .	8
1.2 Scope and structure of the course . . . . .	10
1.3 Example applications of cementitious composites . . . . .	10
1.4 BMCS Tool Suite . . . . .	11
1.5 Warm-up exercises . . . . .	12
<b>I Debonding</b>	<b>14</b>
<b>2 Pull-Out</b>	<b>15</b>
2.1 Pullout test setup . . . . .	15
2.2 Objectivity of a material model . . . . .	18
2.3 Analytically solvable pullout problems . . . . .	20
2.4 Conclusions and remarks . . . . .	27
<b>3 Bond behavior</b>	<b>28</b>
3.1 Generally nonlinear bond-slip law . . . . .	28
3.2 Bond-slip law with hardening . . . . .	30
3.3 Pullout problem for bond slip law with softening . . . . .	33
3.4 Finite element solution of the pullout problem . . . . .	34
3.5 Iterative solver for a general non-linear finite element simulation . . . . .	34
<b>4 Unloading and Reloading</b>	<b>37</b>
4.1 Experimental observation . . . . .	37
4.2 Phenomenology of the bond behavior . . . . .	38
4.3 Damage model . . . . .	40
4.4 Plasticity model . . . . .	42
4.5 Return mapping algorithm . . . . .	45
4.6 Damage-Plasticity model . . . . .	47

<b>5 Inelastic analysis of pull-out response</b>	<b>50</b>
5.1 Pullout governed by plasticity . . . . .	50
5.2 Pullout governed by damage . . . . .	50
<b>II Cracking</b>	<b>52</b>
<b>6 Softening and fracture</b>	<b>53</b>
6.1 Is energy dissipation an objective material property? . . . . .	53
6.2 Energetic interpretation of the nonlinear structural response . . . . .	54
6.3 General formula for energy supply . . . . .	54
<b>7 Cohesive zone, softening, energy dissipation</b>	<b>57</b>
7.1 Sensitivity of strain-softening models with respect to size of the localization zone . . . . .	57
7.2 Softening function accounting for fracture energy . . . . .	58
7.3 Energy dissipation for strain softening . . . . .	59
7.4 Correspondence between softening and damage functions . . . . .	61
<b>8 Softening and finite elements</b>	<b>63</b>
8.1 Effect of element size on the strain localization for linear softening law . .	63
8.2 Regularization of the softening law in finite element code . . . . .	64
8.3 Implementation of softening in finite-element codes . . . . .	65
8.4 Implementation of softening behavior in finite element code . . . . .	66
<b>9 Crack propagation</b>	<b>69</b>
9.1 Propagation of a straight crack . . . . .	69
9.2 Petersen three-point bending test series . . . . .	71
9.3 Onset of damage . . . . .	73
<b>10 Onset of inelasticity in a continuum</b>	<b>75</b>
10.1 Representation of strain and strain in a continuum . . . . .	75
10.2 Examples of yield conditions . . . . .	77
<b>11 Shear &amp; Crack</b>	<b>81</b>
11.1 Double-edge notched test . . . . .	82
11.2 Elementary tests of material models for concrete cracking . . . . .	87
11.3 Examples . . . . .	89

<b>III Cracking &amp; Debonding</b>	<b>91</b>
<b>12 Tensile response of brittle-matrix composites</b>	<b>92</b>
12.1 Pseudo-ductility . . . . .	92
<b>13 Influence of heterogeneity</b>	<b>96</b>
<b>14 Shear loading</b>	<b>97</b>
<b>A Multilayer model</b>	<b>98</b>
A.1 Governing equations . . . . .	98

## List of Figures

1.1	Examples of considered brittle-matrix composites . . . . .	9
1.2	Examples of textile-reinforced concrete shells . . . . .	11
1.3	TRC bridge, Albstadt . . . . .	11
1.4	Examples of material parameters of textile-fabrics reinforcement . . . . .	13
2.1	RILEM pull-out test to characterize the bond between steel and concrete. . . . .	16
2.2	Pullout of GFRP bar from the concrete matrix. . . . .	16
2.3	Beam tests focused on the bond characterization. . . . .	17
2.4	Double sided pullout test applied to carbon textile fabrics. . . . .	17
2.5	Double sided pullout test for a single fiber with a predefined pullout length at one side using a cut at one side. . . . .	18
2.6	Relation between material behavior and structural behavior . . . . .	19
2.7	One dimensional idealization of the pullout test as boundary value problem	20
2.8	Assumptions included in the pullout-model with constant bond stress . . .	21
2.9	Variables and parameters describing the constant bond model . . . . .	21
2.10	Profile of strains in the pullout-model with constant bond stress; a) Matrix supported at loaded end, b) Matrix supported at unloaded end . . . . .	25
3.1	Structural interpretation of bond hardening and softening . . . . .	28
3.2	Prediction of the constant bond model . . . . .	32
3.3	Length dependence . . . . .	32
3.4	Linear finite elements applied in the BMCS tool suite. . . . .	34
3.5	Nonlinear time stepping procedure following the Newton algorithm. . . . .	36
4.1	Double-sided pullout test with several unloading and reloading steps . . .	38
4.2	Bond governed by damage . . . . .	39
4.3	Bond governed by plasticity/friction . . . . .	39
4.4	Damage function governing the deterioration process . . . . .	40
4.5	Slip - bond stress curve of damage model; left : hardening, right: softening	41
4.6	What happens beyond elastic domain? Example of elastic-ideally plastic bond. . . . .	46
4.7	Return mapping of the plasticity model . . . . .	46

---

6.1	Energy bilance for the pullout with constant bond-slip law . . . . .	55
7.1	Finite-element computation of with a softening zone . . . . .	57
8.1	Material with linear softening. . . . .	63
8.2	Example of a tension bar with a softening zone of a finite size. . . . .	68
9.1	Geometry and boundary donditions of the three-point bending test. . . . .	70
9.2	Finite element disretization used for the verification of mesh-independency of the numerical model. . . . .	70
9.3	Fracture energy dissipation including the self-weight. . . . .	71
9.4	(a) Dimensions of notched three-point-bending test series by Petersson, loading and boundary condition; (b) finite element descritization; (c) damage propagation; (d) load-displacement curves from test and simulations with fracture energy $G_f = 124 \text{ N/mm}$ ; (e) range of load-displacement curves from test and simulations with variation of fracture energy $0.115 \text{ N/mm} \leq G_f \leq 0.137 \text{ N/mm}$ . . . . .	73
11.1	Fracture modes 1,2 and 3: opening crack, shearing crack and tearing crack	81
11.2	(a) Test setup and dimensions of the Nooru-Mohamed tests; (b) loading history of horizontal force $F_s$ ; (c) loading history of vertical force $F$ . . . . .	82
11.3	(a) Crack pattern of Nooru-Mohamed test: (a) load path 4a; (b) load path 4b . . . . .	83
11.4	Tensile response of Microplane damage model (MDM) and Concrete damage plasticity (CDP) calibrated for the simulation of Nooru-Mohamed tests . . . . .	84
11.5	Comparison of the crack pattern in Nooru-Mohamed test (load paths 4a and 4b) with damage evolution from the model with biquadratic elements with $2.5 \text{ mm} \times 2.5 \text{ mm}$ mesh size and reduced integration schemes using <i>concrete damage plasticity</i> model . . . . .	84
11.6	Load-displacment curves of the Nooru-Mohamed test from test and finite element simulation using <i>concrete damage plasticity</i> model (a) load path 4a; (b) load path 4b . . . . .	85
11.7	Decomposition of strain components in a material point in 2D stress state.	85
11.8	Example of damage evolution in a material point loaded in uniaxial tension.	86
11.9	Damage envelope calculated for the microplane-damage model. . . . .	87
11.10	Load-displacment curves of the Nooru-Mohamed test from test and finite element simulation using <i>microplane damage model</i> (a) load path 4a; (b) load path 4b . . . . .	88
11.11	Load-displacment curves of the Nooru-Mohamed test from test and finite element simulation using <i>microplane damage model</i> (a) load path 4a; (b) load path 4b . . . . .	88
11.12	Willam test illustration . . . . .	89

11.13 Willam-test, $\sigma_{xx}, \sigma_{yy}, \sigma_{xy}$ versus $\varepsilon_{xx}$ . . . . .	89
11.14 Willam-test, evolution of directions of principal stress $\sigma_{11}$ and strains $\varepsilon_{11}$ .	90
11.15 Willam-test, evolution of principal stresses . . . . .	90
12.1 Tensile response of a composite specimen, random, deterministic matrix .	94
12.2 Stress and strain state of a single crack bridge with constant bond . . . .	94
12.3 Stress and strain state along the tensile specimen at increasing remote stress levels . . . . .	95
A.1 Schematic picture of a typical pull-out test . . . . .	98
A.2 A simplified mechanical model of the pull-out problem . . . . .	98

## List of examples

1.1	Material stiffness of a composite cross section . . . . .	12
1.2	Volume fractions and reinforcement ratio . . . . .	13
2.1	Pullout from rigid matrix . . . . .	23
2.2	Pullout from rigid matrix with extra bar length at the loaded end . . . . .	24
2.3	Pullout from elastic matrix clamped right . . . . .	25
2.4	Pullout from elastic matrix clamped left . . . . .	26
2.5	Pullout of a short fiber with decreasing bond length . . . . .	27
3.1	Piecewise-linear bond slip laws . . . . .	29
3.2	Simulation of the RILEM pullout test . . . . .	30
3.3	Simulation of debonding between CFRP sheet and concrete . . . . .	33
3.4	Demonstration of the solution algorithm . . . . .	36
4.1	What happens if a pullout with multilinear bond-slip law gets unloaded? .	38
4.2	Bond behavior governed by damage . . . . .	42
4.3	Bond behavior governed by plasticity . . . . .	44
5.1	Pullout response simulated using plastic material model . . . . .	50
5.2	Pullout simulated using damage model . . . . .	50
6.1	Energy dissipation in a pullout test with constant bond . . . . .	56
7.1	Tensile behavior of a specimen with a softening zone . . . . .	60
7.2	Transformation of a softening function to damage function . . . . .	62
8.1	Mesh bias for discretized bar with linear softening . . . . .	64
8.2	Discretized bar with regularized linear softening . . . . .	65
8.3	Iterative solution of the localization problem . . . . .	67
8.4	Standard finite element code . . . . .	67
9.1	Regularized numerical model of a bending test . . . . .	69
10.1	Tensorial invariants and deviatoric strain tensor . . . . .	80

# 1 Introduction

## 1.1 What is this course about?

Composite	The aim of the course is to provide a unified view to the behavior of materials and structures made of composites that combine brittle matrix with tensile reinforcement. The term "composite" denotes a material made up of constituent materials that play different roles in the material behavior. In cementitious composites the constituents are specialized on compressive and tensile behavior. The concrete matrix material with high compressive strength surrounds and supports the relative position of the reinforcement material (steel, carbon or glass) with high tensile strength.
Brittle matrix	The term "brittle" implies a sudden local failure that is observed as a distinguished fracture of material. In the usual sense, this property is associated with glass, ceramics and carbon. Such materials exhibit perfectly elastic deformation and sudden failure.
Behavior of concrete	To large extent, concrete and cementitious matrices can also be regarded as brittle. Upon tensile stresses, a macroscopically observable cracks develop that initiate a sudden failure. However, in comparison to the brittle materials mentioned above, the material structure of concrete is consisting of coarse aggregates and cement paste, the process of cracking is more complex. The evolution of a macroscopically observable crack involves a coalescence of microcracks, a process that is not purely elastic-brittle. It is governed by local dissipative mechanisms of internal friction and sliding between aggregates at the scale of the material structure. Such kind of gradual material disintegration is specific to concrete. The local failure is not a sudden event but gradual process involving the development of microcracks and their localization to a macrocrack. Phenomenologically, this process leads to nonlinear stress-strain behavior. In fact, concrete is neither elastic, nor plastic and even not purely brittle. It is something in-between so that its material behavior is referred to as "quasi-brittle". The complexity of the crack localization process makes a an objective general description of concrete material behavior a challenging task and remains a subject of an ongoing research.
Behavior of reinforced concrete	Simply speaking, one could say, that the only reason for putting steel into concrete is to prevent the failure upon the appearance of a crack. But this view would undervalue the role of concrete within the composite. One could also say, that in combination with the reinforcement the cracking becomes a positive feature of the material behavior. Without cracks, the reinforcement could not really exploit its strength. This symbiosis results in a large deformation capacity at a slowly increasing loading providing the desired ductile behavior. More precisely, we speak about "quasi-ductility" because the large deformation is owing to interacting cracking and debonding to distinguish it from the ductility achieved by plastic yielding of material.
Relation to practice	Compared to materials with a more regular and uniform material skeleton, a realistic and generally valid description of concrete material behavior remains a challenging task and subject of ongoing research. Only a few finite-element tools are available on a commercial

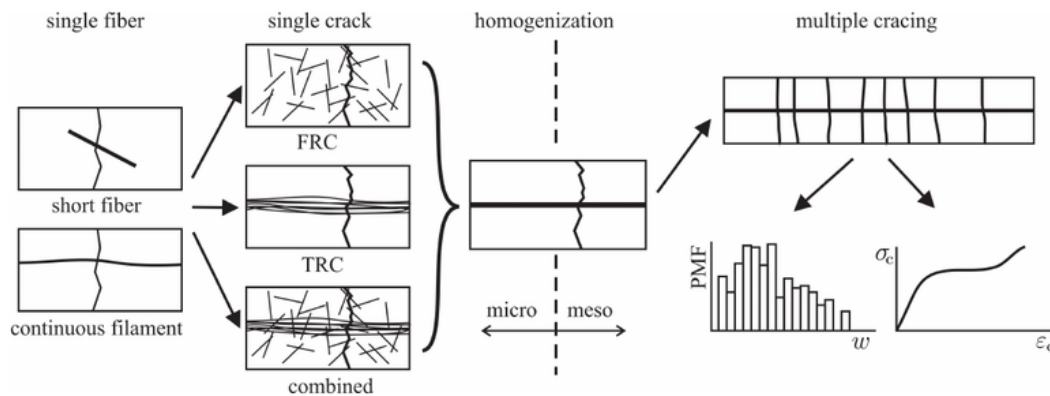


**Figure 1.1** Examples of considered brittle-matrix composites

market that provide a support for realistic simulation of concrete material behavior. Due to inherent limitations of the standard finite element solvers, these tools must be used with care and knowledge of the specifics of the quasi-brittle material behavior.

To provide a focused view at elementary mechanisms of material disintegration, a set of software applications has been developed to support the course. It contains both analytical, closed form models and finite-element models of debonding and crack propagation. The BMCS-Tool Suite is available online. It is implemented within the general purpose scientific-computing environment "Canopy". Students can seamlessly start to learn the rich and powerful functionality of the tools that can be applied for fast prototyping of models and dimensioning and assessment rules or for evaluation of experimental data.

The explained concepts are applicable to the following types of composites exemplified in Fig. 1.1

Tools to look inside

Considered types of composites

**A: Continuous, discrete reinforcement elements** which are explicitly placed by design at a given location. This represents the bar reinforcement in steel-reinforced concrete or reinforcement using CFRP or GFRP bars. The cross-sectional area of individual bars is of the order of centimeters.

**B: Dispersed continuous reinforcement** denoting fine meshes and grids of reinforcement, for example textile fabrics or mats. This reinforcement represents a layer acting in two dimensions. Profiled textiles and prefabricated three-dimensional structures are also included in this category.

**C: Discontinuous, dispersed short fiber reinforcement** with randomly distributed and oriented fibers. This type of reinforcement is a part of the concrete mixture.

The behavior of the three types of composites is certainly different and should be considered complementary. Each of them is associated with different type of behavior and different manufacturing methods so that they are suitable for different types of applications in architecture and structural engineering. The description of their behavior, even though quantitatively different, can be boiled down to the same key mechanism, the interacting matrix cracking and debonding of matrix and reinforcement.

The detailed knowledge provides possibility to design a material structure combining all the mentioned types of composite. By combining different types of concrete mixtures, fiber cocktails, textile reinforcement and discrete bar reinforcement the design space becomes

Material design

huge. The level of initial stiffness, the ductility, the ultimate tensile strength can be modified as desired.

**Research method** Finally, the course will present the concepts following the scientific practice of material research clarifying the notions of experimental design, model calibration, model validation, parametric study, sensitivity analysis.

### 1.2 Scope and structure of the course

**Three structural levels** This course aims to present this knowledge by three cases of macroscopic, structural behavior. In the first part of the course, we look into the debonding process between two material components on an example of a pullout test. In the second part, we will describe the crack propagation in concrete by considering a bending test and its modifications. In the third part, we describe the interaction of cracking and debonding using tensile, and bending test of a composite specimen.

**Three perspectives** In each of these three parts we will use these perspectives of observation. The subjective perspective will be used to evaluate the experimental observation of the structural response, i.e. the test results. In the second perspective, a model of the observed structural behavior will be presented and will be used to "play around" with the experiment asking the question:

*What happens when something gets changed?*

The third, most objective perspective will then regard the process from the perspective of a material point or zone.

**Putting it together** By following this scheme, we will develop a general and in-depth understanding of material and structural behavior applicable to wide range of materials. Except of traditional, steel-reinforced concrete we will apply it to innovative composite materials using nonmetallic reinforcement materials, like carbon bars. In the last part of the course, we will sketch a design of a structure that exploits the material quasi-ductile behavior of cementitious composite in a safe and economic way. We will discuss the aspects of the structural behavior, in view of stress-redistribution and ductility both at the level of a cross section and at the level of the whole structure. Then, we will compare this view with the linear-elastic analysis and prediction of ultimate failure. This discussion will provide the basis for understanding of structural redundancy and safety assessment.

### 1.3 Example applications of cementitious composites

**Application domain** The application domain of brittle-matrix composites is still rapidly growing. Except of the traditional domain of steel-reinforced concrete (reinforcement of type A), innovative composites applying non-metallic reinforcement are included. Lightweight structural elements, like thin-shells provide appealing features, like low material consumption and high durability.

Many examples of structures applying also non-metallic reinforcement already exist and a number of them has been realized in the framework of research projects at the Institute of Structural Concrete of the RWTH Aachen University. On the one hand, thin walled



(a) Campus Melaten, Aachen



(b) T3 Pavillon, RWTH Aachen

**Figure 1.2** Examples of textile-reinforced concrete shells**Figure 1.3** TRC bridge, Albstadt

shells made of textile-reinforced concrete 1.2 applying the reinforcement layout of type B demonstrate the feasibility and the specific features of the new composite materials. On the other hand an application of CFRP as bar reinforcement (type A) has realized in collaboration is shown in Fig. 1.3.

However, their broader applicability is hindered by a missing support for engineering design rules. The traditional design codes cannot be simply adopted, because of qualitative differences in their material behavior. Application of these new types of composites requires the development of new codes and assessment methods from scratch. Standardization of testing methods is also an important issue.

Except of the mentioned cases, the methods described in this course are also relevant for the analysis of FRP sheet lap joints applied for retrofitting of aging structures. At the same time, they are relevant also for application of TRC as a strengthening layer of existing structures, such as bridges.

Design rules  
for new com-  
posites

## 1.4 BMCS Tool Suite

The BMCS Tool Suite is a package of specialized programs that can be used by the course participants to study particular effects of the material- and structural behavior. The idea is to show the students an implemented model of a particular test setup in an

Interactive  
demonstra-  
tion of the  
taught  
concepts

interactive form first so that they can perform some virtual experiments. After showing a few examples of what kind of behavior the model can describe, the theory behind the model can be explained with a clear specification about the purpose and assumptions related to the model.

Open-source  
bundle for  
scientific  
computing

The BMCS Tool Suite has evolved from several years of research in the field of material modeling of brittle-matrix composites. This development has been carried out using open-source scientific computing libraries developed in Python language. The computing environment consists of several hundreds of open-source, free libraries. For convenience, they are packaged within the Canopy software bundle, which is free for academic purposes. The Installation of Canopy can easily be performed on all existing platforms including, Windows, Mac and Linux operating systems.

Role of the  
BMCS  
models in the  
course

The models implemented in BMCS-Tool can be installed on any computer platform. The implementations are computationally efficient, they are equipped with a simple interactive user interfaces that allows the students to start with a study of a problem at hand from scratch without any prerequisite knowledge. At the same time, students have a chance to learn modern implementation concepts of models during the course using a high-level programming language with a large expressive power. Just to mention an example, this environment enables us to implement a finite-element solver of a pull-out problem on some 15 lines of code, which is very closely related to the mathematical description of the model. These features make this environment ideally suited for the teaching concept followed within the BMCS course.

The installation guide to the Canopy and BMCS is provided at the moodle page of the course and can be directly accessed [here](#)

### 1.5 Warm-up exercises

#### Example 1.1: Material stiffness of a composite cross section

What is the initial stiffness of a reinforced concrete cross section shown in Fig 1.4 with the thickness of 10 mm and width of 100 mm. The cross-section is reinforced with 6 layers of textile fabrics made of CAREP3300 specified in Table 1.1.

Evaluation script is available [here](#)

```
A_roving = 1.84 # [mm**2]
n_layers = 6 # -
spacing = 25.77 # [mm]
thickness = 10 # [mm]
width = 100 # [mm]
E_carbon = 240000 # [MPa]
E_concrete = 28000 # [MPa]

A_composite = width * thickness
n_rovings = width / spacing
A_layer = n_rovings * A_roving
A_carbon = n_layers * A_layer
A_concrete = A_composite - A_carbon
E_composite = (E_carbon * A_carbon + E_concrete * A_concrete) / (A_composite)

print ('E_composite', E_composite , 'MPa')
```

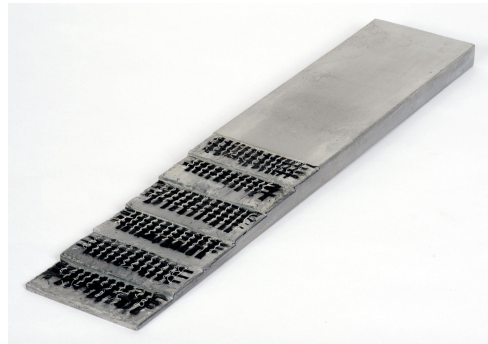


**Figure 1.4** Examples of material parameters of textile-fabrics reinforcement

**Table 1.1** Cross sections characteristics; parameters of performed tests in boldface font, derived values in normal font

Label	Material	Area [mm <sup>2</sup> ]	Grid spacing [mm]	Stiffness [MPa]	Strength (characteristic) [Mpa]
CAR-EP3300	carbon/proxy	1.84	25.77	240000	3500
solidian GRID Q95	carbon/proxy	3.62	36.0	240000	3200

### Example 1.2: Volume fractions and reinforcement ratio

Given a concrete matrix with  $E$  modulus of 28 GPa, carbon reinforcement of 200 GPa, and glass textile fabrics with of 70 GPa ... design a material cross section with the overall stiffness of 45 GPa.

Evaluation script is available [here](#)

```
A_concrete = 50 * 50 # [cm**2]
E_concrete = 28 # [GPa]
A_carbon = 0.08 * A_concrete # [cm**2]
E_carbon = 200 # [GPa]
A_glass = 0.184 * A_concrete # [cm**2]
E_glass = 70 # [GPa]
A_composite = A_concrete + A_carbon + A_glass
E_composite = (
    (E_concrete * A_concrete + E_carbon * A_carbon + E_glass * A_glass) / A_composite
)
print('E_composite', E_composite)
```

---

# **Part I**

## **Debonding**

## 2 Pull-Out

**Outline:** In this chapter we introduce elementary test setups for the pullout of a bar from a cementitious matrix. The goal is set up the playground for questions of test design. Tests are mostly focusing on isolated effects of material behavior, like debonding between two material components. However, it is seldom possible to completely avoid additional effects. The pull-out test setup can be conveniently used to demonstrate the dilemmas involved in a test setup design. By raising these questions we shall motivate the deeper look at the material behavior versus the structural behavior in Chapter 3.

### Addressed questions:

- How to identify a bond law describing the bond behavior between matrix and reinforcement?
- How to design a test for the calibration of the bond characteristics?
- What kinds of tests exist? What are their advantages and disadvantages?
- Which tests are appropriate for the different types of reinforcement? (steel, carbon/-glass fiber-reinforced polymer, carbon or glass textile fabrics reinforcement).

### 2.1 Pullout test setup

The development of a test suitable for characterization of the bond behavior between a reinforcing steel bar and concrete matrix dates back to sixties. The RILEM-FIB-CEB recommendation test has been proposed in 1973. Fig. 2.1 shows the prescribed boundary conditions and measuring equipment that records the pull-out curve in terms of the pull-out force versus slip displacement of the bar at the loaded  $s_l$  and unloaded  $s_u$  free ends. The loading process is controlled by the prescribed pullout displacement and the corresponding force is recorded. In this way, also pullout curve with diminishing force after the peak value can be measured.

The curves displayed in right diagram of Fig. 2.1 exemplify two observations that can be made using this test setup:

- The pullout curve strongly depends on the embedded length and on the diameter of the bar.
- The displacement measured at the loaded and unloaded end differ and this difference is strongly affected by the embedded length.

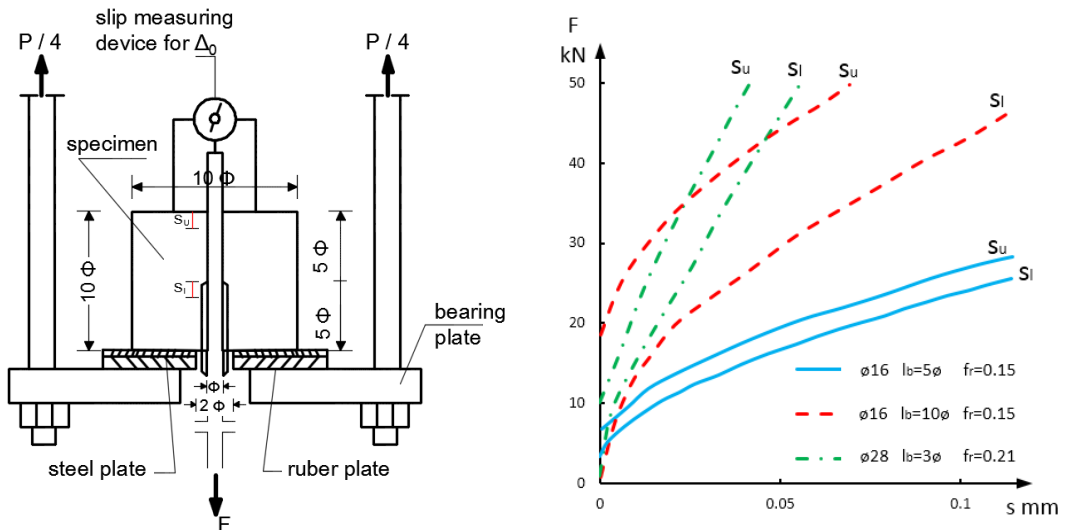


**Figure 2.1** RILEM pull-out test to characterize the bond between steel and concrete.

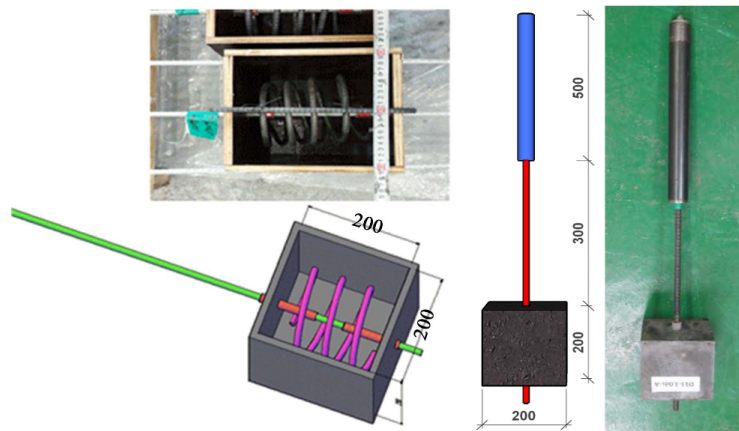


**Figure 2.2** Pullout of GFRP bar from the concrete matrix.

Obviously, the experimentally observed trends must be governed by the principles of physics and mechanics. It is our ambition to capture the underlying phenomena of the bond behavior with the goal to predict the pullout behavior for changed test parameters.

#### Derived pull-out tests

But before approaching a more fundamental view to the effects governing the bond behavior let us span the scope of the bond description to other materials and other types of test setup. A similar type of the pullout test setup has been used to test the behavior of nonmetallic reinforcement as exemplified in Fig. 2.2. Notice that in both mentioned pullout test setups, the bond zone is located inside the specimen and there is a bond-free zone of a predefined depth starting at the loaded side. This bond-free zone is introduced with the goal to render uniform material properties along the tested bond length and to avoid the effect of a boundary zone.

#### Undesired compression

The described pullout test setup is very common in practice, primarily to its simplicity. However, it is not ideal in all situations because it does not really correspond to the situation in the structural elements. The reason is that due to the placement of supports at the loaded side of the specimen, non-negligible compressive stresses develop within bond zone of the concrete matrix. Such a stress state does not represent the state in the bond zone

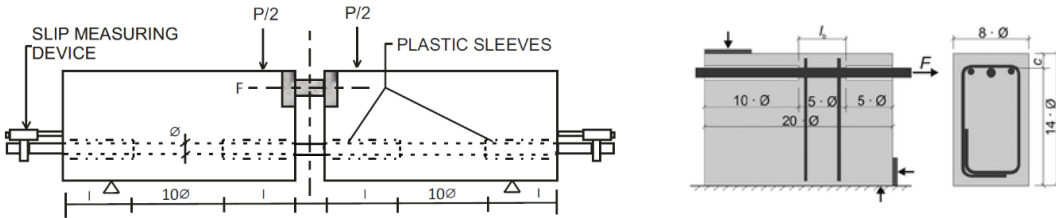


**Figure 2.3** Beam tests focused on the bond characterization.

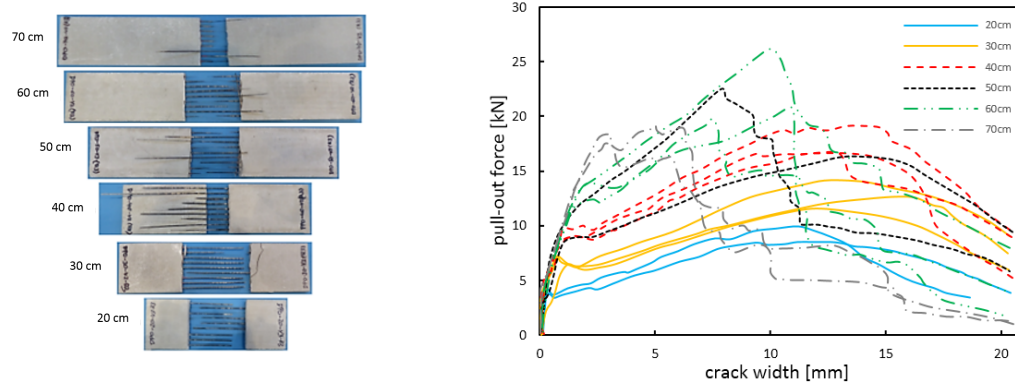


**Figure 2.4** Double sided pullout test applied to carbon textile fabrics.

of a structural element which is mostly loaded in tension. As documented by experimental studies, e.g. in [de2008bond] the effect on the bond behavior is significant.

The refined setup for bond characterization has been proposed in the form of beams or beam-end-sections as exemplified Fig. 2.3. Apparently, this test configuration is closer to the condition of a crack in a tensile zone of a structural specimen. The pullout displacement is measured as the opening of the crack. The test is controlled by the vertical displacement and the corresponding load is measured. It is important to note that the debonding propagates in both directions. Symmetry of the debonding process is provided until the ultimate load has been achieved. Once the pullout force has been reached at one side, the process becomes non-symmetric. As we shall discuss later on, this might become a problem in cases of materials that exhibit a so called bond softening. However, in case of steel rebars this test configuration provides a suitable solution.

Beam anchorage test

Further step in the development of experimental methods for the bond characterization is depicted in Fig. 2.3; right showing the beam-end test. Its boundary conditions, i.e. the placement of supports and loading are designed with the goal to render the stress state equivalent to the end zone of a tensile reinforcement in a beam. It aims to combine the positive features of both the pull-out test and of the beam anchorage test.

Beam-end test

In case of flexible, fine scale reinforcement further types of test setups for bond characterization have been developed. An example of such a test is shown for testing the pullout behavior of textile fabrics. An example in Fig. 2.4 shows a test series performed on double sided pullout test of textile fabrics. The planar test specimens were clamped using steel plates positioned near to the middle section containing a notch and pulled apart. The opening of the notch that we refer to as crack opening displacement (COD) was recorded

Test setups for fine-scale reinforcement

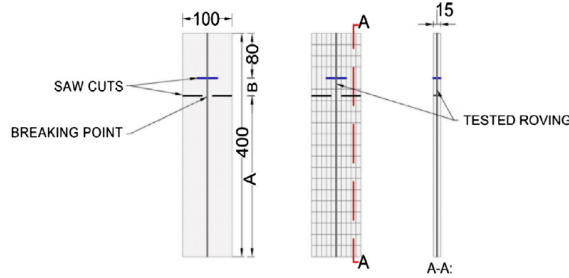


**Figure 2.5** Double sided pullout test for a single fiber with a predefined pullout length at one side using a cut at one side.

during the test. This test setup can be seen in analogy to the beam anchorage length rendering a symmetric debonding on both sides up to the maximum pullout force. From there on, the process becomes non-symmetric. This fact makes it impossible to characterize the bond in material exhibiting a so called softening, i.e. decreasing shear for increasing slip after the peak value. Up to the peak, the end slip can be assumed as a half of the crack-opening displacement  $s = COD/2$ .

To cover also the bond behavior exhibiting softening, a small-scale test setup depicted in Fig. 2.5 has been proposed. This test setup has been derived from the double sided test setup with the goal to prescribe which side will start debonding. This test setup demonstrates the dilemma involved in the pullout test design. The stress profile should be as close as possible to the condition of crack bridge. Let us remark, that the test response must be treated with care as it contains the transition from a symmetrical debonding to a non-symmetrical one.

The brief survey of test setups demonstrates the existing variety of characterization methods that are specialized for individual types of materials. The purpose of this survey is to motivate a unified view to these experimental setups using the objective description of the bond behavior that is independent on the particular test configuration. The theoretical description of the correspondence between the local bond behavior and the global (structural) response of the pullout test is a must for a sound and detailed interpretation of experimental data.

**Question:** The double sided pullout test includes two debonded zones. Can we simply say that the whole process is symmetric and just calculate the pullout displacement at one side by setting  $w = COD/2$ ?

## 2.2 Objectivity of a material model

The bond-slip law represents an objective material property characterizing the material behavior at any point within the interface. Fig. 2.6 shows the bond-slip law  $\tau(s)$  defining the material behavior at any material point  $x$  along the embedded length.

The structural behavior that is measurable as a force-displacement relationship is represented by the pull-out curve  $P(w)$  relating the displacement of the loaded fiber or

reinforcement end with the applied pull-out force. Given a continuous slip  $s(x)$  along the interface we can visualize the pullout force  $P$  as the green area representing the integral

$$P = \int_0^L \tau(s(x)) dx.$$

By identifying a "true" bond-slip law we get the possibility to predict the pull-out curve for diversity of loading scenarios. It is the key to the prediction of structural response. The question is how to identify the bond slip law from an experimental observation, e.g. from the measured pull-out curve  $P(u)$ .

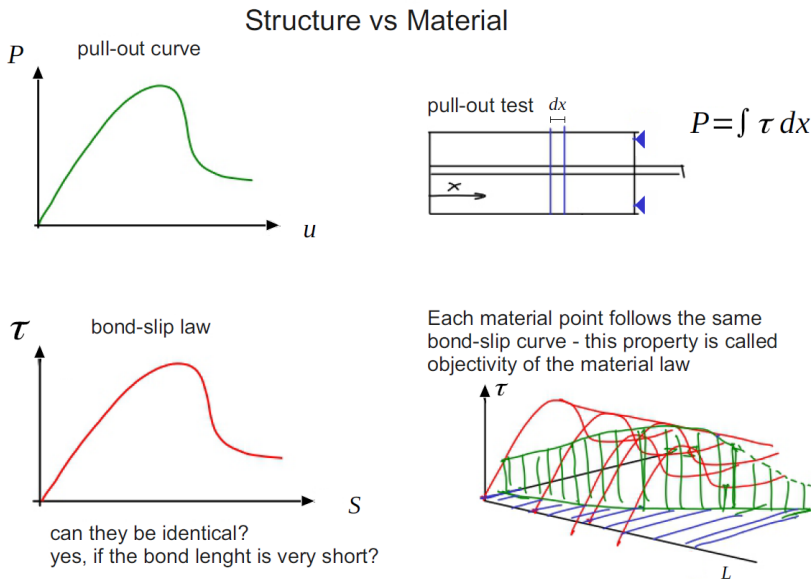


**Figure 2.6** Relation between material behavior and structural behavior

A simple experimental strategy to identify the bond slip law attempts to use a very short embedded length with the goal to achieve a uniform slip along the whole interface length. Then, the front and end slip of the pullout test are the same. In such a case, the pull-out curve can be directly transformed to the bond-slip relation by dividing the force with the interface area given as the product of the perimeter  $p$  and length  $L$

$$\tau(s) = \frac{1}{pL} P(s).$$

However, it is rather difficult to design such a short test setup in a reproducible way. The short section of the material along the interface zone exhibits a relatively large scatter of properties so that many tests have to be conducted. Furthermore, the production of small size specimens results in a material behavior that is different from the *in-situ* conditions.

Realistic prediction of the pullout behavior is needed to support both the efficient and goal oriented material design with tuned material behavior. At the same time, it provides a valuable input for the formulation of design codes. In the sequel we will exemplify this issue on the example of the identification of the anchorage length.

The structural configuration of the pullout test is depicted in Fig. 2.7, including the elastic parameters of the material components. The Figure also shows the boundary conditions BC1, BC2 that can be considered to solve the pullout test. The boundary condition BC3

with the clamped reinforcement represents a configuration of a crack bridge in a tensile test that we will discuss in the context of a multiple cracking behavior of brittle-matrix composites.

S1

[S1:] can I add Parameters'(Lb, Lf, A, E, etc.) definition on the right side of the figure?

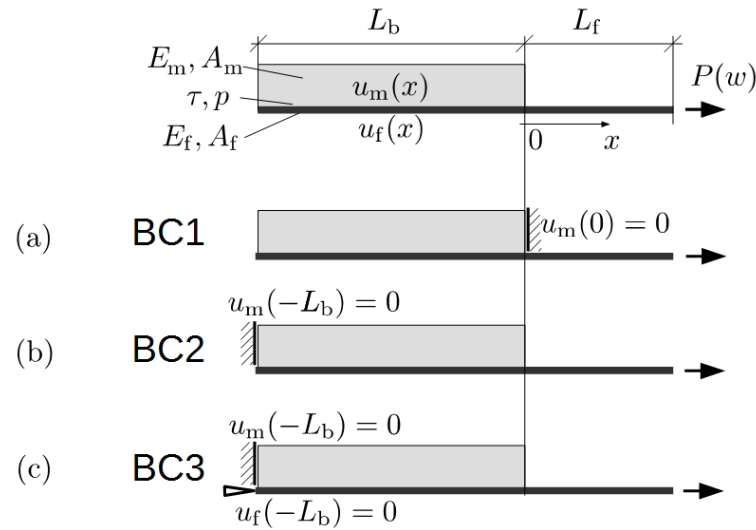


**Figure 2.7** One dimensional idealization of the pullout test as boundary value problem

All the displayed configurations can be associated with different types of material behavior. If we assume rigid matrix and constant or linear bond-slip law, it is possible to derive analytical solutions of the pullout problem.

In case of a generally non-linear bond slip law, including inelastic effects, like friction and damage, numerical solutions are available. In Sec. 2.3 we will construct a simple analytical solution of the pullout problem that can cover all the configurations depicted in Fig. 2.7. Each model will be accompanied with an executable script providing the possibility to study the effect of the geometrical and material parameters on the response of the pullout test.

## 2.3 Analytically solvable pullout problems

Special case of bond behavior used for quick characterization of bond is described by a constant bond-slip function.

$$\tau(s) = \bar{\tau} \quad (2.1)$$

With this assumption, we can derive an analytic expression for the relation between the pull-out force  $P$  versus pull-out displacement  $u_{f,0}$ . This solution deserves our attention because of its frequent use in interpretation of experimental results of pull-out tests and also in design rules for composite materials. Therefore, it is helpful to understand the correspondence between the stress, strain and displacement profiles and the boundary conditions.

The most simple theoretical description of a non-linear structural behavior is provided for the uni-axial idealization of the pullout test assuming a frictional type of bond exhibiting a stick-slip behavior. The assumed shape of bond law is sketched in Fig. 2.8.

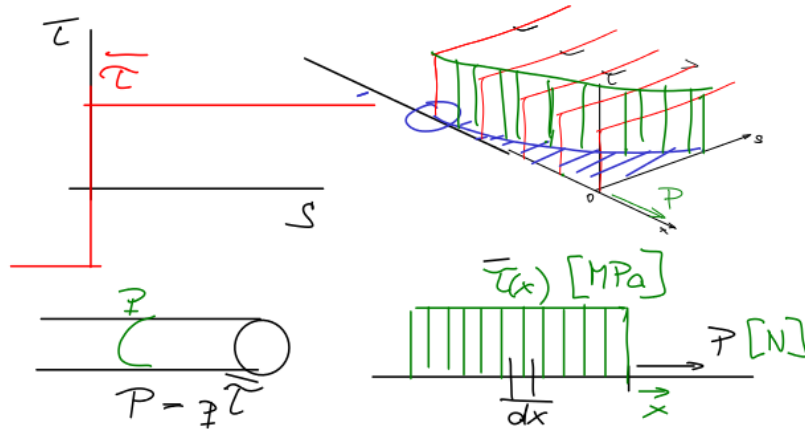


**Figure 2.8** Assumptions included in the pullout-model with constant bond stress

### 2.3.1 Constant shear bond to a rigid matrix

Regarding an infinitesimal element of an interface area within a composite cross section shown in Fig. 2.9 we can formulate the local equilibrium condition as

Just one unknown field  $u_f(x)$

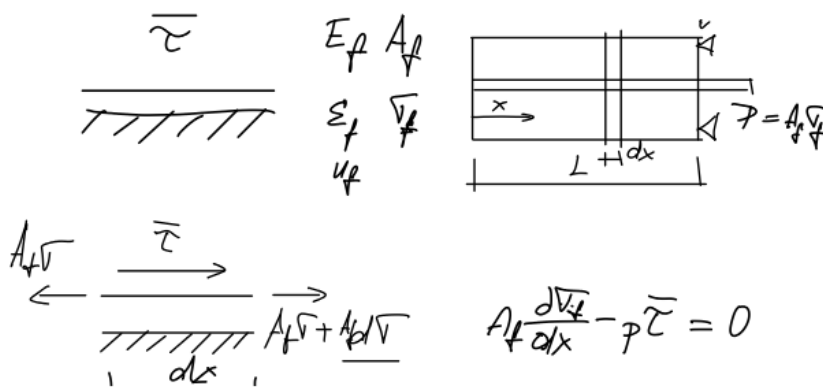


**Figure 2.9** Variables and parameters describing the constant bond model

$$A_f \sigma_{f,x} - p \bar{\tau} = 0 \quad (2.2)$$

where  $A_f$  is the area of the reinforcement,  $\sigma_{f,x}$  the derivative of the fiber stress with respect to the length coordinate  $x$ ,  $p$  is the perimeter, and  $\bar{\tau}$  stands for the constant shear/frictional bond stress. Integration of Eq. (2.2) reveals that the stress  $\sigma(x)$  is linear, i.e.

$$\sigma_f(x) = \frac{p \bar{\tau}}{A_f} x + C \quad (2.3)$$

Assuming a linear elastic reinforcement behavior with the material stiffness  $E_f$  at every point  $x$  of the reinforcement ( $\sigma_f = E_f \varepsilon_f$ ) we rewrite this condition for strain along the debonded zone as

$$\varepsilon_f(x) = \frac{1}{E_f} \sigma_f(x) = \frac{1}{E_f} \left( \frac{p \bar{\tau}}{A_f} x + C \right) \quad (2.4)$$

Local equilibrium

Kinematics

and then into the kinematic condition

$$u_f = \int \varepsilon_f(x) dx = \frac{1}{E_f} \left( \frac{p\bar{\tau}}{2A_f} x^2 + Cx \right) + D = \frac{1}{2} \frac{p\bar{\tau}}{E_f A_f} x^2 + \frac{1}{E_f} Cx + D \quad (2.5)$$

we obtain the quadratic function of the reinforcement displacement with the two parameters  $C, D$  to be determined using the boundary conditions.

Resolve constants

To determine the constant  $C$  we recall that the force distribution along the bar given as

$$F_f(x) = \sigma_f(x) A_f = p\bar{\tau}x + CA_f, \quad (2.6)$$

must be equal to the applied load  $P$  at the pulled end ( $x = 0$ ), i.e.

$$F(0) = \sigma_f(0) A_f = P \implies C = P/A_f. \quad (2.7)$$

Global equilibrium

By substituting Eq. (2.7) into Eq. (2.5) the displacement field of the reinforcement can be rewritten as

$$u_f(x) = \frac{1}{2} \frac{p\bar{\tau}}{E_f A_f} x^2 - \frac{P}{E_f A_f} x + D. \quad (2.8)$$

Compatibility

To factor out the parameter  $D$  another condition is needed. This condition can be introduced by realizing that in zones, where the reinforcement is still bonded to the matrix, there is no slip and, thus, the displacement in the reinforcement at point  $a$  is zero. Knowing that the debonded zone starts from the loaded end and propagates inwards through the bond layer, we can require

$$u_f(a) = 0 \implies D = -\frac{a}{2A_f E_f} (2P + ap\bar{\tau}) \quad (2.9)$$

Still, the problem has one unknown variable, namely the debonded length  $a$ . To resolve it, we need another condition. Realizing that also the strain at  $a$  must vanish we can substitute  $a$  for  $x$  in Eq. (2.4) and resolve for the state variable  $a$  to get

$$\varepsilon_f(a) = 0 \implies a = -\frac{P}{p\bar{\tau}}. \quad (2.10)$$

State fields

With all the variables at hand, the sought reinforcement displacement corresponding to the given boundary conditions has the form

$$u_f(x) = \frac{1}{2} \frac{p\bar{\tau}}{E_f A_f} x^2 - \frac{P}{E_f A_f} x + \frac{1}{2E_f A_f} \frac{P^2}{p\bar{\tau}}. \quad (2.11)$$

Particularly interesting is the displacement at the loaded end  $u(x = 0)$

$$u_f(0) = w = \frac{1}{2} \frac{P^2}{p\bar{\tau} E_f A_f}. \quad (2.12)$$

Pullout curve

By solving this equation for  $P$  we finally obtain an explicit function describing the pull-out curve in the form

$$P(w) = \sqrt{2p\bar{\tau} E_f A_f w}. \quad (2.13)$$

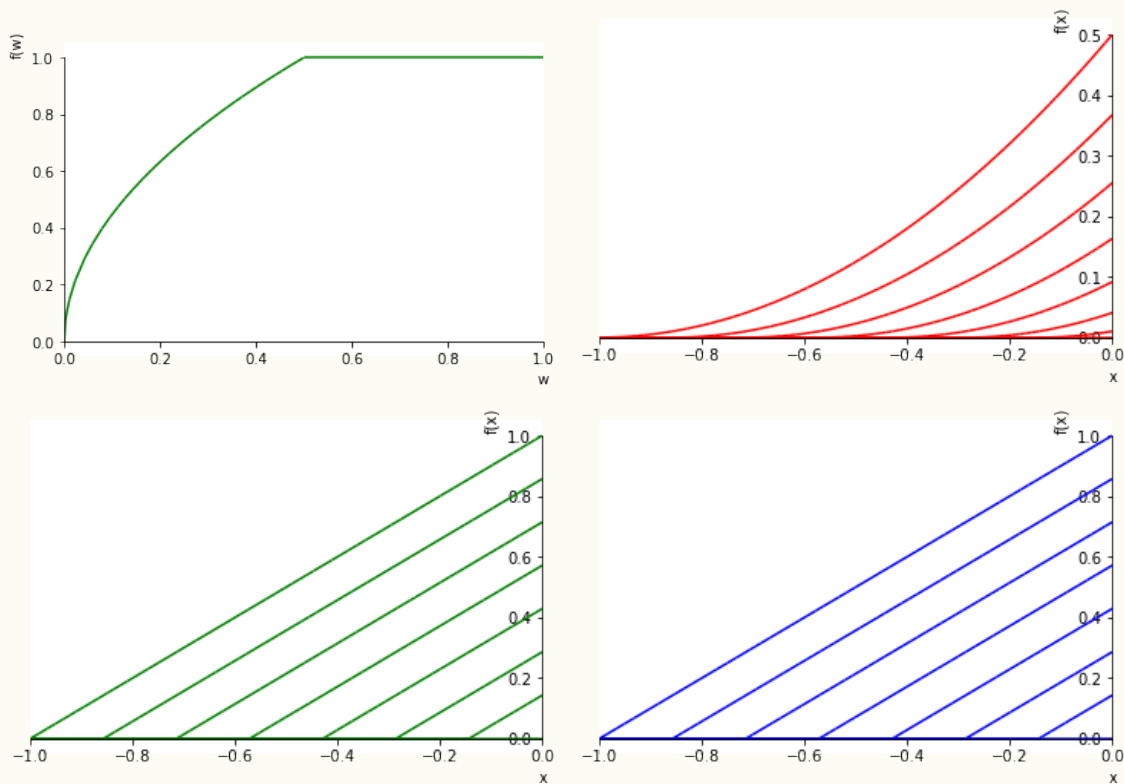
### Example 2.1: Pullout from rigid matrix

**Question:** Consider the pullout test depicted in Fig. 2.1. Evaluate the pullout curve assuming that there is deformation in concrete and that the bond behavior corresponds to the purely frictional bond derived previously. The boundary value problem idealizing such structural behavior is depicted in Fig. 2.7ab.

**Solution:** A python script evaluating the problem using the derived model (2.13) has been prepared [here](#) to perform calculations using the model. It can be readily used to test the model and evaluate the pullout curves and also the stress, strain and displacement fields. Exemplified results are provided here for the values of parameters

$$E_f = 1, \quad A_f = 1, \quad \bar{\tau} = 1, \quad L_b = 1 \quad (2.14)$$

**Results:** The top-left diagram shows the  $P(w)$  curve, the top right diagram shows the slip along the bond length for several load levels, the bottom diagrams visualize the strain and stress along the bond length. Since  $E_f A_f = 1$ , they are equal.



**Task:** Change the material parameters given in the script to reproduce the test results of the RILEM pullout test presented in Fig. 2.1. Is it possible to set up the model such that it can reproduce the results?

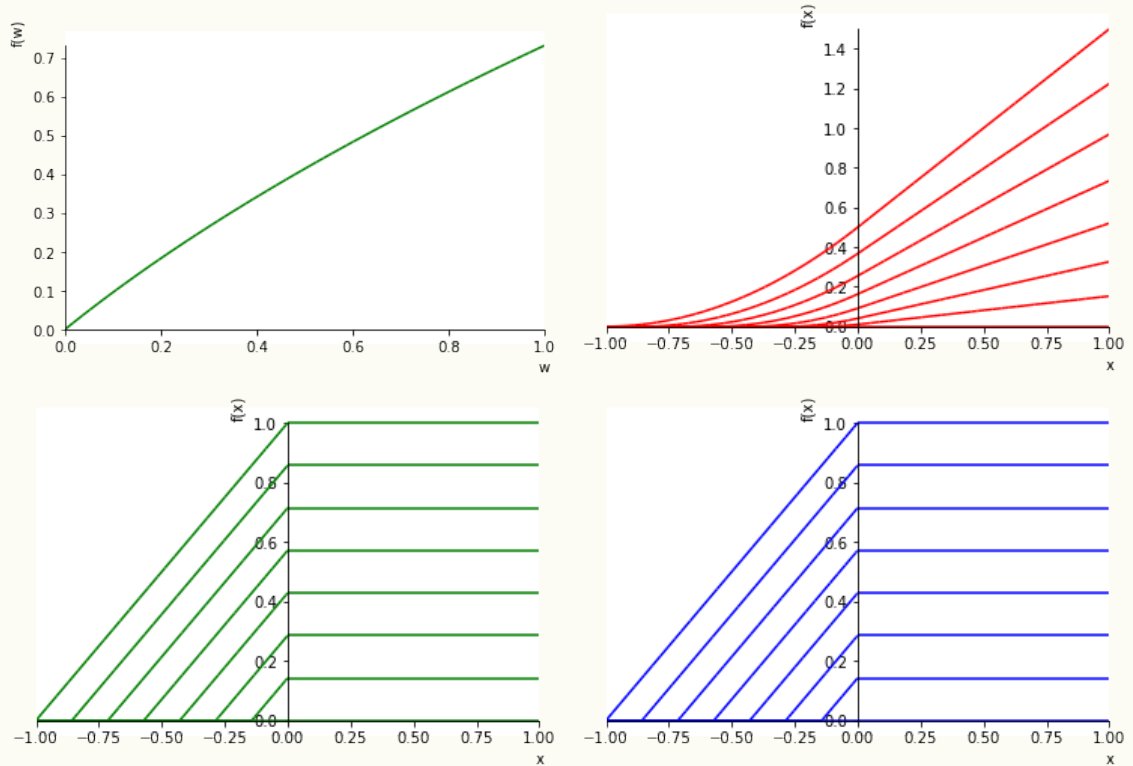
### Example 2.2: Pullout from rigid matrix with extra bar length at the loaded end

**Question:** The bar in test shown in Fig. 2.1 does not start immediately at the beginning of the bonding zone. Extend the model by including the deformation of the bar along the free length such that it is possible to place the LVDT measuring the displacement on the steel bar at some distance from the bond zone. In the evaluation use the parameters

$$E_f = 1, \quad A_f = 1, \quad \bar{\tau} = 1, \quad L_b = 1, \quad L_f = 1 \quad (2.15)$$

**Solution:** The required extension of the analytical model requires another spring attached to the model previously derived and to impose a compatibility condition. The derivation has been done using the symbolic algebra package in the Python language. The executable jupyter notebook can be downloaded [here](#).

**Results:** The diagrams demonstrate the difference with respect to Example 2.1 for  $P(w)$  pullout curve, displacement, strain and stress fields along the bar.



**Task:** Test the effect of the changing free bar length. How does the pullout curve  $P(w)$  look like qualitatively if the free length of the bar gets very long?

**Task:** Name all possibilities how this pullout test can ultimately fail.

#### 2.3.2 Constant shear bond to elastic matrix

What if the  
matrix  
deforms as  
well?

An extension of the previous model for elastic matrix can be done by refining the condition of compatibility. Let us exemplify this extension for two kinds of boundary conditions depicted in Fig. 2.10. Given the strain in the concrete matrix and in the fabric reinforcement,  $\varepsilon_m$  and  $\varepsilon_f$ , respectively we can evaluate the relative slip at  $x = 0$  as

$$w = \int_{-a}^0 \varepsilon_f - \varepsilon_m \, dx. \quad (2.16)$$

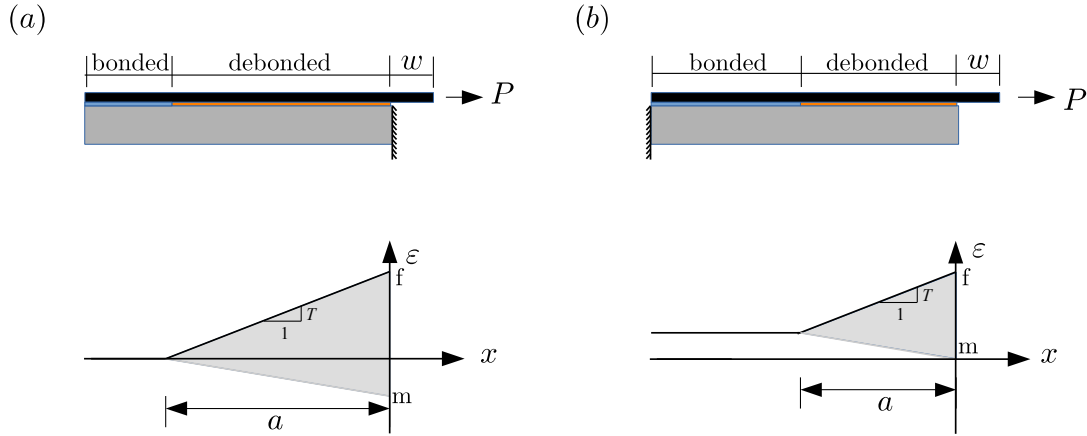


**Figure 2.10** Profile of strains in the pullout-model with constant bond stress; a) Matrix supported at loaded end, b) Matrix supported at unloaded end

It is represented by the shaded area in Fig. 2.10. In the simple case of constant bond, the area is of triangular shape so that the derivation can be simplified. In order to determine the area of the triangle, the following parameters are required: the strains  $\varepsilon_f(x = 0)$  and  $\varepsilon_m(x = 0)$ , as well as the debonded length  $a$ .

### 2.3.2.1 Matrix supported at the loaded end (BC1)

When the matrix is fixed at  $x = 0$  as shown in Fig. 2.10a, the required parameters can be determined as

$$\varepsilon_f(0) = \frac{P}{E_f A_f}, \quad \varepsilon_m(0) = \frac{-P}{E_m A_m} \quad (2.17)$$

$$T = \frac{p\tau}{E_f A_f} \quad (2.18)$$

$$a = \frac{\varepsilon_f(0)}{T} = \frac{P}{p\tau}. \quad (2.19)$$

Thus, the crack opening can be expressed as the area of the triangle

$$\begin{aligned} w &= \frac{1}{2} [\varepsilon_f(0) - \varepsilon_m(0)] a \\ &= \frac{1}{2} \frac{P^2}{p\tau} \left[ \frac{1}{E_f A_f} + \frac{1}{E_m A_m} \right]. \end{aligned} \quad (2.20)$$

By solving this equation for  $P$  we obtain the pullout curve in the form

$$P(w) = \sqrt{2wp\tau \frac{E_f A_f E_m A_m}{E_f A_f + E_m A_m}}. \quad (2.21)$$

#### Example 2.3: Pullout from elastic matrix clamped right

Pullout from rigid matrix with extra bar length at the loaded end. The described procedure can be applied with further extensions considering different position of supports, inclusion of free-length of the reinforcement at the pulled-out end. The script containing this model

is provided [here](#).

**Task:** Use the model with the material parameters appropriate to carbon reinforcement and concrete with the stiffness  $E_m = 28 \text{ GPa}$  and find out for which ratio of cross-sectional areas  $A_m/A_f$  does the pull-out curve change.

### 2.3.2.2 Matrix supported at unloaded end (BC2)

For the case shown in Fig.2.10b where the matrix is fixed at the left side, the values of  $\varepsilon_f(x = 0)$  and  $T$  remain the same, while

$$\varepsilon_m(x = 0) = 0 \quad (2.22)$$

$$\varepsilon_f(x = -a) = \frac{P}{E_f(A_m + A_f)}, \quad (2.23)$$

and the debonded length

$$a = \frac{\varepsilon_f(x = 0) - \varepsilon_f(x = -a)}{T} \quad (2.24)$$

$$= \frac{PA_m}{p\tau(A_f + A_m)}. \quad (2.25)$$

Then the slip at  $x = 0$  can be written as

$$w = \frac{1}{2} \frac{P^2 A_m}{p\tau E_f A_f (A_f + A_m)} \quad (2.26)$$

and finally the pull-out response is given by

$$P(w) = \sqrt{2wp\tau \frac{E_f A_f (A_f + A_m)}{A_m}} \quad (2.27)$$

### Example 2.4: Pullout from elastic matrix clamped left

Pullout from rigid matrix with extra bar length at the loaded end. The described procedure can be applied with further extensions considering different position of supports, inclusion of free-length of the reinforcement at the pulled-out end. The script containing this model is provided [here](#).

**Task:** Use the model with the material parameters appropriate to carbon reinforcement and concrete with the stiffness  $E_f = 28 \text{ GPa}$  and find out for which ratio of cross-sectional areas  $A_m/A_f$  does the pull-out curve change.

**Task:** Answer the question: Assuming steel rebar, at which level of reinforcement ratio does the elasticity of matrix change the maximum pullout force by 10% compared to the case of rigid matrix?

### Example 2.5: Pullout of a short fiber with decreasing bond length

Pullout from rigid matrix with extra bar length at the loaded end. The described procedure can be applied with further extensions considering different position of supports, inclusion of free-length of the reinforcement at the pulled-out end. The script containing this model is provided [here](#).

**Task:** Use the model with the material parameters appropriate to carbon reinforcement and concrete with the stiffness  $E_f = 28 \text{ GPa}$  and find out for which ratio of cross-sectional areas  $A_m/A_f$  does the pull-out curve change.

**Task:** Answer the question: Assuming steel rebar, at which level of reinforcement ratio does the elasticity of matrix change the maximum pullout force by 10% compared to the case of rigid matrix?

#### 2.3.3 Piecewise linear bond-slip law

Besides the case of the frictional model, analytical solution can be derived also for linear-elastic bond as presented in [one] <sup>S2</sup> [S2] [Can I correct the citation number? one?](#)

$$P(u_{f,0}) = \frac{k \tanh(\alpha L)}{\alpha} u_{f,0}, \quad \text{with } \alpha = \sqrt{pk \left( \frac{1}{E_f A_f} + \frac{1}{E_m A_m} \right)} \quad (2.28)$$

This solution can describe the initial stages up to the onset of debonding. Notice that the relation  $P(w)$  is linear. This solution can be generalized for piecewise linear bond-slip law as exemplified in [yuan\_full-range\_2004]. Then a solution of the pullout problem with non-linear bond-slip law can be obtained by putting together the analytical solutions along every segment. However, a more general and efficient solution can be obtained within the framework of the standard non-linear finite element solver. In the following chapter such a solver will be presented including the executable code to solve examples.

## 2.4 Conclusions and remarks

This class of pull-out models is particularly useful as a basic component of models studying statistical aspects of scatter in heterogeneous materials in the vicinity of crack bridges.

## 3 Bond behavior

**Outline:** By saying that we want to capture the "material behavior" we mean that we realistically describe the relation between the strain and stress in a general material point. With the focus on a one-dimensional interface between two material components we can reduce this task to the relation between bond stress and slip. In Chapter 2, we simply assumed two shapes of the bond-slip relation, i.e. the constant bond-slip law for the stick-slip interface and a linear relation. The only reason we chose these two shapes was that for such laws, analytical solutions of the pullout boundary value problem can be found. However, the stick-slip interface cannot realistically describe the behavior of steel-concrete or FRP-concrete bond. In this chapter, we investigate more complex shapes of bond slip laws and their effect on the observed pullout response.

### Addressed questions:

- How to characterize the bond.
- What parameters influence the bond behavior?
- What is a material law? What is a material point?
- At which scale can we characterize a material behavior?
- What is meant with a validity of a model?

### 3.1 Generally nonlinear bond-slip law

To solve a pullout problem for a generally nonlinear bond-slip law, we have to solve the initial boundary value problem numerically. We shall use a finite-element code implemented within the BMCS tool to study the behavior for two examples. To make only a small step from the constant bond-slip law discussed in Chapter 2 we modify this bond slip law only slightly in a way depicted in Fig. 3.1. The shown modifications represent the increasing shear and decreasing shear during the sliding of the two surface over each other.

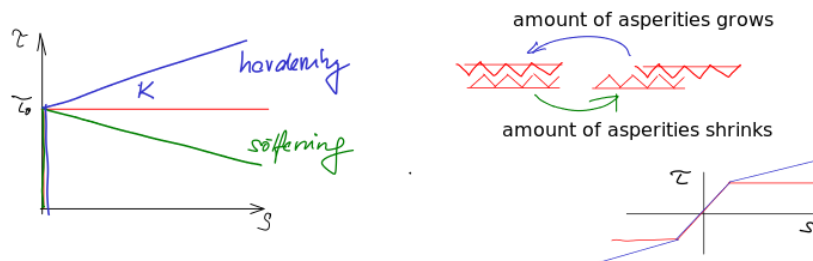


**Figure 3.1** Structural interpretation of bond hardening and softening

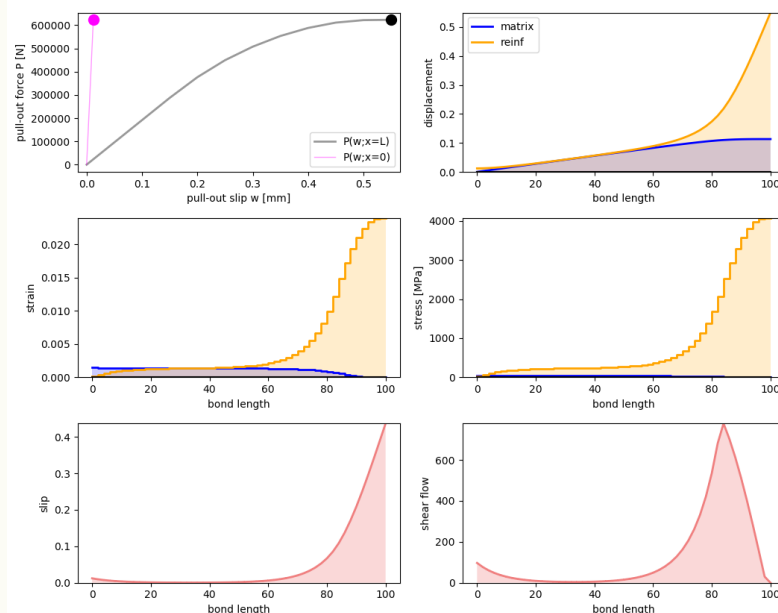
Even though analytical solutions for a piecewise-linear bond slip law have been derived it is more effective to apply general numerical finite-element solvers. Therefore, before proceeding to the study of the effect of the nonlinear bond-slip law on the pullout response, let us briefly touch the topic of the solution algorithm needed to solve the generally nonlinear problem. There are actually two questions that need to be addressed separately:

1. How to find the unknown displacement  $u_f$  satisfying the conditions of equilibrium, constitutive behavior and kinematics that we introduced in Sec 2.3.2 for a given level of load  $P$  assuming linear bond-slip law? A very brief answer to this question is provided in Sec. 3.4.
2. Based on the answer to question 1, how to define an iterative scheme that can handle non-linear type of bond-slip laws considered here? The principle approach to solving the nonlinear problem is shown using an elementary type of function in Sec. 3.5.

To provide an insight into the way how do the finite-element tools solve the problem an open implementation of the nonlinear solver, first in form of an open script that can be modified and tested. This type of solver is provided in the BMCS tool suite to perform virtual tests and discuss the structural behavior later on. The same type of scheme is available in the most finite-element programs available on the market. The detailed explanation of the theoretical background is provided in the Master's courses on linear structural analysis focused on the theoretical background of the finite-element method and on the nonlinear structural analysis.

### Example 3.1: Piecewise-linear bond slip laws

**Task:** Use the corresponding jupyter notebook with the preconfigured pullout-model with piece-wise linear bond slip law to test the correspondence between the local bond law and the structural behavior. Cover the range of hardening and softening bond behavior.



**Task:** Answer the question: how does the response of the pullout curve evolve displayed for further increased pullout displacement  $w = 0.15$  mm in the top left Figure ( $P(w)$ ) and in the other diagrams showing the strain and stress state of the specimen?

**Task:** Answer the question: Based on the state variables (slip and shear stress along the bond zone) shown in the Figure: reconstruct the bond-slip law that was used in the simulation.

### 3.2 Bond-slip law with hardening

With the solution tool at hand let us return to the original question studying the effect of the hardening and softening in the bond-slip law. Assuming a bond slip law with hardening, To start with, let us return to the test results displayed in Fig. 2.1 of Sec. 2.1. The tests were using the steel with the diameter  $d = 15$  mm with two embedded length. Thus, it should be possible to describe the pullout response of the two studied embedded lengths using the same bond-slip law.

If we can describe the two curves using an objective material model, i.e. a single bond-slip law, we might be able to predict the response in general and address the question of the anchorage length required for the particular type of a bar. Our first goals are the following:

**Calibration** Choose one of the tests displayed in Fig. 2.1 (e.g.  $L_b = 5d$ ) and adjust the bond-slip law in such a way that the pullout curve roughly corresponds to the test response.

**Validation** Change the embedded length according to the other test, i.e.  $L_b = 10d$  and calculate the pullout curve. Check if it corresponds with the experimental response.

**Parametric study** Calculate the anchorage length, i.e. at which length does the bar yield or rupture?

This procedure introduces the notions of calibration, validation and parametric study that need to be explicitly distinguished when using models in combination with experimental data. Very often they are mixed up and it is not explicitly said if the modeled curve is a pure prediction, or if the parameters were adjusted to fit the experimental data.

The validation tells us to what extent is the model able to predict the behavior if we change the geometry or boundary conditions. It evaluates the quality and applicability of the model. If the model can reflect the essential effects included in the material behavior, it can be used to predict the response for changed parameters and boundary conditions. In our particular example, we might save experiments if we can trust the model that it can to some extent really substitute the experiment.

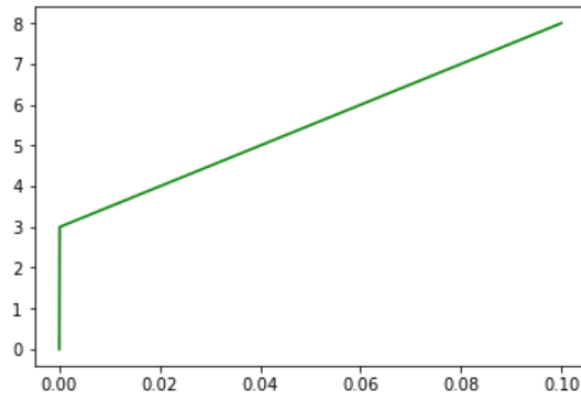
#### Example 3.2: Simulation of the RILEM pullout test

**Question:** As an example of the three steps regarding the calibration, validation and parametric studies, the script provided on the server shows the bond-slip procedure using the finite-element simulator of the pullout within the BMCS tool suite.

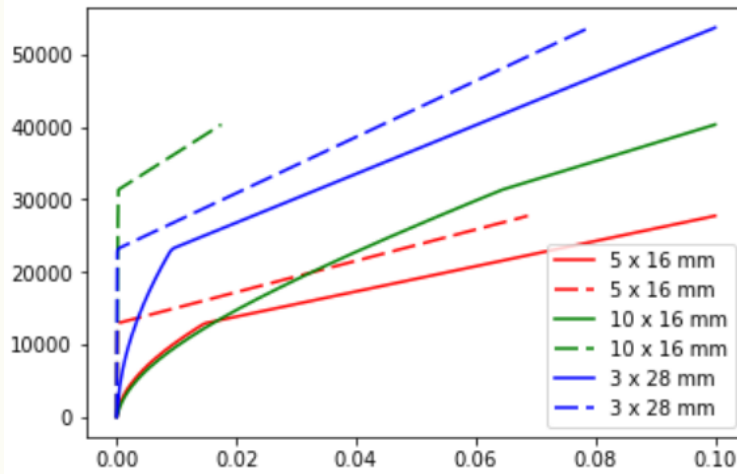
$$d = 16 \text{ mm}, E_f = 210 \text{ GPa}, E_m = 28 \text{ GPa},$$

$$A_f = \pi \left(\frac{d}{2}\right)^2 \text{ mm}^2, A_m = (10d)^2 \text{ mm}^2, p = \pi d$$

The bond-law roughly reproducing the standard RILEM test setup was identified in the form



**Task:** Use the bond-slip law to predict the other combinations of material parameters, i.e length of the bond zone  $L_b = 10d$  and different diameter  $d = 28 \text{ mm}$  and  $L_b = 3d$ .



**Task:** Find out at which length  $L_b$  the yielding of steel would start. question of anchorage length by repeated calculation of the pullout test with increasing anchorage length.

### 3.2.1 How to determine the anchorage length in case of the constant bond-slip law?

Let us consider the case of pull-out model with constant bond strength presented in Sec. 2.3 and qualitatively analyze the length-dependent pull-out response. Let us assume that the level of  $\tau$ , which is the only material parameter needed to characterize the bond-slip behavior, has been determined from a calibration experiment with embedded length  $L_1$ . We can now make a prediction of the pull-out curves for embedded lengths  $L_2$  and  $L_3$  to obtain the respective pull-out curves depicted in Fig. 3.2.

The maximum achievable pull-out force of a test with an embedded length  $L_b$  is given as

$$P_L = \tau p L_b \quad (3.1)$$

Predict the pull-out response of the changed embedment length

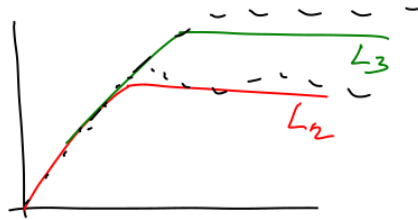


**Figure 3.2** Prediction of the constant bond model

where  $p$  denotes the perimeter, equal in all experiments. The force at which the reinforcement attains the strength  $\sigma_{f,mu}$  and breaks is

$$P_{f,mu} = \sigma_{f,mu} A_f \quad (3.2)$$

so that the anchorage length obtained by setting  $P_\tau = P_{f,mu}$  reads

$$L_{anc} = \frac{\sigma_{f,mu} A_f}{\tau p}. \quad (3.3)$$

The length-dependent maximum pull-out force is a bilinear function with a linear branch starting at zero and achieving the point  $[L_{anc}, P_{f,mu}]$  as indicated in the right diagram of Fig. 3.3

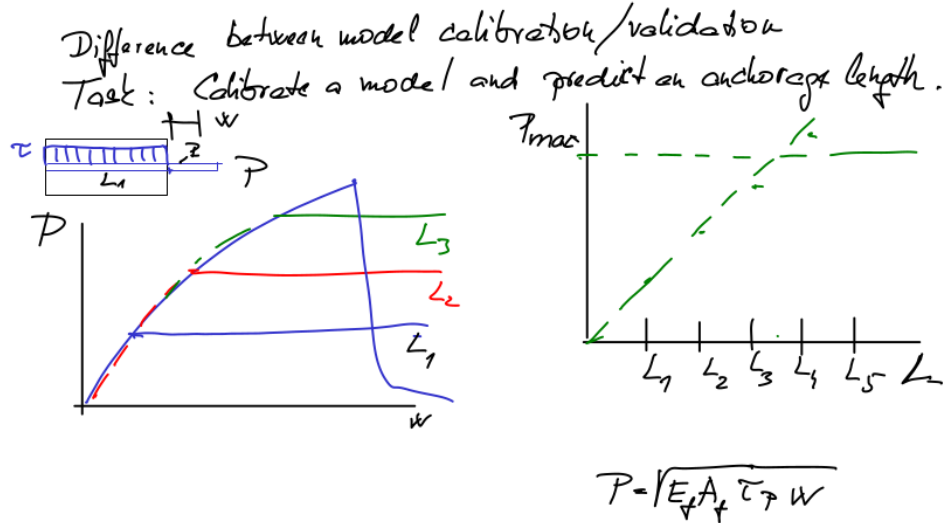


**Figure 3.3** Length dependence

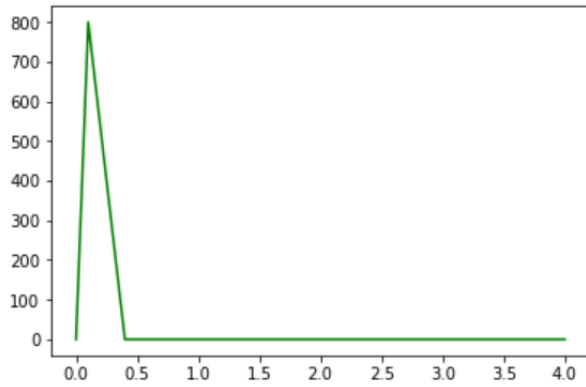
The simple bond-slip law allowed us to derive an explicit relation between the anchorage length, as a design parameter required for dimensioning of structures. This concept is used in design equations. However, it must be used with care, since it is only valid for bond-slip laws that do not exhibit softening behavior as we shall document next.

### 3.3 Pullout problem for bond slip law with softening

A fundamentally different length-dependent behavior can be obtained if a bond-slip behavior exhibits softening. Assuming a bond-slip law with a peak bond stress  $\tau_{mu}$  at slip  $s_{mu}$  and decreasing shear stress for slip  $s > s_{mu}$  we shall now perform the same analysis of length dependency.

#### Example 3.3: Simulation of debonding between CFRP sheet and concrete

**Question:** Considering FRP sheet used for strengthening, the bond-slip law with softening has been identified in a pullout test

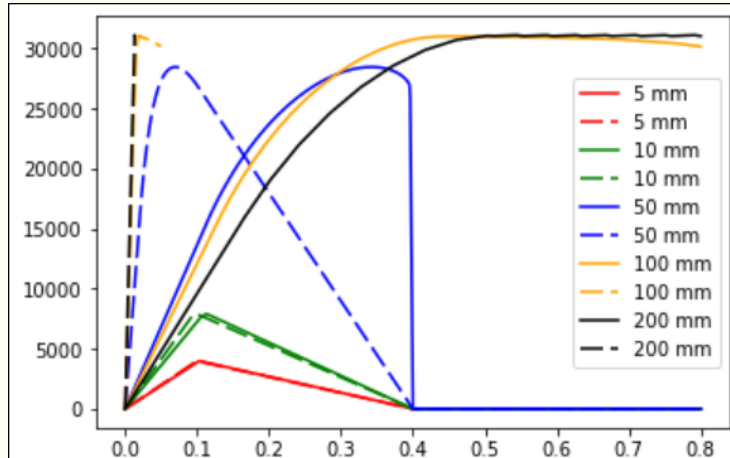


The cross sectional parameters have been set to

$$A_f = 16.67 \text{ mm}^2, A_m = 1540.0 \text{ mm}^2, E_f = 170000 \text{ MPa}, E_m = 28000 \text{ MPa}$$

The perimeter  $p = 1.0$  was considered that means the bond slip law was related to the whole width of the sheet.

**Task:** find out the length-dependent response. The pullout curves calculated for the bond length  $L_b \in (50, 200)$  mm are obtained in the form



**Task:** Answer the question: what is the anchorage length of the studied FRP?

### 3.4 Finite element solution of the pullout problem

The provided code shows an application of these methods for the uniaxial discretization of the interface representing the embedded length. Every single point along the embedded length follows the behavior prescribed by the bond-slip law. The studies in the sequel will use linear finite elements representing the piecewise linear discretization of the embedded zone. Fig. 3.4. The displayed functions are non-zero only on a small subdomain. The

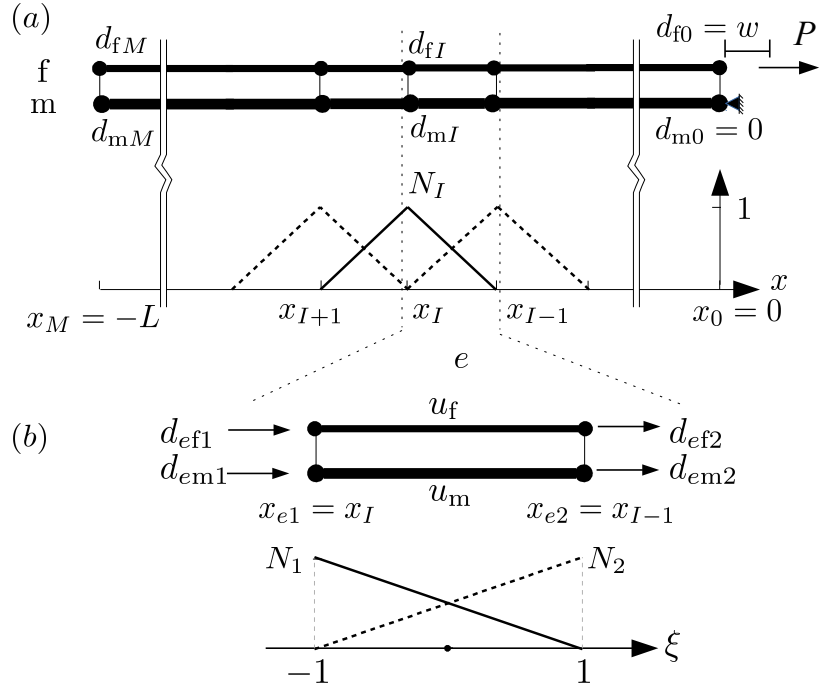


**Figure 3.4** Linear finite elements applied in the BMCS tool suite.

sought displacement field of the reinforcement is approximated using the shape functions shown in Fig. 3.4a,

$$u_f = N_I d_{fI}$$

with the index  $I = 1, 2, \dots, M$  representing the  $I$ -th node.

### 3.5 Iterative solver for a general non-linear finite element simulation

To demonstrate the idea of a non-linear solver even in simple terms, let us consider a nonlinear function with just one unknown variable  $f(u) = \bar{f}(t)$ . Then, we assume to know the derivatives of the sought function with respect to the state variable  $u$ . The time stepping algorithm provides us a means how to travel through the space of state variables along an admissible path satisfying the governing equations. The director of the travel is the pseudo-time variable  $t$ .

In order to illustrate the concept, let us consider the simple function

$$\bar{f}(t) = \sin(u) \quad (3.4)$$

Think of this equation as the equilibrium requirement of our mechanical model. On the left hand side, there is the prescribed history of loads  $\bar{f}(t)$ . On the right hand side, the force of response of the structure. Now, for prescribed history on the right hand side  $\bar{f}(t)$ , we want to find the corresponding history of displacements satisfying the equilibrium  $u(t)$ .

Of course, we might solve this equation just inverting the function to obtain the result

$$u(t) = \arccos f(t) \quad (3.5)$$

but an inverse function is not available in a general case of a discretized structure. We thus pretend, that the inversion of the function  $\sin(u)$  is not available and define the residuum of the problem as an implicit function

$$R = \sin(u) - \bar{f}(t) = 0. \quad (3.6)$$

In a numerical code, the values of the function  $\bar{f}(t)$  is given in incremental steps. For each increment of  $\bar{f}(t)$  an iteration loop must be performed to find the value of  $u$  satisfying the residuum.

To get the numerical algorithm, we first expand the residuum using the first two terms of the Taylor series as

$$R(u^{k+1}, t) = R(u^k, t) + \left. \frac{\partial R(u)}{\partial u} \right|_{u^k} \Delta u^{k+1} = 0. \quad (3.7)$$

In the considered case of  $\sin u$ , the derivative of the residuum with respect to  $u$  is calculated as

$$\left. \frac{\partial R(u)}{\partial u} \right|_{u^k} = \cos(u^k) \quad (3.8)$$

The iteration loop can then be obtained by solving the expanded residuum for the increment of the displacement  $\Delta u^{k+1}$  as

$$\Delta u^{k+1} = - \left[ \left. \frac{\partial R(u)}{\partial u} \right|_{u^k} \right]^{-1} R(u^k) \quad (3.9)$$

The new value of the variable  $u$  can be given as

$$u^{k+1} = u^k + \Delta u^{k+1} \quad (3.10)$$

The last two equations are repeated until the residuum is (almost) zero. Graphical representation of this procedure is shown in Fig. 3.5 for a residuum given as function  $R(\varepsilon) := f(\varepsilon) - \hat{f} = 0$ .

This kind of incremental time-stepping procedure is used in the following examples that are solved either using the applications of the BMCS tool suite or using the ABAQUS, ANSYS, DIANA, ATENA, RFEM, InfoGraph, etc. Our goal is to illuminate the correspondence between the basic types of the bond-slip law and the observed pullout response.

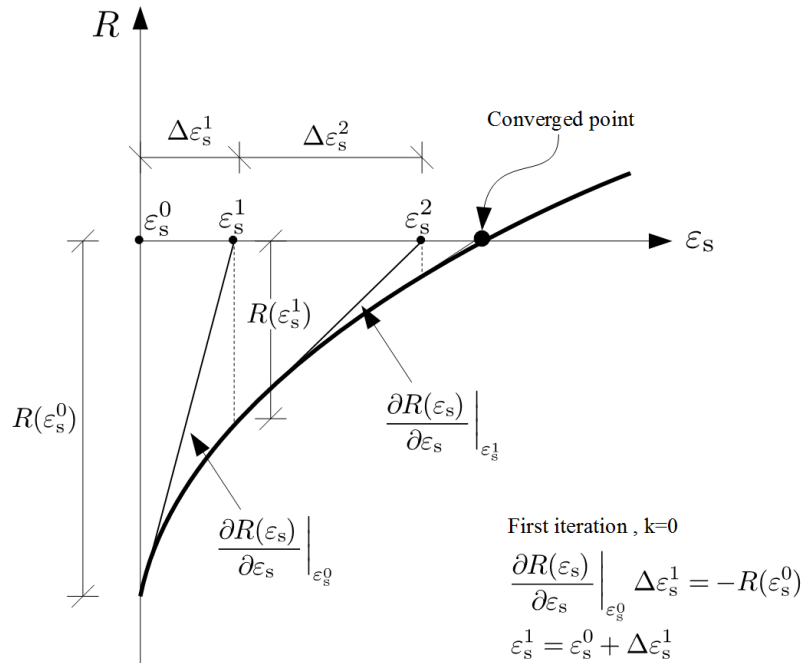


**Figure 3.5** Nonlinear time stepping procedure following the Newton algorithm.

### Example 3.4: Demonstration of the solution algorithm

As an exercise, use the script provided on the server to see how the solution works. The script discusses several types of responses represented by the three functions  $\sin u$ ,  $u^2$  and  $\sqrt{u}$ . They indicate the issues that must be addressed in the non-linear finite element solver implementation.

#### 3.5.1 Related questions

The models establish the basis for the consideration of further issues related to pull-out test and bond behavior.

- Plot a shape profile of a shear along the specimen at the maximum level of the pull-out force, how does it change during the loading
- How does a shape of a shear flow correspond with a bond law?
- How does the lateral pressure influence the bond behavior?
- What is the influence of lateral cracking?

---

## 4 Unloading and Reloading

**Outline:** In this chapter, we introduce two concepts of inelasticity: damage and plasticity. These fundamental phenomena can be experimentally observed and distinguished upon unloading. The amount of persisting deformation shows the amount of plastic deformation (slip or strain) and the amount of stiffness reduction can be regarded as damage. These concepts allow us to model path dependent material behavior with "memory" of what loading history has it gone through so far.

### Addressed questions:

- What happens in the bond structure upon unloading
- Which form of inelasticity can occur?
- Difference between plasticity and damage
- What is hardening, what is softening?
- How does the implementation of a material model for damage and plasticity work?

### 4.1 Experimental observation

To motivate a more general development of the model for the bond-slip behavior let us consider the case of non-monotonic loading. What happens in the material structure of the bond if the load is reduced and than it grows again? An experimental observation of the structural behavior is shown in Fig. 4.1 on an example of a double sided pullout test. The specimens had the form depicted in Fig. 2.4 and the embedded length was 300 mm. This test has been conducted with textile reinforced concrete specimens reinforced with carbon fabrics.

**Question:** Can the pullout model from Chapter 3 be used to describe such kind of behavior? Can you explain what bond stress – slip history experienced a material point within an interface? What was the loading history leading to this test result?

The answer is, that the bond-slip models presented so far only considered monotonically increasing load and cannot reproduce the real material behavior upon unloading. The constant-bond slip model from Sec 2.3 and the nonlinear model using the multilinear bond-slip law exemplified in Sec 3.2 did not consider any change of behavior upon unloading. To document this statement and to show how to introduce unloading and reloading into the interactive numerical models that we used in Sec 3.2 an example has been prepared showing how to introduce a more complex type of loading into the model.

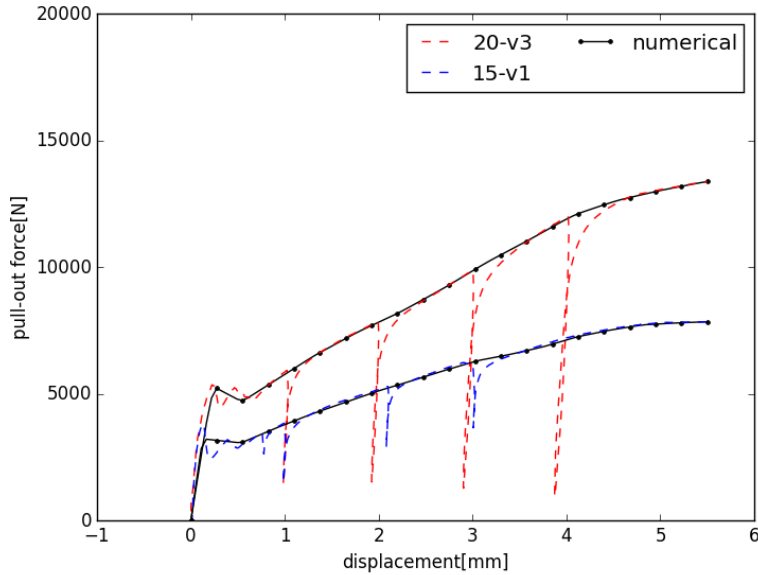


**Figure 4.1** Double-sided pullout test with several unloading and reloading steps

#### Example 4.1: What happens if a pullout with multilinear bond-slip law gets unloaded?

We will use the numerical examples to test the behavior interactively. The example is provided [here](#).

These solutions are limited to the monotonically increasing loading without the possibility to impose cyclic or even fatigue loading. To describe the exemplified behavior mathematically we need to introduce the irreversible phenomena of material behavior. In this lecture we will first classify the types of the bond slip and establish their relation to the microscopic structure of the bond layer constituting the material behavior considering a single material point of the interface. Different types of bond material structures lead to different types of material behavior. Cyclic loading can reveal the phenomenology of the bond we can make some conclusions about the quality of the bond: is it governed by adhesive reversible bond, or cohesive sliding or mechanical interaction between the ribs of the steel rebars and microcrack evolution within the concrete matrix?

## 4.2 Phenomenology of the bond behavior

Idealization  
of the  
material  
structure

Regarding a small segment of the bond interface with a nearly constant shear stress  $\tau$  and constant slip  $s$  let us try to describe the correspondence between the micro- and meso-scopic mechanisms that actually govern bond-slip relation  $\tau(s)$ . To classify the elementary mechanisms behind the observed of bond behavior, let us can idealize the material structure of the bond using two types of bindings:

- as a series of elastic springs that can break once they achieve their strength and
- as a series of asperities representing an unevenness or roughness of the surface area. Sliding of these surfaces is accompanied with a stress required to cross over the

asperities. During this process the asperities can deform elastically or get abraded. With this simple image of the material interface we can try to associate the structure of the bond layer with the basic types of inelastic material behavior, namely, damage and plasticity. In most cases both types of material behavior occur. The question is, how to distinguish them.

Considering the infinitesimal material point of the interface the damage type of behavior by a nonlinear shape of the stress-strain or (shear-slip) curve and by unloading to origin as shown in Fig. 4.2. This behavior can be reproduced by a series of springs within the considered material point representing a zone of the interface covered by elastic springs with scattered strength. The failure of a spring reduces the material stiffness. Since all the remaining springs are elastic, they unload all to the origin so that after unloading, the zero slip and zero stress gets recovered.

Damage

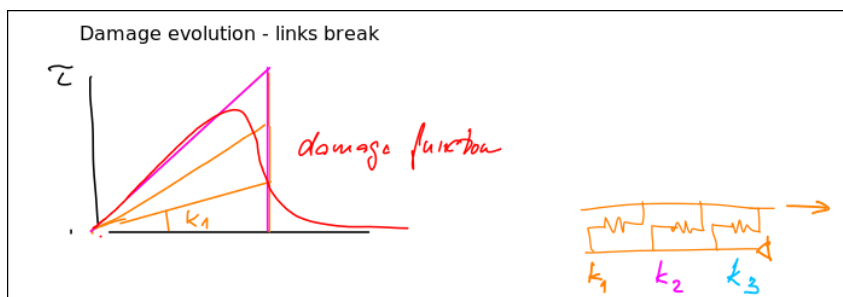


**Figure 4.2** Bond governed by damage

On the other hand, if a bond stress is transferred by asperities, we can distinguish two phases of response. Before the stress necessary to skip over an asperity has been reached, the slip is zero. At the onset of sliding over the asperities, the slip can increase at constant level of stress. Once the stress level is reduced, the slip does not change. Or putting it differently, the stress needed to induce sliding over the surface is constant. Once the sliding direction should be changed, also the sign of the shear stress must change. The described type of behavior is referred to as ideally plastic. This kind of material response is shown as the curve (2) in Fig. 4.3. If asperities can deform before reaching the onset of

Plasticity

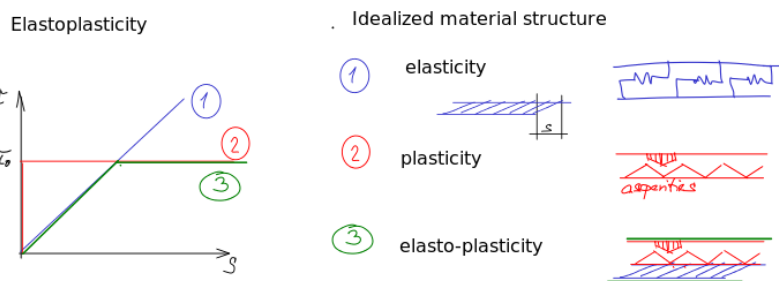


**Figure 4.3** Bond governed by plasticity/friction

sliding, an elastic deformation can be observed as indicated by the curve (3) in Fig. 4.3. Usually, both damage and plasticity encounter simultaneously in the material behavior. Both introduce energy dissipation. While damage is connected with the reduction of the material stiffness, plasticity leads to permanent deformation after unloading of the

structure. To understand the effect of damage and plasticity at the level of a material point, we will construct simple models that can be used within the BMCS interactive sheets to understand the two types of material behavior in detail.

### 4.3 Damage model

stress-slip  
relation

Instead of explicitly prescribing the bond slip law as a nonlinear curve let us prescribe a nonlinear curve governing the evolution of stiffness.

$$\tau = (1 - g(\kappa))E_b s \quad (4.1)$$

where  $g$  is the damage function and  $\kappa$  is the state variable that depends on slip as will be explained later on. The only difference with respect to the models used in Chapter 2 is that the bond slip model introduces the initial bond stiffness  $E_b$  and prescribes its reduction in terms of the damage function  $\omega = g\kappa$ . The values of damage at the beginning of loading with intact material structure is equal to 0, and for the fully damage material it takes the value 1. By rearranging the terms in Eq. (4.1) we can introduce the notion

effective  
stress

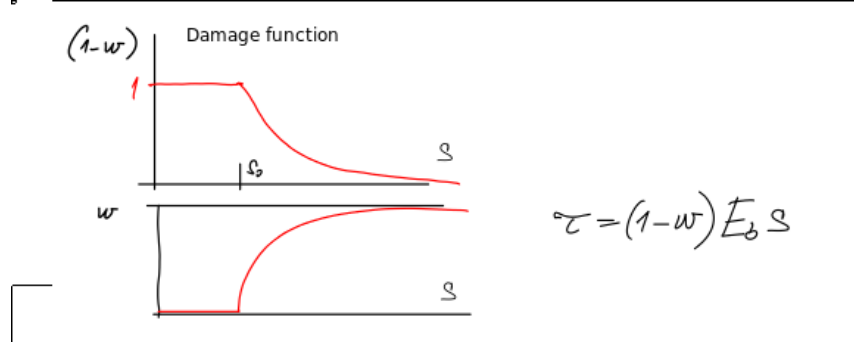


**Figure 4.4** Damage function governing the deterioration process

of effective stress as

$$\tilde{\tau} = \frac{\tau}{1 - \omega} = E_b s \quad (4.2)$$

Apparently, this effective stress  $\tilde{\tau} \geq \tau$ . It can be interpreted as the stress acting on the diminishing number of springs. We can regard the damage process as the reduction of the cross-sectional area due to the loading. The effective stress is related to the instantaneous, or still effective, cross section and not to the initial cross sectional area of the unit material zone.

Damage  
function

By specifying the limit values of the damage function,  $\omega \in (0, 1)$  the question remains, what shape does the damage function have between these two values? The answer to this question is not unique and depends on the particular type of material. In other words, it can only be determined using an experiment. Let us provide two examples of the damage function that will be used later on on examples.

### 4.3.1 Softening function [Jirasek]

$$\omega = g(\kappa) = 1 - \left[ \frac{s_0}{\kappa} \exp \left( -\frac{\kappa - s_0}{s_f - s_0} \right) \right] \quad (4.3)$$

where  $s_0, s_f$  are parameters controls the exponential damage function,  $s_0$  is controlling the elastic limit and  $s_f > s_0$  is another parameter controlling ductility.

### 4.3.2 Softening function [Abaqus]

The second example of the damage function taken from the finite-element program Abaqus has the form

$$\omega = g(\kappa) = 1 - \left( \frac{s_0}{\kappa} \right) \left[ 1 - \frac{1 - \exp(-\alpha(\frac{\kappa-s_0}{s_u-s_0}))}{1 - \exp(-\alpha)} \right] \quad (4.4)$$

where  $s_u$  is the slip at complete failure and  $\alpha$  is a parameter controls the exponential damage function.

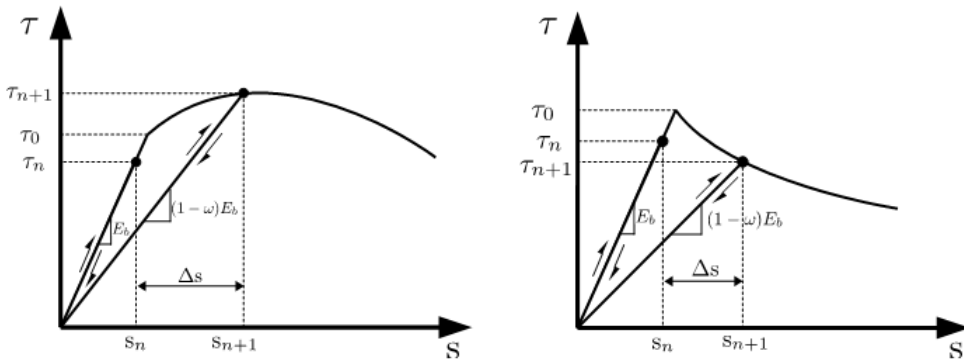


**Figure 4.5** Slip - bond stress curve of damage model; left : hardening, right: softening

### 4.3.3 Hardening function [Li]

The damage function is usually used to prescribe a material softening behavior. However, it can be adjusted rather flexibly to prescribe also hardening behavior. An of an analytical function is provided in the BMCS tool in terms of the function

$$\omega = g(\kappa) = \frac{\alpha_1}{1 + \exp(-\alpha_2 \kappa + 6)} \quad (4.5)$$

where  $\alpha_1, \alpha_2$  are parameters controls the exponential damage function.

However, the exemplified damage functions do not depend directly on the slip  $s$  but on a variable  $\kappa$ . This variable is defined as the maximum absolute value of slip achieved during the loading history, i.e.

$$\kappa = \max\{|s|\}. \quad (4.6)$$

This parameter actually introduces the "memory" of the material point and introduces the different response of the material upon loading, unloading and reloading.

The incremental time stepping used in the numerical simulation is sketched in Fig. 4.5. The transition between the linear elastic unloading response and the nonlinear growth of damage upon increased loading is completely controlled by the state variable  $\kappa$ . The damage is initiated when  $\kappa > s_0$ , where  $s_0 = \tau_0/E_b$  is the damage threshold slip. During the further simulation, damage can grow only if  $s > \kappa$ .

### Example 4.2: Bond behavior governed by damage

**Task:** Study the influence of the parameters of the damage functions on the response of a single material point.

```
In [4]: bs1.mats_eval.omega_fn.trait_set(s_f = 10, plot_max=0.05)
bs1.mats_eval.omega_fn
```

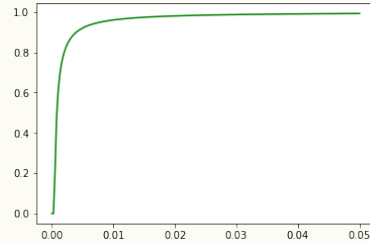
Out[4]: Damage function (Jirasek)

$$\omega = g(\kappa) = 1 - \left[ \frac{s_0}{\kappa} \exp\left(-\frac{\kappa - s_0}{s_f - s_0}\right) \right]$$

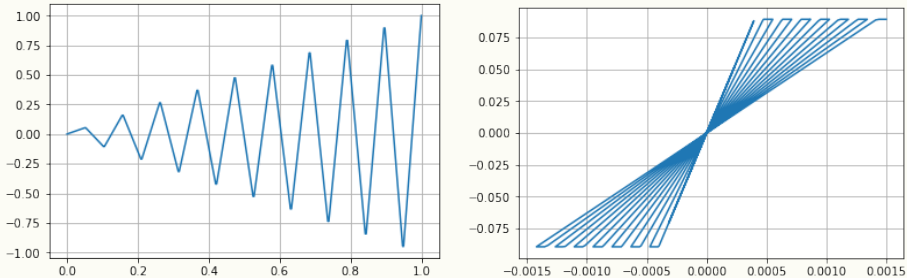
where  $\kappa$  is the state variable representing the maximum slip that occurred so far in the history of loading.

$s_f$   $s_f = 10.0$  [mm/mm] derivative of the damage function at the onset of damage

$s_0$   $s_0 = 0.0004$  [mm] elastic strain limit



Use the available damage functions to reproduce both softening and hardening behavior. An example of a loading scenarios and the corresponding shear-slip relation is shown below.



The other one applies slip in the range of  $-\hat{s}, \hat{s}$ . The interactive sheet that can be used to test this type of behavior is provided on the server.

## 4.4 Plasticity model

Considering the plastic behavior, the introduction of the material "memory" is slightly more complex. Instead of prescribing the reduction of the material stiffness, we split the deformation into two variables: the elastic slip  $s_e$  representing the reversible deformation, and the plastic slip  $s_p$  expressing the irreversible deformation that would persist after unloading. Let us note, that the development of the plastic slip  $s_p$  depends on the loading history. As a consequence, the variable  $s_p$  introduces a kind of material "memory" that

remembers the loading events and their levels that the material point experienced so far. This variable plays a similar role as the variable  $\kappa$  introduced for the damage model in Sec. 4.3

The total slip is defined as

$$s = s_e + s_p. \quad (4.7)$$

We can start to construct the bond-slip behavior by expressing the elastic behavior of the material  $\tau = E_b s_e$  as

$$\tau = E_b(s - s_p). \quad (4.8)$$

where  $\tau$  is the bond stress,  $E_b$  is the bond stiffness and  $s, s_p$  are the total slip and the plastic slip respectively. As a next step, we require that the bond stress yields once it achieves the prescribed level. This is done in terms of an inequality

$$f = |\tau - X| - h \leq 0 \quad (4.9)$$

imposing a yield limit on the value of shear stress  $\tau$ . This function defines the elastic range of the material response. Once this limit is reached, an inelastic yielding occurs. The symbols  $h$  and  $X$  introduce two different types of limit of the bond stress.

The variable  $h$  represents the so called isotropic limit relative to the zero stress. In other words, the limit stress is the same for the negative and positive stresses. It is defined as

$$h = \max\{0, (Kz + \tau_0)\} \quad (4.10)$$

where  $K$  is the isotropic hardening parameter,  $\tau_0$  is the yield stress.  $z$  represents the state variable of a material point. It is a part of the "memory" in addition to plastic slip  $s_p$ .

The variable  $X$  represents the kinematic limit. It is relative to the level of stress achieved during the history. A linear kinematic hardening behavior is defined as

$$X = \gamma \alpha \quad (4.11)$$

where  $\gamma$  is kinematic hardening parameter and  $\alpha$  is the kinematic hardening state variable that "memorizes" the effect of the loading history.

By defining the threshold or yield limit we specify the range of elastic behavior. As a next step we need to tell what happens once this limit has been reached and the loading still increases. The usual way to define the response in an inelastic regime is to introduce the flow rule governing the plastic deformation, i.e. plastic slip, as the derivative of the yield limit with respect to the stress  $\tau$

$$\dot{s}^p = \dot{\lambda} \frac{\partial f}{\partial \tau} = \dot{\lambda} \operatorname{sign}(\tau - X). \quad (4.12)$$

where  $\dot{\lambda}$  is an unknown scalar multiplier. In this way, we have defined the direction of flow but not its magnitude that is represented by  $\dot{\lambda}$ . The flow rules for the remaining state

variables  $z$  and  $\alpha$  are defined in the same way, i.e. by differentiating the yield limit with respect to the corresponding (conjugate) stress, i.e.  $h$  and  $X$

$$\text{Isotropic hardening} \quad \dot{z} = \dot{\lambda} \quad (4.13)$$

$$\text{Kinematic hardening} \quad \dot{\alpha} = \dot{\lambda} \operatorname{sign}(\tau - X). \quad (4.14)$$

Having expressed the evolution of the state variables in terms of a single scalar parameter  $\dot{\lambda}$  we need to find another criterion to get its value. This criterion is derived from the fact, that upon loading beyond the elastic limit, the state of a material point must stay on the yield surface. The only way how this can be accomplished is that the yield surface changes during the yielding process. Let the change of the yield limit is expressed as  $\dot{f}$ , representing the derivative with respect to a control parameter of the loading.

Then, two conditions can be imposed in an inelastic regime.

- The first is the requirement that the stress state does not exceed the yield limit, i.e.

$$\dot{\lambda} \geq 0, \quad f \leq 0, \quad \dot{\lambda} f = 0 \quad (4.15)$$

This form is the so called Kuhn-Tucker condition (loading-unloading condition). It says that the plastic multiplier  $\dot{\lambda}$  must be zero in elastic regime and it grow only if the yield limit has been reached.

- Second, we require that the derivative of the yield limit stays also zero

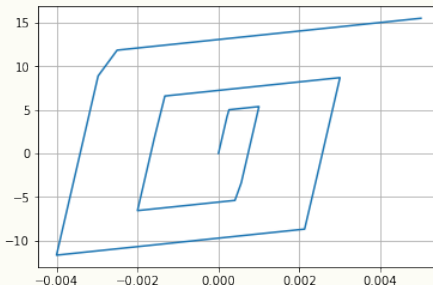
$$\dot{\lambda} \geq 0, \implies f = 0, \implies \dot{f} = 0 \quad (4.16)$$

which means that the inelastic variables can only grow if the stress stays on the yield limit. Thus, during the yielding, the yield limit can grow or shrink.

This fact is closely related to the phenomena of hardening and softening discussed in the previous lectures. Closer look at the considered yield limit given in (4.9) reveals that the material parameters  $K$  and  $\gamma$  define the rate of expansion or shrinkage of the elastic domain. Negative values of  $K$  and  $\gamma$  introduce a linear softening behavior. The condition (4.9) represents the equation that delivers the value of the plastic multiplier  $\dot{\lambda}$  to deliver the amount of yielding corresponding to the current load.

### Example 4.3: Bond behavior governed by plasticity

The example presents a plastic material model with isotropic and kinematic hardening. Two loading scenarios are shown, one for increasing amplitude and unloading to zero slip.



The other one applies slip in the range of  $-\hat{s}, \hat{s}$ . The interactive sheet that can be used to

test this type of behavior is provided on the server

Thus, to solve for  $\dot{\lambda}$  the derivative of the yield surface needs to be expressed using the previously introduced equations

$$\begin{aligned}
 \dot{f} &= \frac{\partial f}{\partial \tau} \dot{\tau} + \frac{\partial f}{\partial z} \dot{z} + \frac{\partial f}{\partial \alpha} \dot{\alpha} \\
 &= \frac{\partial f}{\partial \tau} E_b (\dot{s} - \dot{s}_p) + \dots \text{complete} \\
 &= \text{sign}(\tau - X) E_b ((\dot{s} - \dot{s}_p) + \dots \text{complete}) \\
 &= \text{sign}(\tau - X) E_b (\dot{s} - \dot{\lambda} \text{sign}(\tau - X)) + \dots \text{complete} \\
 &= \text{sign}(\tau - X) E_b \dot{s} - \text{sign}(\tau - X) \text{sign}(\tau - X) E_b \dot{\lambda} + \dots \text{complete} \\
 &= \text{sign}(\tau - X) E_b \dot{s} - E_b \dot{\lambda} + \dots \text{complete} \\
 &= 0
 \end{aligned} \tag{4.17}$$

As a result the plastic multiplier for the current step can be expressed as

$$\dot{\lambda} = \text{sign}(\tau - X) \dot{s} + \dots \text{complete} \tag{4.18}$$

The resolved multiplier can than be substituted back into the evolution equations (4.12), (4.13) and (4.14) to obtain the explicit first-order differential equations

$$\dot{s}^p = \text{sign}(\tau - X) \text{sign}(\tau - X) \dot{s} = \dot{s} \tag{4.19}$$

$$\dot{z} = \text{sign}(\tau - X) \dot{s} \tag{4.20}$$

$$\dot{\alpha} = \text{sign}(\tau - X) \text{sign}(\tau - X) \dot{s} = \dot{s} \tag{4.21}$$

Note that isotropic hardening grows regardless of the sign of the total slip rate. It's sign gets canceled by the term  $\text{sign}(\tau - X)$  which is the same as the of  $\dot{s}$ . On the other hand, the plastic slip and kinematic hardening grow consistently with the direction of the total (control) slip.

The described derivation delivers the differential evolution equations that are continuous. To solve them for a particular problem at hand, an integration scheme to derive a time-stepping algorithm must be applied. The standard procedure applied in the nonlinear material models for finite-element simulations applies the return mapping algorithm sketched in the next section.

## 4.5 Return mapping algorithm

The algorithmic treatment of plasticity requires the incremental formulation of the evolution equations. To provide a robust implementation, we need to make the distinction between an elastic and plastic state of the material. If the material is a plastic state, than the consistency condition is used to return back to the yield limit as shown in Fig. 4.7.

input date :  $s_n, \Delta_s, \tau_n, s_n^p, \alpha_n, z_n$   
 output date :  $\tau_{n+1}, s_{n+1}^p, \alpha_{n+1}, z_{n+1}$   
 constant material parameters:  $E_b, \tau_0, K, \gamma$

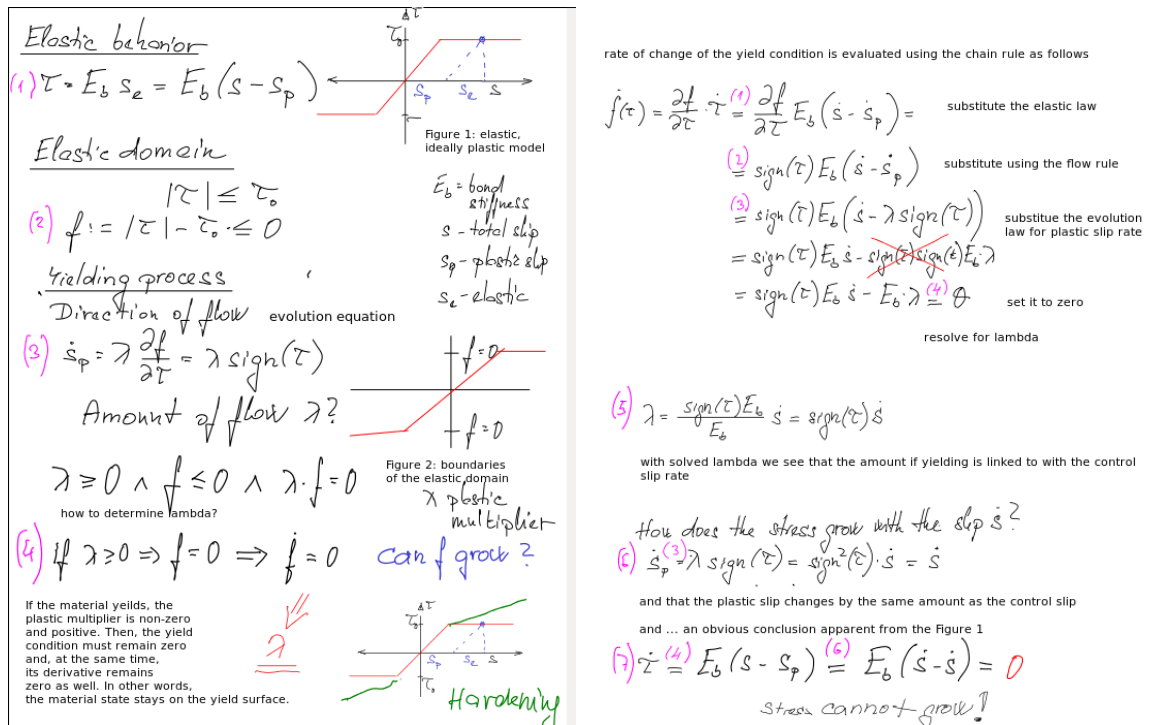


Figure 4.6 What happens beyond elastic domain? Example of elastic-ideally plastic bond.

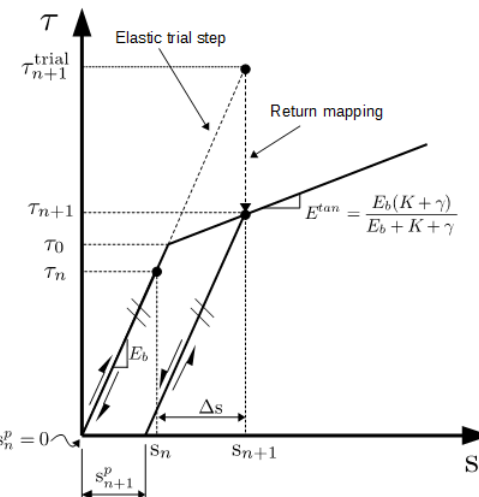


Figure 4.7 Return mapping of the plasticity model

$$s_{n+1} = s_n + \Delta_s$$

$$\tau_{n+1}^{trial} = E_b(s_{n+1} - s_n^p)$$

$$X_n = \gamma \alpha_n$$

$$h = \max\{0, (Kz_n + \tau_0)\}$$

$$f_{n+1}^{trial} = |\tau_{n+1}^{trial} - X_n| - h$$

If  $f_{n+1}^{trial} \leq 0 \rightarrow$  Elastic step

$$\tau_{n+1} = \tau_{n+1}^{trial}$$

$$(\cdot)_{n+1} = (\cdot)_n$$

with  $(.)$  denote the state variables  $(s^p, \alpha, z)$

Else  $\longrightarrow$  Plastic step: perform return mapping

$$\begin{aligned}\Delta\lambda &= \frac{f_{n+1}^{trial}}{E_b + |K| + \gamma} \\ s_{n+1}^p &= s_n^p + \Delta\lambda \operatorname{sign}(\tau_{n+1}^{trial} - X_n) \\ z_{n+1} &= z_n + \Delta\lambda \\ \alpha_{n+1} &= \alpha_n + \Delta\lambda \operatorname{sign}(\tau_{n+1}^{trial} - X_n) \\ \tau_{n+1} &= \tau_{n+1}^{trial} - E_b \Delta\lambda \operatorname{sign}(\tau_{n+1}^{trial} - X_n)\end{aligned}$$

## 4.6 Damage-Plasticity model

This section summarizes the contents of the two previous sections within a single model covering both damage and plasticity. Such type of models is implemented in the nonlinear finite element packages and is used for the simulation of concrete behavior.

- Stress-slip relation

$$\tau = (1 - \omega)E_b(s - s^p) \quad (4.22)$$

where  $\omega$  is the damage parameter

- The effective stress

$$\tilde{\tau} = \frac{\tau}{1 - \omega} = E_b(s - s^p) \quad (4.23)$$

- Plastic yield function

$$f = |\tilde{\tau} - X| - h \quad (4.24)$$

where

$$h = \max\{0, (Kz + \tau_0)\} \quad (4.25)$$

- Damage function

for example using the following damage function:

$$\omega = g(\kappa) = \frac{\alpha_1}{1 + \exp(-\alpha_2 \kappa + 6)} \quad (4.26)$$

where  $\alpha_1, \alpha_2$  are parameters control the exponential damage function, and  $\kappa$  is the history parameter which defines the maximum absolute value of the slip during the loading history and can be written as follows

$$\kappa = \max\{|s|\} \quad (4.27)$$

- Damage threshold

The damage is active when  $\kappa > s_0$ , where  $s_0 = \tau_0/E_b$  is the damage threshold slip

- **Flow rule**

$$\dot{s}^p = \dot{\lambda} \operatorname{sign}(\tilde{\tau} - X) \quad (4.28)$$

where  $\dot{\lambda}$  is the incremental multiplier.

- **Hardening rules**

$$\text{Isotropic hardening} \quad \dot{z} = \dot{\lambda} \quad (4.29)$$

$$\text{Kinematic hardening} \quad \dot{\alpha} = \dot{\lambda} \operatorname{sign}(\tilde{\tau} - X) \quad (4.30)$$

with

$$X = \gamma \alpha \quad (4.31)$$

where  $\gamma$  is kinematic hardening parameter.

- **Kuhn-Tucker condition (loading-unloading condition)**

$$\dot{\lambda} \geq 0, \quad f \leq 0, \quad \dot{\lambda} f = 0 \quad (4.32)$$

- **Consistency condition)**

$$\dot{\lambda} \geq 0, \rightarrow f = 0, \rightarrow \dot{f} = 0 \quad (4.33)$$

- **Return mapping algorithm**

input date :  $s_n, \Delta_s, \tau_n, \omega_n, \kappa_n, s_n^p, \alpha_n, z_n$

output date :  $\tau_{n+1}, \omega_{n+1}, \kappa_{n+1}, s_{n+1}^p, \alpha_{n+1}, z_{n+1}$

constant material parameters:  $E_b, \tau_0, K, \gamma, \beta, s_0, s_f$

$$s_{n+1} = s_n + \Delta_s$$

### Damage

If  $s_{n+1} \leq s_0 \rightarrow$  No damage

$$\omega_{n+1} = 0$$

Else  $\rightarrow$  Damage is active

$$\kappa_{n+1} = \max(|s_{n+1}|, \kappa_n)$$

$$\omega_{n+1} = g(\kappa) = \frac{\alpha_1}{1 + \exp(-\alpha_2 \kappa_{n+1} + 6)}$$

### Plasticity

$$\tilde{\tau}_{n+1}^{trial} = E_b(s_{n+1} - s_n^p)$$

$$X_n = \gamma \alpha_n$$

$$h = \max\{0, (Kz_n + \tau_0)\}$$

$$f_{n+1}^{trial} = |\tilde{\tau}_{n+1}^{trial} - X_n| - h$$

If  $f_{n+1}^{trial} \leq 0 \longrightarrow$  Elastic step

$$\tilde{\tau}_{n+1} = \tilde{\tau}_{n+1}^{trial}$$

$$\tau_{n+1} = (1 - \omega_{n+1})\tilde{\tau}_{n+1}$$

$$(.)_{n+1} = (.)_n$$

with  $(.)$  denote the state variables  $(s^p, \alpha, z)$

Else  $\longrightarrow$  Plastic step: perform return mapping

$$\Delta\lambda = \frac{f_{n+1}^{trial}}{E_b + |K| + \gamma}$$

$$s_{n+1}^p = s_n^p + \Delta\lambda \operatorname{sign}(\tau_{n+1}^{trial} - X_n)$$

$$z_{n+1} = z_n + \Delta\lambda$$

$$\alpha_{n+1} = \alpha_n + \Delta\lambda \operatorname{sign}(\tau_{n+1}^{trial} - X_n)$$

$$\tau_{n+1} = (1 - \omega_{n+1})E_b(s_{n+1} - s_{n+1}^p)$$

## 5 Inelastic analysis of pull-out response

### 5.1 Pullout governed by plasticity

#### Example 5.1: Pullout response simulated using plastic material model

This example shows the elementary difference between the pullout behavior modeled using perfect plasticity, isotropic hardening plasticity and kinematic hardening plasticity. The executable notebook is provided [here](#)

#### Questions and tasks:

- Is it possible to model the same type of behavior using kinematic and isotropic hardening? Plot the response of a pullout test assuming cyclic loading with increasing amplitude of the control displacement centered at  $w = 0$ .
- Can the hardening be negative? Try to simulate such a problem by modifying the example above. How does the bond-slip law then look like?

### 5.2 Pullout governed by damage

To relate the modeling to a particular example, let us reproduce the experimental results published in [dai\_development\_2005].

#### Example 5.2: Pullout simulated using damage model

This example shows the pullout behavior for a model based on damage. The damage function has been derived based on the paper [dai\_development\_2005] has been reproduced and allows us to monitor the damage process in during the debonding of FRP sheet from concrete.

#### Questions and tasks:

- How does the pullout response change with an increasing embedded length?
- How does this pullout test unload?

This model has been applied to reproduce the debonding behavior of FRP sheets used for strengthening of concrete structures [dai\_development\_2005]. The bond slip law for the studied interface between FRP and concrete has been assumed in the form

$$\tau(s) = 2BG_F [\exp(-Bs) - \exp(-2Bs)] \quad (5.1)$$

Such prescription can be used to describe the debonding only if the slip monotonically increases in all points along the embedded length. No unloading is allowed. Let us now set this model into the framework of damage material model of the form

$$\tau(s) = (1 - \omega(\kappa))E_b s \quad (5.2)$$

where  $\kappa = \max_t(s(t))$  represents the maximum absolute value of slip achieved during the loading history and  $E_b$  is the initial stiffness of the bond. This stiffness must be equal to the derivative of the bond-slip law given in (5.1), i.e.

$$E_b = \left. \frac{d\tau}{ds} \right|_{s=0} = 2B^2G_F [2\exp(-2Bs) - \exp(-Bs)] \Big|_{s=0} = 2B^2G_F \quad (5.3)$$

Considering a monotonic loading with  $\kappa = s$ , we can require an equivalence of the explicit and of the damage-based bond-slip relations:

$$(1 - \omega(\kappa))E_b s = 2BG_F[\exp(-Bs) - \exp(-2Bs)] \quad (5.4)$$

so that after substituting for  $E_b$  using (5.3) and solving for  $\omega$ , the damage function reproducing the bond-slip law (5.1) reads

$$\omega(s) = 1 - \frac{\exp(-2Bs) - \exp(-Bs)}{Bs} \quad (5.5)$$

In this form, the assumed bond-slip law can be used within a general, nonlinear finite-element solver providing the possibility of unloading and reloading.

**Remark** The interpretation of the material parameter  $G_F$  can be provided as follows: Realizing that the integral of the bond-slip law given in (5.1) is equal to  $G_F$  we recover the physical meaning of fracture energy as the energy needed to produce a stress-free crack of a unit area. This reveals the original idea motivating the construction of this bond-slip law with softening. In fact, the shape of the bond-slip law is a matter of choice and of calibration using the test results. The parameter  $B$  has the unit 1/mm and it scales the bond-slip law and the damage function along the slip domain.

Note that in the case at hand, the damage starts from the very beginning, i.e. the model has no elastic behavior with perfectly linear material response.

This kind of softening model represents a category of fracture-based models possessing the property that the material deterioration localizes into crack. With the chosen bond-slip law, we can view the propagation of the stress-free zone along the embedded length as a propagation of a shear crack. In Chapter 6 this concept will be revisited for the case of a tensile crack propagating through the beam cross-section.

---

## **Part II**

# **Cracking**

---

## 6 Softening and fracture

**Outline** We now include energy as a measure of stored and lost energy within a system into play. We also notice that if the material damage localizes due to softening behavior we observe an energy dissipation in a small volume of material while the whole domain/structure remains elastic. This observation brings to the idea to characterize the deterioration process of the structure by the means of energy release rate.

### Addressed questions

- What is the consequence of the softening material behavior on the damage distribution within a structure?
- How can we numerically express the fact that the stress state in the localization zone remains unchanged during its "travel" through the structure?
- How to evaluate the stored and released energy from the load-displacement diagram of a test?

### 6.1 Is energy dissipation an objective material property?

Up to now, we have described the inelastic material behavior from the perspective of a material point representing a small volume of a continuum. In fact, we considered only a one-dimensional continuum represented by the interface between the two material components. We focused on a point on this interface and followed the stress and strain evolution at this point. The strain at the point was represented by the slip  $s$  and the stress by the bond stress flow  $\tau$ . Our goal was to describe the relation between

Material model as a material point with memory

$$\tau(s; \boldsymbol{\theta}),$$

i.e. between shear stress  $\tau$ , slip  $s$  and state variables  $\boldsymbol{\theta}$ . With state variables  $\boldsymbol{\theta}$ , exemplified by damage, plastic slip, kinematic or isotropic hardening, we introduced a kind of material point *memory*. Recall that in case of an explicitly prescribed *memoryless* bond-slip law

$$\tau(s),$$

as it was introduced in Chapter 3 there was no material memory and no path dependency. For more complex types of material behavior, exemplified by plasticity or damage, the memory in form of state variables has been introduced to allow for complex loading scenarios with unloading and reloading.

In this chapter we focus on the material behavior exhibiting softening. This means that the bond slip relation contains a descending branch as was the case e.g. in Example 3.3. Such type of material behavior leads to a stress concentration within a small volume of material. This volume is called a process zone. In case of debonding, we can observe

Softening, stress concentration, discontinuity

a propagation of the process zone throughout the embedded length for increasing load. The debonding with a distinguished, propagating process zone can be observed in the Example 5.2 simulating the pullout behavior of a CFRP sheets from the concrete matrix using a damage-based softening model. Behind the process zone, a distinguished displacement discontinuity develops. Moreover, if the stress transfer across the newly emerged discontinuity is small, we can regard it as a crack. In the pullout problem, this crack occurs in form of a slip line that us usually referred to as a shear crack or mode II crack.

Process zone	In this case, the structural behavior can be directly related to the characteristics of the process zone. Then, the structural response can be described in an alternative way to the approaches described so far in chapters 3 and 6. Instead of regarding the local stress-strain response at every material point of the structure we can focus on the description of the small, inelastic process zone in an intermediate state of its propagation through the structure. Then, we calculate its impact on the surrounding structure where no inelastic effects occur. This can be done if the size of the process zone is small compared to the size of the structure.
Energy dissipation	The characterization of the process zone includes particularly its size and the energy dissipation associated with its propagation through the structure. Instead of defining the material behavior in terms of the stress-strain relation, we postulate that the size of the process zone and rate of energy dissipated within it remains constant during its propagation through the structure. Thus, we regard it as a material property associated with particular material, objectively characterizing its localization process of damage into a material discontinuity, i.e. crack. As already emphasized, this kind of description is only possible for materials exhibiting strain-softening that are denoted as brittle or quasi-brittle. Examples of such materials include concrete, fiber-reinforced concrete and ceramics.
Introductory example	We will start the explanation by revisiting the example of the pullout test with a damage function that introduces softening. In particular, we will describe the debonding of FRP sheet from the concrete matrix observed in the test and evaluate the amount of work supplied to the structure by the imposed loading.
Correspondence between fracture and damage	Our goal is to prepare the platform for the general explanation of the correspondence between the theoretical concepts of fracture mechanics, i.e. the energetic characterization of the material disintegration, and between the strain-softening types of models used in the finite element simulation of brittle materials exhibiting cracking.

## 6.2 Energetic interpretation of the nonlinear structural response

### 6.3 General formula for energy supply

Work of external force	Assume a tensile specimen with the total energy supply given as an integral of the load over the displacement variable $u$
------------------------	--

$$W = \int P(u) \, du \tag{6.1}$$

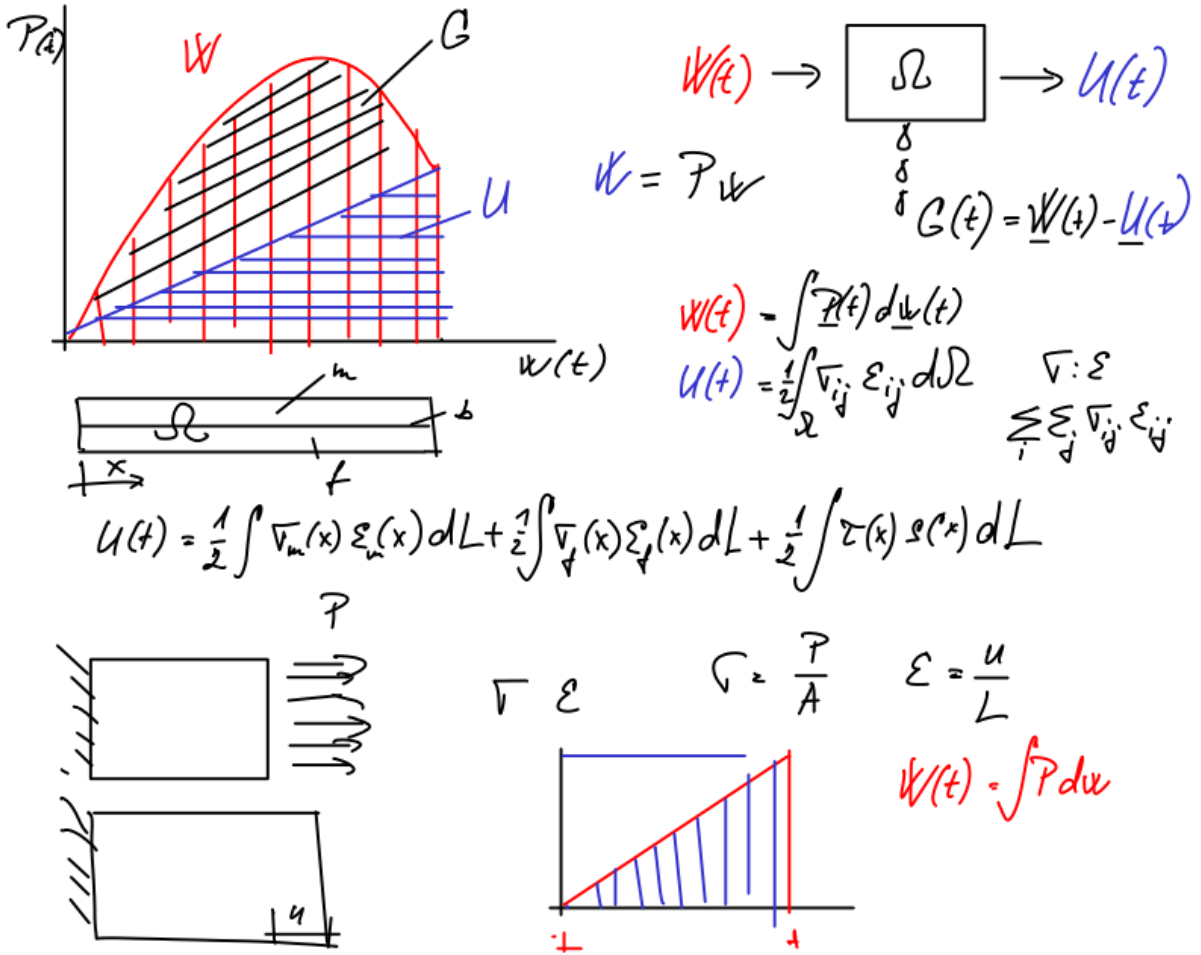


**Figure 6.1** Energy bilance for the pullout with constant bond-slip law

Assuming linear elastic material behavior we can employ the equilibrium condition and kinematic relation to link the load directly to the control displacement  $u$  as

$$P = A\sigma = AE\varepsilon = AE\frac{1}{L}u, \quad (6.2)$$

where  $E$  denotes the Young's modulus,  $\sigma$  the stresses,  $A$  the cross-sectional area and  $\varepsilon$  the strain. Then the total energy supply reads

$$W = \frac{1}{L}AE \int u \, du = \frac{1}{2L}AEu^2 = \frac{1}{2}Pu \quad (6.3)$$

The stored energy is represented by the area below the unloading branch integrated over the whole volume of the structure. In case of the tensile specimen with uniform profile of stress and strain, the integral reduces to

$$\mathcal{U} = \frac{1}{2} \int_{\Omega} \sigma \varepsilon \, dx = \frac{1}{2} AL\sigma\varepsilon = \frac{1}{2}Pu \quad (6.4)$$

By evaluating the difference between supplied and stored energy, we obtain the obvious result

$$G = W - \mathcal{U} = 0 \quad (6.5)$$

Stored elastic energy

rephrasing the fact that the supplied energy is stored in the specimen without any loss.

In case of a pullout test, the work supply remains unchanged. It can be evaluated using Eq. 6.1. The stress distribution is not uniform anymore so that we need to evaluate the integral explicitly. In cases considered so far we assumed linear elastic behavior of the matrix and of the reinforcement. Thus, the integral over the volume of the specimen can be decomposed into

$$\mathcal{U} = \frac{1}{2} \int_{\Omega_m} \sigma_m(x) \varepsilon_m^{el}(x) dx + \frac{1}{2} \int_{\Omega_f} \sigma_f^{el}(x) \varepsilon_f(x) dx + \frac{1}{2} \int_{\Omega_{mf}} \tau_{mf}(x) s_{mf}^{el}(x) dx \quad (6.6)$$

This equation is valid for any kind of material behavior in the bond zone (damage or plasticity), (softening or hardenign). Its evaluation may be regarded as counting of intact, undamaged material links/spring in every single material point along the bond zone. The elastic springs of the matrix remain undamaged by assumption. The bond between the material components may release energy depending on the material behavior that we assume. However, if we can solve the boundary value problem numerically as we did in the previous Chapters assuming damage or plasticity of the bond interface, we can use Eq. 6.6 to evaluate the stored energy and, thus, the overall energy dissipation in the pullout problem.

To explain the concept in simple terms, let us return back to the example of the analytically solved pullout problem given Chapter 2 with the interface governed by a constant, frictional behavior:

### Example 6.1: Energy dissipation in a pullout test with constant bond

The analytical formula of work supply, stored energy and energy dissipation has been derived in Sec. 2 for a rigid matrix and constant level of bond stress. Using the analytical solution we have all state variable needed to evaluate the stored energy available.

**Task:** Consider the pullout state with a fixed value  $w$

**Question:** What the is amount of energy stored in the pullout specimen at a given control pullout displacement:

- assuming that the bar has infinite stiffness
- assuming that the bar has a finite stiffness  $E$  and area  $A$ ?

**Question:** Which amount of energy dissipated in the state  $w$  is larger?

- the one with a bar of infinite stiffness?
- the one with bar of an finite stiffness  $A$ ?

Use the example notebook to confirm your answers to the the questions.

## 7 Cohesive zone, softening, energy dissipation

The notion of energy dissipation, localization and fracture process zone is useful for two purposes:

- regularization of the finite element computation
- size effect on the structural response

In the former case, energy dissipation rate is used as a material parameter to remove mesh dependency from the numerical calculation. The latter case represents an important phenomenon that has to be accounted for in the safety assessment of structures. Let us demonstrate the effect of strain softening on the results of the finite element calculation.

### 7.1 Sensitivity of strain-softening models with respect to size of the localization zone

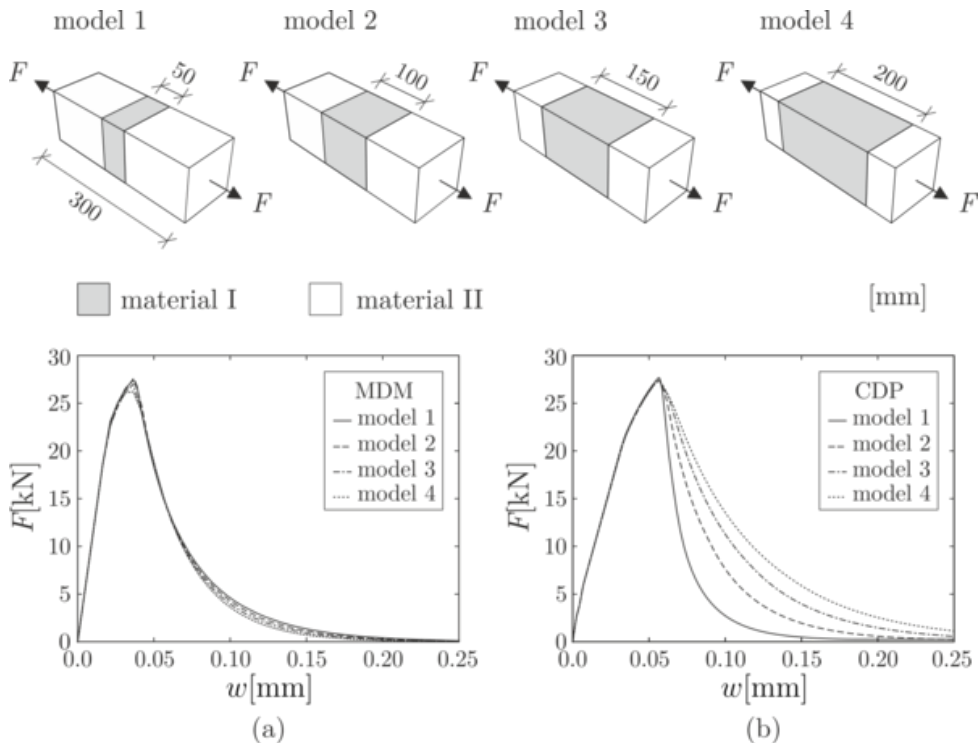


**Figure 7.1** Finite-element computation of a tensile test with a softening zone

The example in Fig. 7.1 shows the calculated response of a tensile test using finite element method with three different sizes of the middle section exhibiting a lower strength than the outer regions.

The structural response calculated with two different models is shown in terms of the tensile force versus the control displacement. The bottom-right diagram shows the different curves obtained using the damage-plasticity model in Abaqus.

The sensitivity of the softening branch with respect to the size of the softening volume can be explained using elementary analysis of a tensile test with a cohesive zone. The basis for this analysis can be provided using the cohesive crack model.

$$\sigma = E\varepsilon_{\text{el}} \quad (7.1)$$

and the softening law

$$\sigma = f(w) \quad (7.2)$$

defining the decay of stress with an increasing crack opening. In the considered case of the tensile test, the stress level in a series of two springs representing the bulk material and the cohesive crack is constant so that we exploit the equilibrium condition to relate the elastic strain to the softening function as

$$\sigma = \text{constant.} \implies f(w) = E\varepsilon_{\text{el}} \implies \varepsilon_{\text{el}} = \frac{f(w)}{E} \quad (7.3)$$

The control displacement  $u$  is given as a sum of the elastic elongation  $\varepsilon_{\text{el}}L$  and the crack opening  $w$

$$u = \varepsilon_{\text{el}}L + w = L\frac{f(w)}{E} + w \quad (7.4)$$

Evidently, the load-elongation curve in tensile test under monotonic extension is completely determined by  $L$ ,  $E$  and  $f(w)$ . Finally, we obtain the effective strain of the tensile test in the softening regime using the kinematic condition and substituting the terms above as

$$\varepsilon(w) = \frac{u}{L} = \varepsilon_{\text{el}} + \frac{w}{L} = \frac{1}{E}\sigma + \frac{w}{L} = \frac{1}{E}f(w) + \frac{w}{L} \quad (7.5)$$

so that we can calculate the global strain for monotonically increasing crack opening. The corresponding value of stress is given by the softening law

$$\sigma(w) = f(w) \quad (7.6)$$

For  $L \rightarrow \infty$  we get  $\frac{w}{L} \rightarrow 0$  then  $\varepsilon(w) = \frac{1}{E}\sigma(w)$  this means that for arbitrary value of crack opening, the quasi-static unloading is only possible by following the linear-elastic branch back to the origin. strain and stress remains linear even upon unloading.

## 7.2 Softening function accounting for fracture energy

To explain the role of energy dissipation in the numerical calculation let us introduce a softening containing the fracture energy as its parameter. The shape of the softening function is assumed in exponential form scaled by two parameters  $c_1$  and  $c_2$

$$\sigma = c_1 \exp(-c_2 w). \quad (7.7)$$

The parameter  $c_1$  can be set equal to the tensile strength  $f_t$  accounting for the fact that softening starts at the level of the material strength

$$\sigma(0) = f_t \implies c_1 = f_t. \quad (7.8)$$

The parameter  $c_2$  is obtained by requiring that the energy dissipated by a unit surface area of a crack equals the fracture energy

$$\begin{aligned} G_F &= \int_0^\infty \sigma(w) dw = \int_0^\infty c_1 \exp(-c_2 w) dw = f_t \left[ -\frac{1}{c_2} \exp(-c_2 w) \right]_0^\infty \\ &= \frac{f_t}{c_2} \implies c_2 = \frac{f_t}{G_F}. \end{aligned} \quad (7.9)$$

With these two parameters the softening function has the form

$$\sigma = f(w) = f_t \exp\left(-\frac{f_t}{G_F}w\right). \quad (7.10)$$

This kind of definition is particularly suitable for explaining the relation between the softening law of a crack surface accounting for the dissipated fracture energy and the energy dissipation due to localized damage in the finite element computations.

### 7.3 Energy dissipation for strain softening

To quantify the energy dissipation at a particular value of crack opening we need to evaluate the energy supply and the energy still stored in the specimen during the softening process:

**Work energy supply** To evaluate the total energy supplied into the tensile specimen we can consider the influx of energy separately for the elastic bulk material and for the softening cross section where the crack develops

$$W = W_{\text{el}} + W_{\text{cr}} \quad (7.11)$$

The elongation of the elastic part of the specimen is given as

$$u_{\text{el}} = \varepsilon_{\text{el}} L = \frac{\sigma}{E} L \quad (7.12)$$

with the work supply equal to that given previously in Eq. (6.3)

$$W_{\text{el}} = \frac{1}{2} A \sigma u_{\text{el}} = \frac{1}{2E} A L \sigma^2 = \frac{1}{2E} A L f^2(w) \quad (7.13)$$

The work within the softening cross section is performed on the crack-opening displacement

$$W_{\text{cr}} = A \int \sigma dw = A \int f(w) dw \quad (7.14)$$

So that the sum reads

$$W = \frac{1}{2E} A L f^2(w) + A \int f(w) dw. \quad (7.15)$$

**Stored energy:** The specimen can be regarded as a series of springs: one for the elastic bulk material and one for the cohesive crack. The volume integral over the two different parts of the specimen can be again split into the elastic unloading and into the softening parts.

$$\mathcal{U} = \frac{1}{2} \int_{\Omega} \sigma \varepsilon(x) d\Omega = \frac{1}{2} A \int_{\Omega_{el}} \sigma \varepsilon_{el} dx + \frac{1}{2} A \sigma w = \frac{1}{2} A (L \sigma \varepsilon_{el} + \sigma w). \quad (7.16)$$

Recalling that during the unloading branch we can set

$$\varepsilon = \frac{1}{E} f(w). \quad (7.17)$$

we obtain

$$\mathcal{U} = \frac{1}{2} A \left( \frac{L}{E} f^2(w) + f(w)w \right) = \frac{1}{2E} AL f^2(w) + \frac{1}{2} A f(w)w. \quad (7.18)$$

The total energy released at the crack opening

$$G = W - \mathcal{U} \quad (7.19)$$

thus reads

$$\begin{aligned} G &= \frac{1}{2E} AL \left( f^2(w) - f^2(0) \right) + A \left( \int f(w) dw - \frac{1}{2} f(w)w \right) \\ &= A \left( \int f(w) dw - \frac{1}{2} f(w)w \right). \end{aligned} \quad (7.20)$$

For  $w \rightarrow \infty$  we realize that  $f(w) \rightarrow 0$  so that the second term will vanish for large crack opening. As a consequence, we can conclude that the total value of fracture energy  $G_F$  required to make the crack stress-free is

$$G = A \int f(w) dw = AG_F. \quad (7.21)$$

This is the expected result rephrasing that  $G_F$  represents the energy dissipated through a unit area of a stress-free crack face.

**Remark:** In the above evaluation of fracture energy, the work supply into the elastic part of the specimen and the amount of stored energy cancel. Therefore, evaluation of the dissipated energy can be limited to the volume of the softening spring. Thus, the dissipated energy owing to cracking can be evaluated locally, ignoring the elastic part of the specimen. This observation is useful for further elaboration on the size of the localization zone characteristic for the particular concrete mixtures.

### Example 7.1: Tensile behavior of a specimen with a softening zone

Consider a chain of springs with softening behavior. The spring chain can be regarded as the simplest possible discretization of a tensile specimen of a length  $L$ . Test the force-displacement response for varying length of the specimen using the script [length dependence](#).

### Questions

- How does the tensile test response change with varying specimen length?
- How does the tensile test response change with the change of the softening zone length  $L_s$ ?
- How does the tensile test response change if the fracture energy is very large/very low?
- Is snap-back a physical property?
- Can the snap-back be measured experimentally?

## 7.4 Correspondence between softening and damage functions

To embed the concept of the controlled energy dissipation within a finite element calculation we establish a link between the softening law and the damage function. Indeed, by deriving the damage function from the softening law, we obtain an implicitly regularized strain-softening model demonstrating the approach used in the most commercial codes.

The behavior of a material point can be decomposed into linear-elastic and inelastic, i.e. general strain-softening material behavior as follows

$$\sigma(\varepsilon) = \begin{cases} E\varepsilon & \varepsilon \leq \varepsilon_0 \\ \phi(\varepsilon - \varepsilon_0) & \varepsilon > \varepsilon_0 \end{cases} \quad (7.22)$$

In order to show the correspondence with the previously used cohesive crack law

$$\sigma = f(w) = f_t \exp\left(-\frac{f_t}{G_F} w\right) \quad (7.23)$$

let us now incorporate the strain-softening function into the framework of a damage model within a finite element computation. Using the softening function governed by the fracture energy we introduce the finite length of the softening zone  $L_s$  as a parameter. Then we can set

$$\phi(\varepsilon - \varepsilon_0) = f(w = (\varepsilon - \varepsilon_0)L_s) = f_t \exp\left(-\frac{f_t}{G_F}(\varepsilon - \varepsilon_0)L_s\right) \quad (7.24)$$

The decomposed representation of the material behavior in terms of the softening law should be equally well reproducible using a damage model describing the strain-softening as a material deterioration, which has been discussed in Chapter in the context of approaches to interface modeling. as

$$\sigma(\varepsilon) = (1 - \omega)E\varepsilon \quad (7.25)$$

where  $\omega$  is a monotonic damage function with values within the range (0,1). The damage function can be related to the softening function introduced above in the following way.

For  $\varepsilon \leq \varepsilon_0$  we obtain  $\omega = 0$  and for the softening regime  $\varepsilon > \varepsilon_0$  the damage function reads

$$\omega(\varepsilon) = \begin{cases} 0 & \varepsilon \leq \varepsilon_0 \\ 1 - \frac{\phi(\varepsilon - \varepsilon_0)}{E\varepsilon} & \varepsilon > \varepsilon_0 \end{cases} \quad (7.26)$$

Substituting from (7.24) we obtain a strain-based damage function with fracture energy  $G_F$  and tensile strength  $f_t$  as parameters

$$\omega(\varepsilon) = \begin{cases} 0 & \varepsilon \leq \varepsilon_0 \\ 1 - \frac{1}{E\varepsilon} f_t \exp\left(-\frac{f_t}{G_F} (\varepsilon - \varepsilon_0) L_s\right) & \varepsilon > \varepsilon_0 \end{cases} \quad (7.27)$$

Deriving a material law with physically meaningful parameters is certainly aesthetically pleasing. However it does not provide us any guarantee that the model will be able to capture the real behavior. Notice that the choice of the exponential function (7.10) was rather intuitive. Other choices, e.g. bi-linear might be taken as well. Nevertheless, the fact that the parameters of damage function have a clear physical interpretation can be exploited during the model calibration as we will discuss in Chapter 9.

### Example 7.2: Transformation of a softening function to damage function

The derivation is provided in an interactive form in the [jupyter notebook](#).

#### Questions

- What is the unit of fracture energy?
- What is the unit of energy release rate?
- How does the fracture energy influence the relation between the stress and crack opening?
- How does the equivalent parameter  $L_s$  in the damage function influence the stress strain response?

## 8 Softening and finite elements

### 8.1 Effect of element size on the strain localization for linear softening law

Instead of a cohesive crack model with the softening behavior described in terms of stress versus crack opening, let us consider a material law of a zone of a material with linear softening depicted in the Figure 8.1. We will use the softening law to discretize a bar subjected to tensile load. The bar with the Young's modulus  $E$  with the total length  $L$  is discretized using  $n$  number of elements. The response of the bar will stay linear elastic until one of the elements reaches its tensile strength  $f_t$ . At this point, the strain in the bar will be  $\varepsilon_0 = f_t/E$ . Thus, the elastic elongation of the bar can be expressed as

$$u_{\text{el}} = \varepsilon_0 L = \frac{f_t}{E} L \quad (8.1)$$

Beyond the elastic limit, the critical element will enter the softening branch while all the remaining elements will unload. Since we assume the linear softening behavior, we can directly obtain the nominal / macroscopic or average stress-strain response. Once the critical element reached the strength, the stress in the bar will decrease following either the unloading/elastic branch in the elastic part of the specimen or the softening branch in the single softening element. At the stress level  $\sigma = 0$ , the elastic part will unload to zero so that it provides no contribution to the overall displacement. The softening part will reach the strain corresponding to the intersection of the softening branch with the  $\varepsilon$  axis, i.e.  $\varepsilon_f$ . Thus, the control load upon reaching the zero strain in the bar be exactly

$$u_f = \frac{L}{n} \varepsilon_f \quad (8.2)$$

As a result, the macroscopic stress-strain response of the bar is described by three data points for strains and stresses, i.e.

$$\varepsilon = [0, f_t/E, \varepsilon_f/n], \sigma = [0, f_t, 0] \quad (8.3)$$

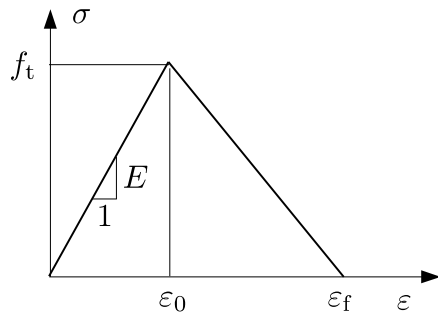


**Figure 8.1** Material with linear softening.

Apparently, the macroscopic response of the bar depends on the number of discretization elements so that we can produce arbitrary results by changing the number of elements or, more precisely, the size of the localizing element.

### Example 8.1: Mesh bias for discretized bar with linear softening

The example demonstrates that the bar response produces different results for different number of discretization elements. See the example in [jupyter notebook](#)

## 8.2 Regularization of the softening law in finite element code

Let us assume that the fracture energy  $G_f$  is known and we want to improve the above model to deliver stable, mesh-independent results. Knowing that the energy dissipation is only happening in the one softening element, we can require that it always dissipates the same amount of energy. Recall that the fracture energy dissipated by a unit area of a stress free crack is evaluated as

$$G_f = \int_0^\infty f(w) dw \quad (8.4)$$

where  $w$  represents the crack opening. In the studied case of linear softening with  $f$  defined as

$$f(w) = f_t \left( 1 - \frac{1}{w_f} w \right) \quad (8.5)$$

and the corresponding fracture energy

$$G_f = \int_0^{w_f} f(w) dw = \frac{1}{2} f_t w_f \quad (8.6)$$

This kind of model is working correctly and reproduces exactly the amount of fracture energy needed to produce the unit area of the stress free crack.

However, in a finite element model, the crack is not represented as a discrete line but is represented by a strain within the softening element of the size  $L_s = L/N$ . Thus, the softening is not related to crack opening displacement (COD) but to a strain in the softening zone using a softening function  $\phi(\varepsilon_s)$ . This model was used in the example above and delivered mesh-dependent results with varying amount of fracture energy.

To regularize the finite element model let us express the crack opening displacement as a product of the softening strain  $\varepsilon_s$  and the size of the softening zone  $L_s$ :

$$w = \varepsilon_s L_s \quad (8.7)$$

Now, the energy dissipated within the softening zone can be obtained as an integral over the history of the softening strain as

$$G_f = L_s \int_0^\infty \phi(\varepsilon_s) d\varepsilon_s \quad (8.8)$$

Coming back to the model with linear softening, the integral of the strain based softening function is expressed as

$$\int_0^\infty \phi(\varepsilon_s) d\varepsilon_s = \frac{1}{2} \varepsilon_f f_t \quad (8.9)$$

so that

$$G_f = \frac{1}{2} L_s \varepsilon_f f_t \implies \varepsilon_f = \frac{2}{L_s} \frac{G_f}{f_t} \quad (8.10)$$

### Example 8.2: Discretized bar with regularized linear softening

This sheet provides the implementation of the above shown regularized softening model that does not change values for a modified size of the softening zone and delivers objective results. See the example in [jupyter notebook](#)

## 8.3 Implementation of softening in finite-element codes

Standard finite-elements are formulated for smooth shape functions and their derivatives within the element volume. Cracks in form of displacement jumps are not possible. Advanced finite-element techniques can be used to provide more accurate representation of strain localization of an emerging crack. These techniques, however, require changes in the mesh structure, remeshing, embedding of discontinuities or non-local integration of state variables including bookkeeping of neighboring relations between elements. Implementation of these methods, however, is rather complex compared to standard finite-element methods so that these methods are rarely available in commercial codes and are mostly provided only in scientific codes.

In practical applications, the most common approach to introducing cracks is based on the concept of strain softening with smeared representation of a crack that resembles the approach studied in topic 7.2. This approach has been developed in the 1970's and is used in the most commercial codes. In its original form the approach did not provide objective results and it was necessary to overcome a number of difficulties regarding the ill-posedness and lack of objectivity.

The common strategy applied in standard finite-element codes is the crack-band regularization technique. The basic idea of the crack band regularization is to relate the amount of energy dissipation to the size of the finite element. To illuminate the concept of crack band regularization, let us consider again the tensile test of a length described in topic 7.2. The length of the softening element is .

We require that the energy needed to make the cohesive zone stress-free is equal to the energy required to produce a stress-free crack. More precisely: the amount of energy dissipated per unit area of an emerged crack must be equal to  $G_F$ . Expressed mathematically, the softening law applied in a finite element computation with strain localization within a single finite element needs to fulfill the condition:

$$G_F = \int_0^\infty f(w) dw = \int_0^\infty \phi(\varepsilon) d\varepsilon \quad (8.11)$$

This can be achieved by the requirement that the strain integral over the element exhibiting softening is set equal to crack opening, i.e.

$$w = \varepsilon h_c \quad (8.12)$$

where  $h_c$  denotes the element length. As a result, we can set

$$\sigma = f_w(\varepsilon h_c) \quad (8.13)$$

## 8.4 Implementation of softening behavior in finite element code

Consider a chain of 2 elements with the total length  $L$ . One element has slightly lower strength  $f_t$ . Then, upon softening we distinguish the elastic part of the length  $L_{\text{el}} = L(N - 1)/N$  and the softening part with the length  $L_s = L/N$ . The total elongation corresponding to the control displacement is then given as

$$u = \varepsilon_{\text{el}} L_{\text{el}} + \varepsilon_s L_s. \quad (8.14)$$

The nominal/average strain in the whole bar can then be written as

$$\varepsilon = \frac{\varepsilon_{\text{el}} L_{\text{el}} + \varepsilon_s L_s}{L}. \quad (8.15)$$

The stress in each of the two elements is

$$\sigma_{\text{el}} = E\varepsilon_{\text{el}} \quad (8.16)$$

The equilibrium condition can then be written as a requirement of stress equality in both parts

$$R = \sigma_{\text{el}} - \sigma_s = 0 \quad (8.17)$$

The stress in the element s is governed by softening prescribed by the damage function derived previously for a softening zone with predefined fracture energy in Eq. (7.27)

$$\omega(\varepsilon) = 1 - \frac{f_t}{E\varepsilon} \exp\left(-\frac{f_t}{G_f}(\varepsilon - \varepsilon_0)L_s\right) \quad (8.18)$$

The resulting stress is provided as

$$\sigma_s = (1 - \omega(\varepsilon))E\varepsilon \quad (8.19)$$

After substituting for stresses in Eq. (8.17) we obtain a residuum function as

$$R = E\varepsilon_{\text{el}} - (1 - \omega(\varepsilon))E\varepsilon_s = 0 \quad (8.20)$$

By using the compatibility equation we can express elastic strain in terms of the control displacement and softening strain as

$$\varepsilon_{\text{el}} = \frac{1}{L_{\text{el}}} (u - \varepsilon_s L_s) \quad (8.21)$$

so that finally the residuum is given as

$$R = \frac{1}{L_{\text{el}}} (u - \varepsilon_s L_s) - (1 - \omega(\varepsilon_s)) \varepsilon_s = 0 \quad (8.22)$$

This nonlinear equation can be solved iteratively using the Newton method. The first step is to use the Taylor expansion

$$\hat{R} = R(\varepsilon_s^k) + \left. \frac{\partial R(\varepsilon_s)}{\partial \varepsilon_s} \right|_{\varepsilon_s^k} \Delta \varepsilon_s = 0 \quad (8.23)$$

Using this approximation, we can calculate the increment of softening strain as

$$\left. \frac{\partial R(\varepsilon_s)}{\partial \varepsilon_s} \right|_{\varepsilon_s^k} \Delta \varepsilon_s = -R(\varepsilon_s^k) \quad (8.24)$$

The derivative of the residuum with respect to the softening strain reads

$$\frac{\partial R(\varepsilon_s)}{\partial \varepsilon_s} = -\frac{L_s}{L_{\text{el}}} + \frac{\partial \omega(\varepsilon_s)}{\partial \varepsilon_s} \varepsilon_s - (1 - \omega(\varepsilon_s)) \quad (8.25)$$

The iterative scheme is then given as

$$\left[ -\frac{L_s}{L_{\text{el}}} + \left. \frac{\partial \omega(\varepsilon_w)}{\partial \varepsilon_s} \right|_{\varepsilon_s^k} \varepsilon_s^k - (1 - \omega(\varepsilon_s^k)) \right] \Delta \varepsilon_s = \frac{1}{L_{\text{el}}} (u - \varepsilon_s^k L_s) - (1 - \omega(\varepsilon_s)) \varepsilon_s^k \quad (8.26)$$

The derivative of the damage function provided in Eq. (7).

$$\frac{\partial \omega(\varepsilon)}{\partial \varepsilon} = \begin{cases} 0 & \varepsilon \leq \varepsilon_0 \\ \frac{1}{EG_F \varepsilon^2} f_t \exp\left(-\frac{L_s(\varepsilon - \varepsilon_0)}{G_F} f_t\right) (G_F + L_s \varepsilon f_t) & \varepsilon > \varepsilon_0 \end{cases} \quad (8.27)$$

### Example 8.3: Iterative solution of the localization problem

The implementation of the described algorithm is provided in the notebook It demonstrates the structure of a nonlinear finite element solver.

Derivation of this example follows the reasoning applied in the implementation of nonlinear finite element computation. In the uni-axial case, we do not need to use numerical integration of stresses. The mapping between local strains and global strains, normally resolved using Jacobi transformation, is done by directly multiplying the particular lengths. The notebook sheet supplied with the example increments the control displacement of the bar in an outer loop and searches for the solution satisfying the equilibrium condition in the inner loop.

Correspondence with the finite element code

### Example 8.4: Standard finite element code

When calculating this example using standard finite element code, the unknowns are the nodal displacements along the bar. Consider an example sketched in Figure 8.2. It represents a bar with one element of a slightly lower strength  $f_t$  in a gray element

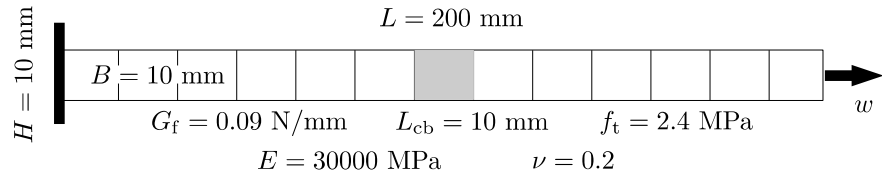


**Figure 8.2** Example of a tension bar with a softening zone of a finite size.

then in the other elements. Upon displacement loading, the damage will localize in the gray element. The given geometrical and material parametric are preset in the BMCS application **Tensile test - isotropic damage**.

### Tasks

- Calculate the response using the jupyter script provided in Example 8.3 and also using the BMCS application **Tensile test - isotropic damage**. Do they match?
- Change the size of the softening zone to half and double size. Check to see if you get mesh-independent results.
- Evaluate and plot the strain profile along the specimen with the three different sizes of the softening zone.
- Compare the total amount of dissipated energy  $G$  at the end of the loading with nearly zero force in the bar with the input value of the damage function  $G_F$ . How are they related?
- Switch off in the regularization using a button on the first page of the application. Then, the damage law is not adjusted to the element size any more. Change the size of the crack band element and test how does it affect the observed response.

# 9 Crack propagation

In the previous lecture, we have analyzed the correspondence between the fracture and damage using a uni-axial example. In the present lecture we apply the same concepts to a two-dimensional case of stable crack propagation. In particular, we are going to use the three-point bending test as a means of rendering an elementary crack-propagation scenario, namely a stable crack running along a predefined straight path. After discussing the test setup, we provide the test results in terms of load-deflection curve. Then, we will construct a numerical model that can reproduce such a behavior, specify the required material parameters and how to identify them. Similarly to the previous lecture, we will consider the link between fracture and damage concepts that are both included in any finite element computation involving strain-softening material behavior.

## 9.1 Propagation of a straight crack

An isolated tensile crack, mode-I crack, can be initiated using a notched specimen. The most common configurations used to study the cracking behavior for a tensile crack denoted as mode I are the wedge splitting test and notched, three-point bending test. Both these tests aim at the characterization of the material behavior in terms of the softening law describing the relation between the tensile stress transmitted across the localization zone and the corresponding crack opening.

Why notched  
three-point  
bending  
test?

Due to its simplicity, three-point-bending test on a notched concrete has become a standard (RILEM) to determine the fracture energy  $G_F$  characterizing the cracking behavior of concrete. The test induces a single crack in the notched section propagating straight upwards from the notch in a stable manner. The energy is dissipated in a local region in the crack vicinity so that it can be directly ascribed to the area of emerging crack surface.

The numerical simulation of this model can be readily performed using the material model with the damage function derived in previous lecture. An example of the geometry and boundary conditions of the three-point bending test including the material parameters of the model is depicted in Fig. 9.2.

### Example 9.1: Regularized numerical model of a bending test

The finite element discretization in this model applies the symmetry condition at the middle section of the beam. Upon loading loading, the damage will localize at the tip of the notch and propagate upwards. This process with simultaneous evaluation of the energy dissipation is provided in the BMCS application **Tensile test - isotropic damage**.

#### Tasks

- Change the size of the softening zone to half and double size. Check to see if you

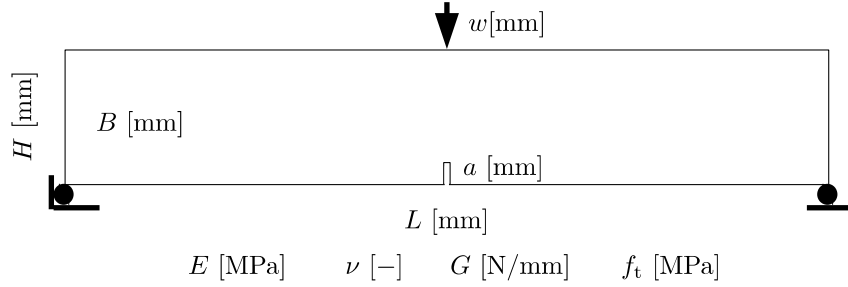


**Figure 9.1** Geometry and boundary conditions of the three-point bending test.

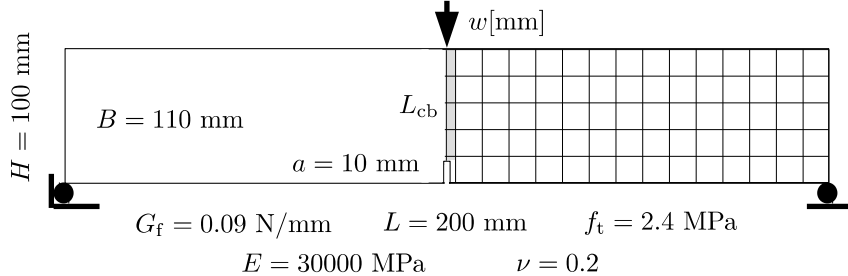


**Figure 9.2** Finite element discretization used for the verification of mesh-independency of the numerical model.

get mesh-independent results.

- Vary the value of fracture energy  $G_f$  - how does it affect the test response?
- Compare the total amount of dissipated energy  $G$  at the end of the loading with nearly zero force with the input value of the damage function  $G_F$ . How are they related?
- Vary the size of the notch and evaluate the amount of dissipated energy. Could a test without a notch be used to obtain a realistic estimate of fracture energy  $G_F$ ?

**Direct evaluation of the fracture energy:** Recalling that we can characterize the stable process of crack propagation by an amount of energy needed to produce a unit crack area, i.e. fracture energy  $G_F$ , we can choose a more efficient and pragmatic approach determining the fracture energy directly from the test without having to perform numerical calibration. This is the idea behind the standardized characterization procedure proposed by the RILEM committee. Recall that at the point of failure, the whole energy has been consumed to produce the crack of a surface area  $A = b(h - a)$ , where  $h$  and  $b$  denote the height and width of the beam and  $a$  is the notch depth. Then assuming uniform dissipation during a stable crack propagation we can set

$$G_F = \frac{W}{b(h - a)}, \quad (9.1)$$

However, this simple approach would ignore the fact that self-weight of the beam also invoked some deflection  $w_0$ . Neither the self-weight load, nor the corresponding deflection

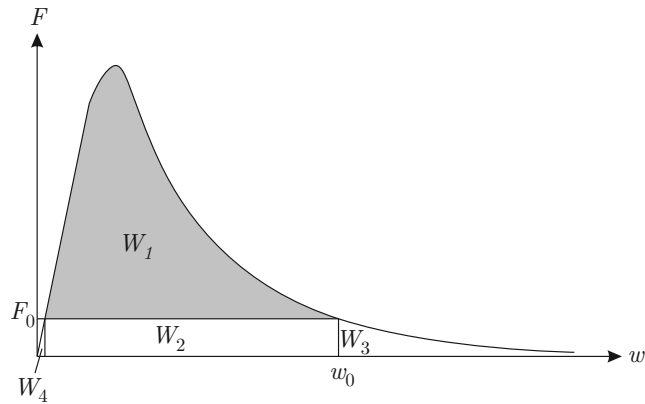


**Figure 9.3** Fracture energy dissipation including the self-weight.

are included in the experimentally recorded curve. The situation is illustrated in Fig. 9.3. This effect might be relevant for large specimens. A simple remedy has been suggested by Petersson in the form

$$G_F = \frac{W_1 + mgw_0}{b(h-a)}, \quad (9.2)$$

where  $mg$  is the weight of the beam. Let us now present an application of the model to tests conducted by Petersson.

## 9.2 Petersen three-point bending test series

The original test setup for three-point bending test has been introduced by Petersson who conducted a series of stable tensile tests and three-point-bending tests on notched concrete specimens aiming at characterization of fracture properties such as tensile strength and fracture energy. In the bending test series a group of large-span beams with span length of  $L = 2000$  mm, height of  $h = 200$  mm and width of  $b = 50$  mm and notch length of  $a = 100$  mm were tested (Fig. 9.4). The ratio of the notch length to the depth of the beam  $a/h$  is set to 0.5. The specimens were loaded at the middle by the vertical force  $F$ . The vertical displacement of the loading point  $w$  was recorded during the test.

Let us now ask the question, what material parameters do we need to model this type of response using a non-linear finite element code. What parameters do we know in advance and what are still missing? We know the  $E$  modulus and the Poisson's modulus  $\nu$ , but we do not know the strain-softening law that would characterize the concrete matrix, i.e. the process of crack localization within a fracture process zone.

Effect of the shape of softening law

**Direct evaluation of fracture energy:** Applying this method to the considered series of tests performed by Petersson mean value of the fracture energy has been quantified to  $G_F = 0.124$  N/mm. This correction is only approximate and leads to a non-negligible error in case of large specimens. Therefore, weight compensation is also employed in order to achieve a zero reference state for the evaluation of energy supply during the bending test.

Iterative calibration of the softening law:  
71

**Table 9.1** Material parameter for simulation of Petersson bending test series

Description	Symbol	Value	Unit
elasticity modulus	$E$	30000	N/mm <sup>2</sup>
tensile strength	$f_t$	3.3	N/mm <sup>2</sup>
fracture energy	$G_f$	0.124	N/mm

This situation resembles the case of the calibration of the bond-slip law discussed. There, we were identifying the parameters of the bond-slip model by iteratively adjusting the damage function and the hardening modulus with the goal to fit the pull-out response of the numerical model with the experiment. The same procedure can be applied here to identify the crack localization and propagation characteristics. Indeed, we can apply the same concept to identify the softening law  $f(w)$  iteratively by adjusting the parameters of its approximation. However, as we have already experienced in case of bond-slip law, this kind of trial-and-error approach is not really efficient. It might be automated using a numerical optimization algorithm that would minimize the lack of fit between the experimental and numerical response curve.

**Numerical simulation of Petersson tests** The simulation shown in Fig. 9.4 is done using 4-node bilinear quadrilateral elements. The model is discretized using fine mesh at the mid-span region, where the localization of the strains is expected. To be sure that there is no numerical bias, let us first verify the convergence of the model. Particular attention needs to be paid to the support regions which are susceptible to stress concentration which can distort the results. The applied finite element discretization of the test is shown in Fig. 9.4b with fine mesh within the fracture process zone using element size of 10 mm × 10 mm. Material parameters used in the simulation are summarized in Table 9.1.

**Simulation results** Fig. 9.4c shows plot of damage parameter  $\omega$  at mid-span of the beam. Load-point deflection  $w$  is plotted versus force  $F$  in Fig. 9.4d for fracture energy  $G_f = 0.124 \text{ N/mm}$ . Petersson also compared the numerical results with the experiments for the range of fracture energy between the lowermost and uppermost obtained values  $0.115 \text{ N/mm} \leq G_f \leq 0.137 \text{ N/mm}$ . The same comparison of load-displacement curves is done here using microplane damage model with variation of fraction energy between the given values (Fig. 9.4e).

**Choice of the softening law:** With the determined amount of the fracture energy  $G_F$  we still do not know the shape of the softening law. Similarly to the previous cases, additional simplifying assumptions on the shape of the softening law need to be made. An example of such an assumption is provided by the exponential cohesive law 7.10 derived previously in Chapter 8.

Last question to be addressed is how can we implement the strain softening law into the finite element code? How to ensure objectivity of results and avoid the mesh bias? Example studies performed in Abaqus.

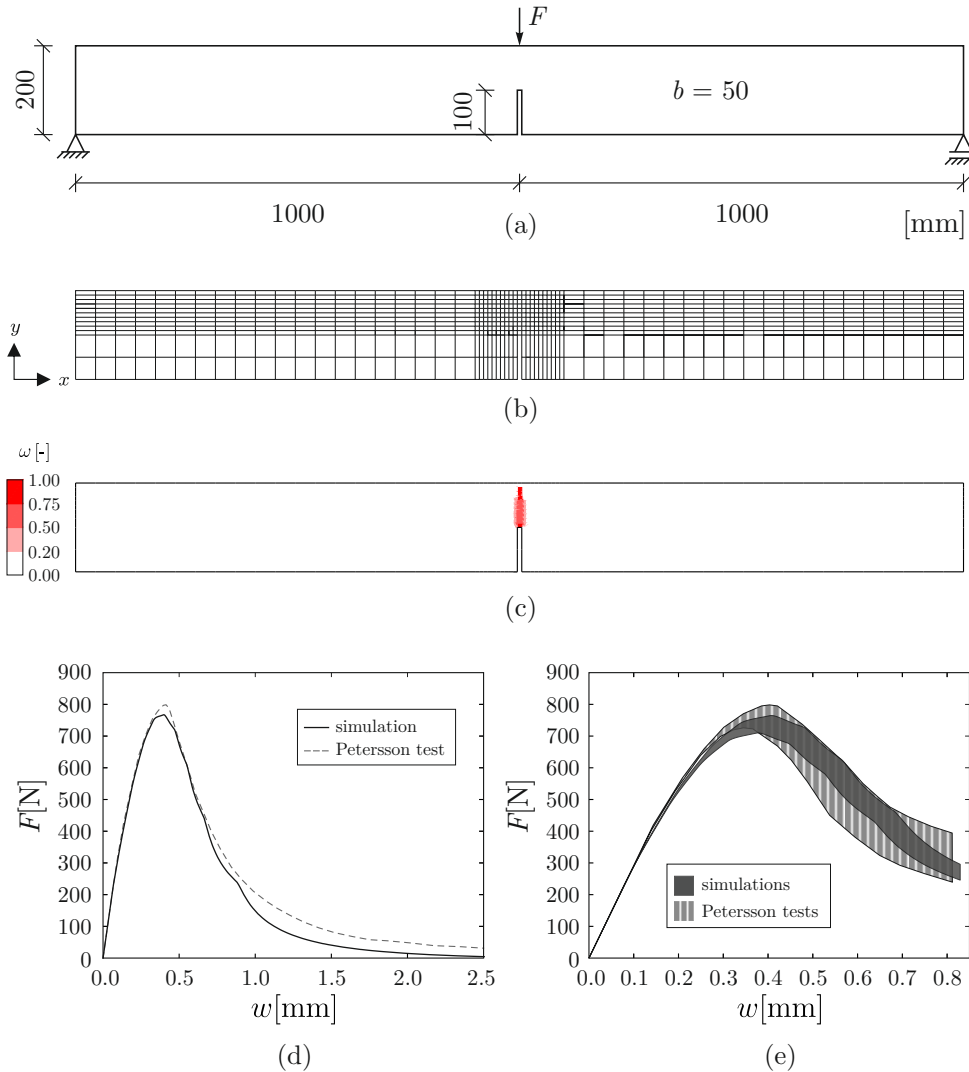


**Figure 9.4** (a) Dimensions of notched three-point-bending test series by Petersson, loading and boundary condition; (b) finite element discretization; (c) damage propagation; (d) load-displacement curves from test and simulations with fracture energy  $G_f = 124 \text{ N/mm}$ ; (e) range of load-displacement curves from test and simulations with variation of fracture energy  $0.115 \text{ N/mm} \leq G_f \leq 0.137 \text{ N/mm}$

### 9.3 Onset of damage

The shown examples are two-dimensional. They describe the strain state and stress state using tensors. But the damage function used so far was based on a scalar input, either the tensile strain  $\varepsilon_{xx}$  or slip  $s$ . However, in 2D, there are three variables and in 3D six independent variables describing the strain state at a single material point. Therefore, an equivalent scalar strain measure must be defined to introduce the damage model.

### 9.3.1 Rankine failure surface

The simplest case of equivalent strain measure is introduced as the maximum value of the principal tensile strain

$$\tilde{\varepsilon} = \frac{1}{E} \max(\sigma_i), \quad i = 1, 2, 3 \quad (9.3)$$

The principal stresses are obtained as the eigenvalues of the stress tensor.

### 9.3.2 Mazars failure surface

Another variant of equivalent yield surface is defined as follows

$$\tilde{\varepsilon} = ||\langle \varepsilon \rangle|| = \sqrt{\langle \varepsilon : \varepsilon \rangle} = \sqrt{\langle \varepsilon_1 \rangle^2 + \langle \varepsilon_2 \rangle^2 + \langle \varepsilon_3 \rangle^2} \quad (9.4)$$

In 9.4, the McAuley brackets  $\langle \cdot \rangle$  means the positive part of  $(\cdot)$ , e.g.  $\langle x \rangle = (x + |x|)/2$ . And  $\varepsilon_1, \varepsilon_2, \varepsilon_3$  are the principal strains.

---

# 10 Onset of inelasticity in a continuum

## 10.1 Representation of strain and stress in a continuum

To achieve strain softening and localization in standard finite element analysis with continuous approximation of stress and strain fields we need to define a failure criterion as a scalar equation in a material point. In 1D models of the bond behavior, the onset of inelasticity has been defined in terms of slip  $s$  and shear stress  $\tau$ . Similarly, the 1D models of crack localization used strain  $\epsilon$  and stress  $\sigma$  in the direction of tensile loading. However, in a 2D and 3D continuum the stress and strain state of a material point is characterized by non-scalar variables, i.e. strain tensor  $\boldsymbol{\epsilon} = \epsilon_{ij}$  and stress tensor  $\boldsymbol{\sigma} = \sigma_{ij}$ . Tensors represent the state of a material frame within a continuum using six and nine variable components in 2D and 3D continuum, respectively.

Consider a strain tensor in 3D

$$\boldsymbol{\epsilon} = \epsilon_{ij} = \begin{bmatrix} \epsilon_{11} & \epsilon_{12} & \epsilon_{13} \\ \epsilon_{21} & \epsilon_{22} & \epsilon_{23} \\ \epsilon_{31} & \epsilon_{32} & \epsilon_{33} \end{bmatrix} \quad (10.1)$$

To introduce a failure criteria in 2D and 3D as a scalar equation of the form  $f(\boldsymbol{\epsilon}) = 0$  or  $f(\boldsymbol{\sigma}) = 0$  we need to define measures of strain and stress tensor. Thus, we need to combine the information stored in a tensor to obtain a single number deciding whether or not the material state is elastic or inelastic. This task requires some understanding of the way a tensor stores the information about the material deformation.

To do that, we exploit two properties of a tensor:

- The strain tensor is symmetric, thus  $\epsilon_{ij} = \epsilon_{ji}$ . As a result, there are only six independent variables included in the strain tensor given in expression (10.1).
- The tensor in expression (10.1) describes the deformation of a material state from a particular position of an observer. In other words, the tensor representation is related to a particular coordinate system. If the observer changes the position, he or she will see the deformed cube with different values of the components. However, the deformation of the material frame did not change. Thus, there must some values hidden in the tensor representation that are invariant with respect to the coordinate system.

Indeed, strain tensor describes the volume and shape change of a unit material frame and this change can be captured using three invariants of a tensor. Volumetric strain is obtained as an average of the normal strain components, i.e.

$$I_1 = \epsilon_{xx} + \epsilon_{yy} + \epsilon_{zz} \quad (10.2)$$

It is convenient to write this expression in an indicial notation using the so called Einstein summation rule, making the mathematical expressions directly "programmable". We shall

use the index notation to directly visualize the yield surfaces and study the differences between them. The first strain invariant given in (10.2) can be rewritten in index notation as

$$I_1 = \varepsilon_{ii} \quad (10.3)$$

The Einstein summation rule introduces an implicit summation over the terms with repeated indexes. The above expression is then evaluated as

$$I_1 = \sum_{i=1}^3 \sigma_{ii}$$

There are another two invariants  $I_2, I_3$  that capture the change of shape of a material frame. Their definition is given as

$$I_2 = \frac{1}{2} [\varepsilon_{kk}^2 - \varepsilon_{ij}\varepsilon_{ij}] \quad (10.4)$$

$$I_3 = \epsilon_{ijk}E_{i1}E_{j2}E_{k3}. \quad (10.5)$$

#### Demo script

Using `numpy` package we can apply directly this convention also in coding a mathematical expression. The first invariant of the stress tensor is then expressed as

```
import numpy as np
epsilon = np.array([[1.0, 2.1, 3.5],
                   [2.1, 3.0, 1.2],
                   [3.5, 1.2, 2.0], dtype=np.float_)]
I_1 = np.einsum('ii', epsilon)
print 'I_1', I_1
```

For some examples of strain tensor invariants and their behavior and evaluation see the interactive page

<http://www.continuummechanics.org/principalstrain.html>.

#### Changing the position of observer

When we change the position of the observer, the invariants must not change. This means that the transformation rules of a tensor must keep the invariants untouched. Such transformation matrix is achieved using the directional cosines representing the rotation between two Cartesian coordinate systems  $x'_i$  and  $x_i$

$$Q_{ij} = \cos(x'_i - x_j). \quad (10.6)$$

Using such a transformation matrix, a tensor can be transformed using the rule

$$\varepsilon'_k l = Q_{ki} Q_{li} \varepsilon_{ij}. \quad (10.7)$$

For details and exercises on tensor invariants and tensor transformation use standard literature on continuum mechanics. An interactive page with the explanation of the strain tensor transformations is provided at the interactive page

<http://www.continuummechanics.org/coordxforms.html>

#### Principal strains

There is one special position of an observer that is very useful for the introduction of failure criteria and for their visualization, namely the perspective, in which the off-diagonal components of the tensor, i.e.  $\varepsilon_{ij}, i \neq j$  vanish. In this configuration, the tensor is given by three principal strains  $\varepsilon_i$ . Given a general tensor, like the one in the above example script, we can obtain the principle strains and the coordinate transformation matrix transforming the current values of the tensor to the shear-free view of the same tensor using the eigenvalue analysis. In `numpy`, this can be readily performed using the method `np.linalg.eig`:

```
eps_eigvals, Q = np.linalg.eig(epsilon)
print eps_eigvals, Q
```

To verify that the eigenvectors  $Q$  transform the tensor `epsilon` into the shear-free perspective let us use the transformation rule (10.7) using the `np.einsum` utility

```
epsilon_prime = np.einsum('ki,lj,ij->kl', Q, Q, epsilon)
print epsilon_prime
```

To provide a more straightforward interpretation of the tensor state derived tensor invariants can be constructed with the goal to relate failure criteria to some particular mode of deformation, e.g. pure shear. A useful example of a modified tensor is a deviatoric strain tensor which is constructed by subtracting the volumetric strain from the total strain tensor. As a result, we obtain a tensor with zero change of volume

$$\varepsilon_{ij}^D = \varepsilon_{ij} - \frac{1}{3} I_1 \delta_{ij}. \quad (10.8)$$

Here, the symbol Kronecker delta is by definition

$$\delta_{ij} = \begin{cases} 1 & \text{if } i = j \\ 0 & \text{if } i \neq j \end{cases} \quad (10.9)$$

and represents a standard operand introduced within the index notation that can be regarded as a unit matrix.

As  $\varepsilon_{ij}^D$  is again a tensor, we can evaluate its invariants using the expressions (10.3), (10.4) and (10.5). As the volume deformation has been subtracted, the first invariant is implicitly zero,

$$J_1 = \varepsilon_{ii}^D = 0.$$

Its second invariant represents the actual measure of shear used in many yield functions relevant also concrete modeling:

$$J_2 = \frac{1}{2} \varepsilon_{ij}^D \varepsilon_{ji}^D. \quad (10.10)$$

Its interpretation can be provided if we align the coordinate system of a material point with the principal axes of the tensor. In this setting, the tensor has only normal components and no shear components.

Deviatoric strain

## 10.2 Examples of yield conditions

The tensor invariants and tensor transformation introduced using a strain tensor apply also to the stress tensor. In modeling of inelastic behavior of materials we can either use a strain based threshold function to define an onset of damage, i.e.  $f(\boldsymbol{\varepsilon}) = 0$  or a stress based yield condition  $f(\boldsymbol{\sigma}) = 0$  that marks the elastic range of the material behavior. Two examples of a damage threshold functions have been shown in Sec. 9.3 and Sec defined in terms of equivalent strains. Note that these strains represent derived invariants of a strain tensor and, thus, fulfill the requirement of independence on the chosen coordinate system.

In this section, we review several yield conditions defining the failure criterion in terms of a stress tensor using the function function

$$f(\sigma_{xx}, \sigma_{yy}, \sigma_{zz}, \sigma_{xy}, \sigma_{yz}, \sigma_{zx}) \leq 0. \quad (10.11)$$

or, in indicial notation

$$f(\sigma_{ij}) \leq 0, \quad i, j \in (1, 2, 3), \quad \sigma_{ij} = \sigma_{ji}. \quad (10.12)$$

The requirement of objectivity with respect to the chosen coordinate system is again required. A compact specification of the elastic domain treat loading configurations that are equivalent with respect to the spatial axes simultaneously. This means that for example a uni-axial loading  $\sigma$  in  $x$  direction

$$\sigma_{xx} = \sigma, \quad \sigma_{yy} = 0, \quad \sigma_{zz} = 0, \quad \sigma_{xy} = 0, \quad \sigma_{yz} = 0, \quad \sigma_{zx} = 0$$

delivers the same value of  $f(\sigma_{ij})$  as a uni-axial loading in  $y$  direction

$$\sigma_{xx} = 0, \quad \sigma_{yy} = \sigma, \quad \sigma_{zz} = 0, \quad \sigma_{xy} = 0, \quad \sigma_{yz} = 0, \quad \sigma_{zx} = 0.$$

Thus, we have to use The mathematical means of describing this symmetry can be achieved using stress tensor invariants. The simplest yield function suitable for simulation of metals has been introduced by von Mises in the form

$$f := J_2 - k^2 \leq 0. \quad (10.13)$$

This simple yield function can be visualized by choosing the view in the space of principal stresses. Let us show the values of  $f(\sigma_i) = 0$  in the 3D visualization by evaluating the values in the range  $\sigma_i \in (\sigma_{\min}, \sigma_{\max})$ .

---

```

import numpy as np
# define the boundaries of a cube in stress space
min_sig = -20.0 # maximum compression
max_sig = 5.0 # maximum tension
n_sig = 100j # number of values in each stress direction
sig_1, sig_2, sig_3 = np.mgrid[min_sig: max_sig: n_sig,
                                 min_sig: max_sig: n_sig,
                                 min_sig: max_sig: n_sig]
# make a four dimensional array
sig_abcj = np.einsum('jabc->abcj', np.array([sig_1, sig_2, sig_3]))
# Kronecker delta
DELTA = np.identity(3)
sig_abcij = np.einsum('abcj,jl->abcjl', sig_abcj, DELTA)
# first invariant of the stress tensor
I1 = np.einsum('...ii,...ii', sig_abcij, DELTA)
# deviatoric stress tensor in each point
s_ij = sig_abcij - np.einsum('...,ij->...ij', I1 / 3.0, DELTA)
# second deviator of the stress tensor
J2 = np.einsum('...ii,...ii', s_ij, s_ij) / 2.0
# threshold defining the radial distance from hydrostatic axis
k = 2.
f = J2 - k ** 2
# visualization using Mayavi package
import mayavi.mlab as m
f_pipe = m.contour3d(
    sig_1, sig_2, sig_3, f, contours=[0.0], color=(0, 1, 0))
m.axes(f_pipe)
m.show()

```

---

**Questions:**

- What is the meaning of the parameters  $k$ ?
- What happens when loading the material point hydrostatically? Does the material fail?
- Meridians
- Deviatoric plane
- Plane stress representation

**Drucker-Prager** While in  $J_2$  plasticity, the yielding is triggered by achieving a certain level of shear, there is no failure upon volumetric tension or compression. On the one hand we get On the one hand, hydrostatic tensile loading would initiate relatively early failure. Moreover, shear loading that would initiate inelastic internal friction within the material structure is affected by the lateral pressure. For such materials, often referred to as pressure-sensitive, the first invariant  $I_1$  can be used to introduce the interaction between the volumetric pressure and shear. The mostly used example of this function is presented by the Drucker-Prager yield surface defined as

$$f := \alpha I_1 + \sqrt{J_2} - k \leq 0 \quad (10.14)$$

Special cases of this condition can be constructed by specifying the parameters using the meridians of the yield surface.

**Question:** Consider the role of the parameter  $\alpha$ . What happens for its limiting values  $\alpha \rightarrow 0$ .

An example of such a yield surface is provided by the Mohr-Coulomb criterion postulating that shear stress necessary to induce yielding on a certain plane increases with increasing compressive stress normal to that plane:

$$f := |\tau| + \sigma \tan \phi - c \leq 0 \quad (10.15)$$

**Question:** Special case of this criterion is given by the angle of internal friction  $\phi = 90^\circ$  rendering the Rankine yield condition. Plot its representation for plane stress in  $\sigma_1, \sigma_2$  plane with  $\sigma_3 = 0$

**Abaqus** The yield condition used in the damage-plasticity model implemented in Abaqus has the following form

$$\begin{aligned} f &:= \frac{1}{1-\alpha} (\alpha I_1 + \sqrt{3 J_2} + \beta \sigma_{\max}) \leq 0 \\ \alpha &:= \frac{f_b - f_c}{2f_b - f_c} \\ \beta &:= \frac{f_c}{f_t} (\alpha - 1) - (1 + \alpha) \\ \sigma_{\max} &:= \max(\sigma_1, \sigma_2, \sigma_3) \end{aligned} \quad (10.16)$$

where  $f_t$  is the uniaxial yield tensile stress,  $f_c$  the uniaxial yield compressive stress and  $f_b$  the biaxial yield compressive stress. Apparently, it has some common features with the Drucke-Prager condition.

**Questions:** What are the added aspects? Explore the limits. What happens upon compressive volumetric loading?

**Willam-Warnke** Another example proposed of a yield surface proposed for the modeling of concrete and of masonry has been introduced by Willam-Warnke. It also introduces the pressure-sensitivity in terms of the stress tensor invariants  $I_1$  and  $J_2$ . In addition, the third invariant of the deviatoric stress tensor

$$J_3 = \det(\mathbf{s}) = \frac{1}{3} s_{ij} s_{jk} s_{ki}$$

The role of the third invariant is to "deform" the shape of deviatoric sections so that the meridian for uni-axial stress loading or bi-axial stress loading are differ from each other which is not the case for the previous examples.

### Example 10.1: Tensorial invariants and deviatoric strain tensor

The manipulation of strain tensor explaiend in this section are provided in form of an interactive notebook [here](#)

**Exercise** : Use the BMCS tool suite to explore the difference between the three described yield surfaces.

## 11 Shear & Crack

The standard finite-element code on the market applies mostly the combination of damage and plasticity models to simulate the cracking behavior of concrete. Besides the yield surface exemplified in the previous chapter, further also the evolution equations specifying the criteria for evaluation of state variables. Even though the models can be used to realistically capture many cases structural configurations, they still do not guarantee that correct results for complex loading scenarios. Particularly difficult and challenging tasks is the correct description of the crack development through a zone with combined tensile and shear loading.

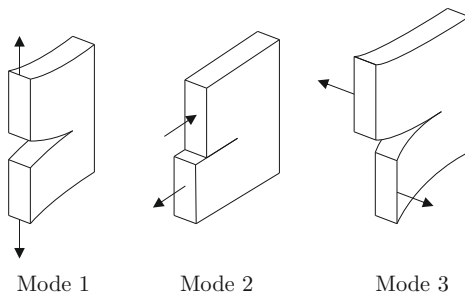


**Figure 11.1** Fracture modes 1,2 and 3: opening crack, shearing crack and tearing crack

In our brief tour through the approaches to the description of complex material behavior we only touch the problem by visualizing the source of the difficulties that are encountered when using material models formulated in the framework of plasticity and damage mechanics. These models are formulated in tensorial form and are based on the stress invariants described in section 10.1.

In the context of fracture mechanics, three fracture modes that we deal with can be distinguished: mode 1: opening crack, mode 2: shearing crack and mode 3: tearing crack (Fig 11.1). A failure process containing a combination of fracture modes (mixed mode fracture) is characterized by interaction of fracture modes I and II, leading to the "*mixed-mode*" fracture process. To motivate the detailed view to the problem, let us start with an experimental setup that has been designed to render two symmetric cracks with combined tensile and shear loading. We will consider the analysis of the test performed on the double-notched specimen by Nooru-Mohamed [**nooru\_mixed\_1992**] and compare the behavior of the relatively widely used concrete-damage-plasticity model implemented in Abaqus. In parallel, we will introduce an alternative "non-tensorial" model using the concept of microplane and explain its basic features.

We will then explore the model behavior using a verification test that studies the model behavior by defining loading paths within the principal stress space close to the yield condition. An extreme condition, occurs when moving through the stress space along a path parallel to the surface of the yield condition. Such loading path can be used to

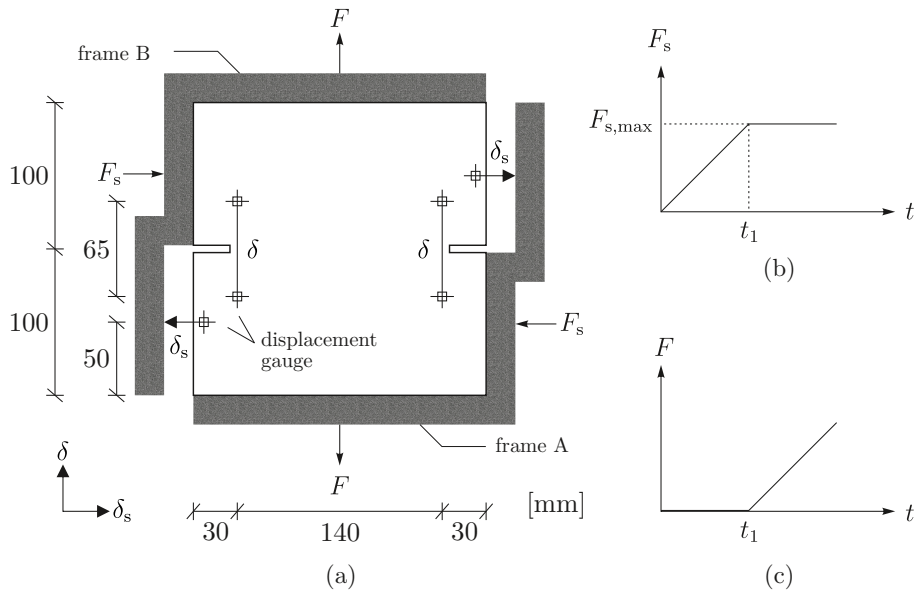


**Figure 11.2** (a) Test setup and dimensions of the Nooru-Mohamed tests; (b) loading history of horizontal force  $F_s$ ; (c) loading history of vertical force  $F$

visualize pathological features of the models in general and to explain why a model is not able to reflect the reality in some loading scenario.

To explain the better performance of the microplane-based modeling approach we look at the fundamental concept of the microplane modeling approach at the end of the lecture.

## 11.1 Double-edge notched test

**Test setup** Nooru-Mohamed [nooru\_mixed\_1992] tested square-shaped double-edge notched concrete specimens of  $200 \text{ mm} \times 200 \text{ mm}$  with constant thickness of  $t = 50 \text{ mm}$  subjected to different loading conditions (Fig. 11.2a). The bi-axial testing machine consists of two loading frames which can independently move in horizontal and vertical directions.

**Loading scenario** Test was performed in a sequence of transmitted loads  $F_s$  and  $F$  using loading steel frames. At first, the test specimen was loaded in horizontal direction by force  $F_s$  to a predefined level  $F_{s,max}$  at time  $t_1$  (Fig. 11.2b). Then, the force  $F_s$  was kept constant and test specimen was loaded in vertical direction using displacement-controlled force  $F$  up to the failure (Fig. 11.2c). Vertical displacement  $\delta$  was measured using displacement gauges with the length of  $t = 65 \text{ mm}$ . Horizontal gauges were used to measure the displacement  $\delta_s$ .

**Observed crack development** Fig. 11.3 shows the test results for two different levels of the horizontal, shear-inducing force  $F_{s,max} = 5 \text{ kN}$ , and  $F_{s,max} = 10 \text{ kN}$ , respectively. Apparently, the described test setup and the applied loading history leads to a formation of rotating cracks. The low shear force  $F_{s,max} = 5 \text{ kN}$  leads to almost horizontal evolution of cracks (Fig. 11.3a), while the increased horizontal force of  $F_{s,max} = 10 \text{ kN}$  induces curved cracks (Fig. 11.3b).

In the following paragraphs we compare the simulation results from two different material models, *microplane damage model* and *concrete damage plasticity model* from ABAQUS

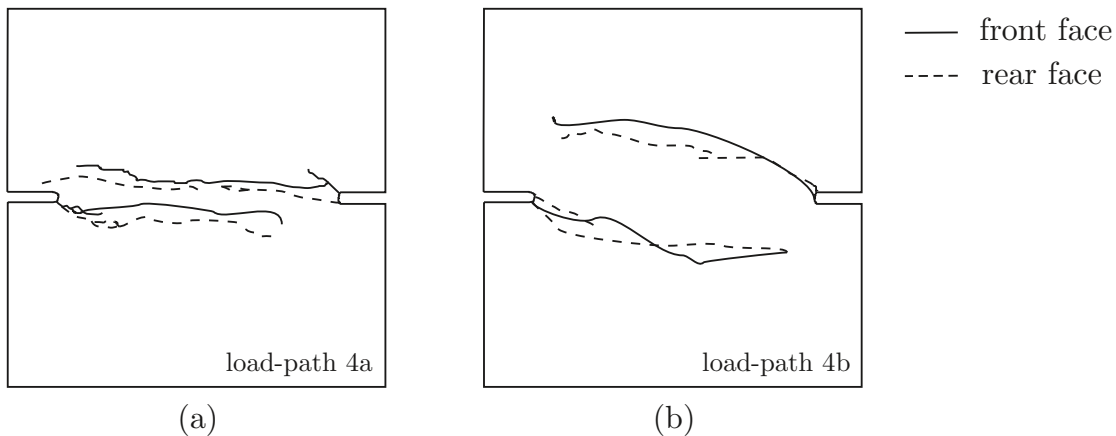


**Figure 11.3** (a) Crack pattern of Nooru-Mohamed test: (a) load path 4a; (b) load path 4b

**Table 11.1** Material parameter for simulation of Nooru-Mohamed tests

Description	Symbol	Value	Unit
elasticity modulus	$E$	29000	N/mm <sup>2</sup>
tensile strength	$f_t$	3.0	N/mm <sup>2</sup>
fracture energy	$G_f$	0.11	N/mm

and discuss their ability to simulate the mixed-mode fracture. Finite element simulation of Nooru-Mohamed test is done using two-dimensional microplane damage model in combination with biquadratic elements of  $2.5 \text{ mm} \times 2.5 \text{ mm}$ .

### 11.1.1 Numerical simulation using concrete damage plasticity model

**Brief characterization of the model** This material model uses the concepts of isotropic damage in combination with plasticity. The stress-strain relation of the material in compression or tension is defined as

$$\boldsymbol{\sigma} = (1 - \omega) \boldsymbol{D}^e (\boldsymbol{\varepsilon} - \boldsymbol{\varepsilon}^{pl}). \quad (11.1)$$

In Eq. 11.1, damage in the model is described using the scalar parameter  $\omega \leq 1$  which is multiplied by the elastic stiffness tensor of the material  $\mathbf{D}^e$ . In other words, the stiffness tensor of the damaged material  $\mathbf{D}$  is obtained as  $\mathbf{D} = (1 - \omega) \mathbf{D}^e$ . All components of tensor  $\mathbf{D}$  are reduced by the same factor  $1 - \omega$ , regardlessly of the mode of loading (normal or shear).

Material model used for the simulation of Nooru-Mohamed tests are summarized in Table 11.1. For the modeling of the Nooru-Mohamed test using concrete damage plasticity model, the softening rule shown in Fig. 11.4 was used. In this Figure, also a response of a single biquadratic element with reduced integration imposed to pure tension is shown for the  $2.5 \text{ mm} \times 2.5 \text{ mm}$  mesh size. The obtained strain softening from *concrete damage plasticity* model assures the same softening behavior and fracture energy as in microplane damage model under pure tension. Further parameters required for the *concrete damage plasticity* model are dilation angle  $\theta = 35^\circ$ , eccentricity  $\epsilon = 0.1$ ,  $\frac{\sigma_{b0}}{\sigma_{c0}} = 1.16$  and  $K_c = \frac{2}{3}$ .

## Material parameters

## Simulation results

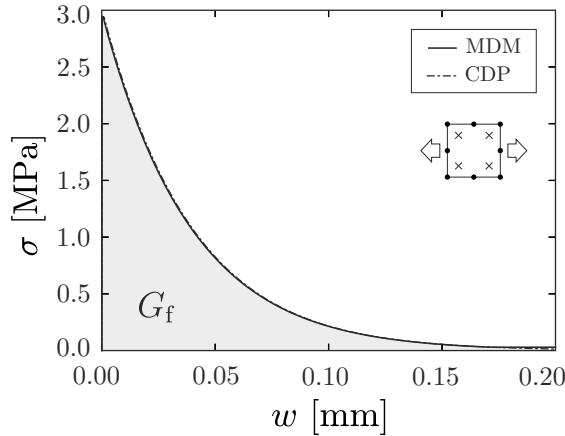


**Figure 11.4** Tensile response of Microplane damage model (MDM) and Concrete damage plasticity (CDP) calibrated for the simulation of Nooru-Mohamed tests

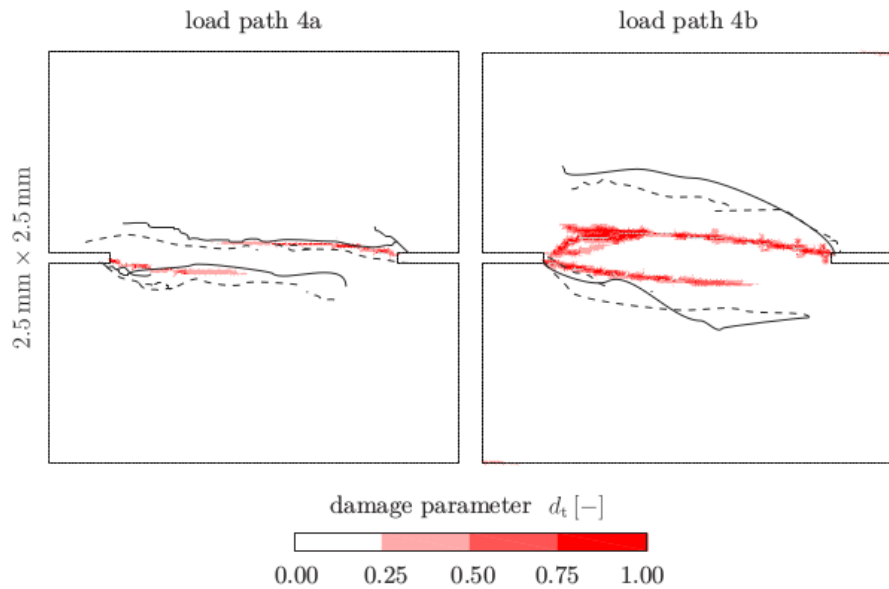


**Figure 11.5** Comparison of the crack pattern in Nooru-Mohamed test (load paths 4a and 4b) with damage evolution from the model with biquadratic elements with  $2.5 \text{ mm} \times 2.5 \text{ mm}$  mesh size and reduced integration schemes using *concrete damage plasticity* model

Evolution of damage obtained by the simulation using *concrete damage plasticity* model is compared to the crack pattern of the test for load paths 4a and 4b. Considering the load path 4a, the results are sufficiently good compared to the test. The good conformity with the test results justifies the capability of the *concrete damage plasticity* model in realization of fracture mode I with minor shear force included. Now considering the load path 4b, once the shear force  $F_s$  becomes proportionally larger than load path 4a, the model is unable to realize the mixed-mode fracture. The model is obviously unable to represent the inclined and rotating form of the crack pattern.

The load displacement curves of  $F - \delta$  are shown in Fig. 11.6.

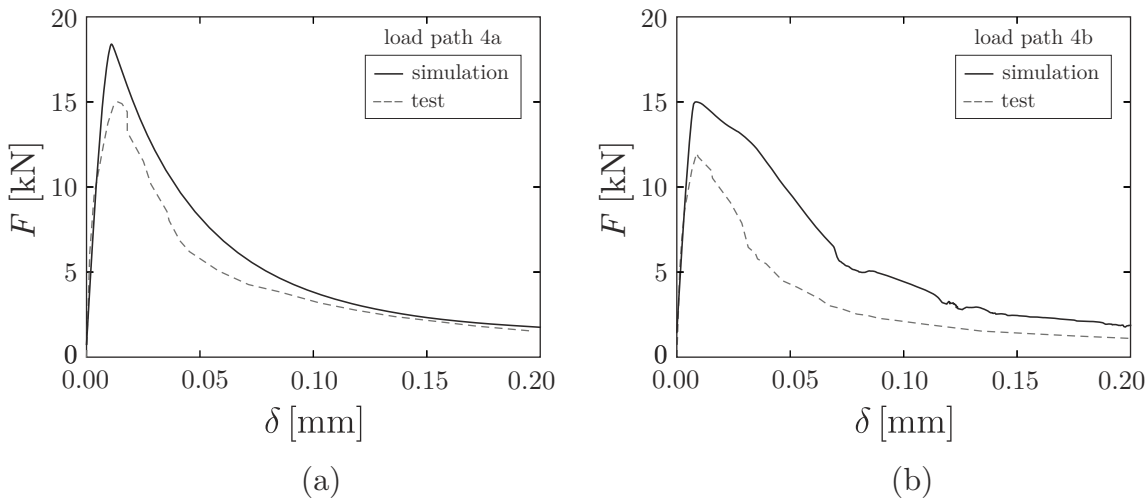


**Figure 11.6** Load-displacement curves of the Nooru-Mohamed test from test and finite element simulation using *concrete damage plasticity* model (a) load path 4a; (b) load path 4b

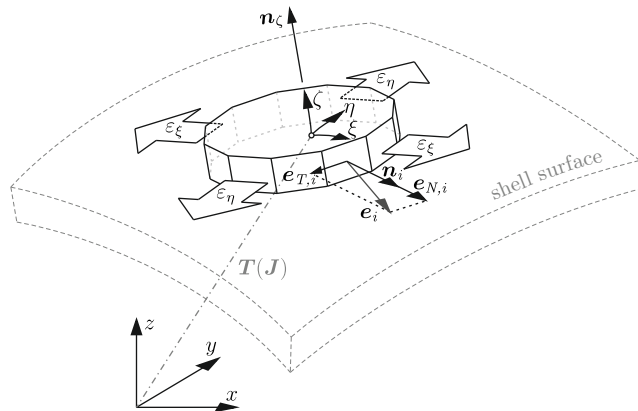


**Figure 11.7** Decomposition of strain components in a material point in 2D stress state.

### 11.1.2 Numerical simulation using *microplane damage model*

The principle idea behind the microplane damage model is to formulate the damage not-within the stress invariants but to resolve the stress state in a material point into individual directions. The concept is indicated in Fig. 11.7.

## Brief characterization of the model

Then, the damage function is not related to all strain components equally, but is related to a direction on a circle or sphere. Therefore, an anisotropic damage evolution can be described and in this way also an emerging, oriented crack. Fig. 11.8 shows an example of a single material point loaded in tension. The loading factor  $\lambda$  is plotted along the vertical axis of the cylinder. Thus, the changing indicate the evolution of damage with the increasing level of loading. The directions oriented in perpendicular direction with respect to the loading direction are almost undamaged. In this way, the material model can describe an oriented crack. This model belongs to the category of anisotropic damage models but possesses a clear geometrical interpretation of the material point state.

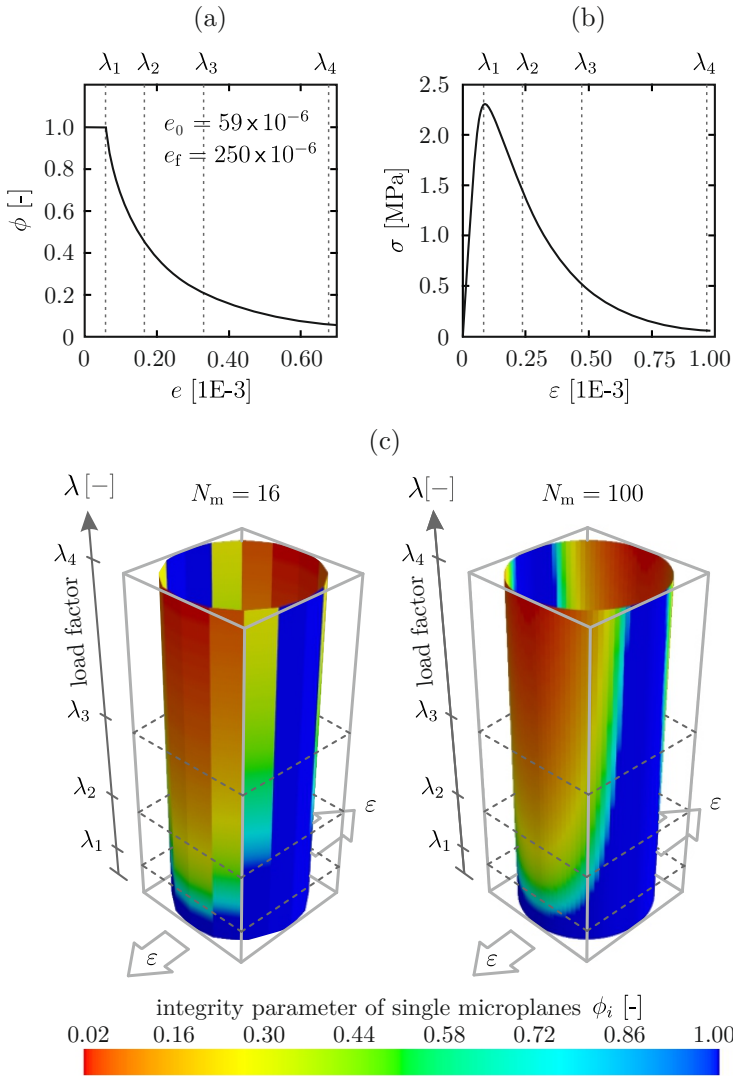


**Figure 11.8** Example of damage evolution in a material point loaded in uniaxial tension.

It is useful to set the model into the context of the models formulated in tensorial form with an explicitly defined failure surface within the principal stress space. The failure envelope can be calculated by repeated simulations with different ratios of the strains  $\varepsilon_{xx}$  and  $\varepsilon_{yy}$ . Fig. 11.9a shows the cut through the plane stress plane. The other three stress-strain diagrams shown in Figs. 11.9 show the response for biaxial tension (a), uniaxial tension (b), and uniaxial compression (c). Note that, this version of the model does not define an envelop for biaxial compression.

**Material parameters** The material parameters needed for the present version of the microplane model were set equivalent to the parameters used for the concrete damage-plasticity model given in Table 11.1. The input for the microplane model is represented by the damage function defined at the microplane level. In order to achieve equivalence, of calculation, we need to ensure the same fracture energy dissipation for both models.

**Simulation results** Fig. 11.10 shows the evolution of damage in the finite element simulation using biquadratic elements with comparison to the crack pattern from the test for load path 4a and 4b. Results from Fig. 11.10 give clearer localization zone with crack branches going across the

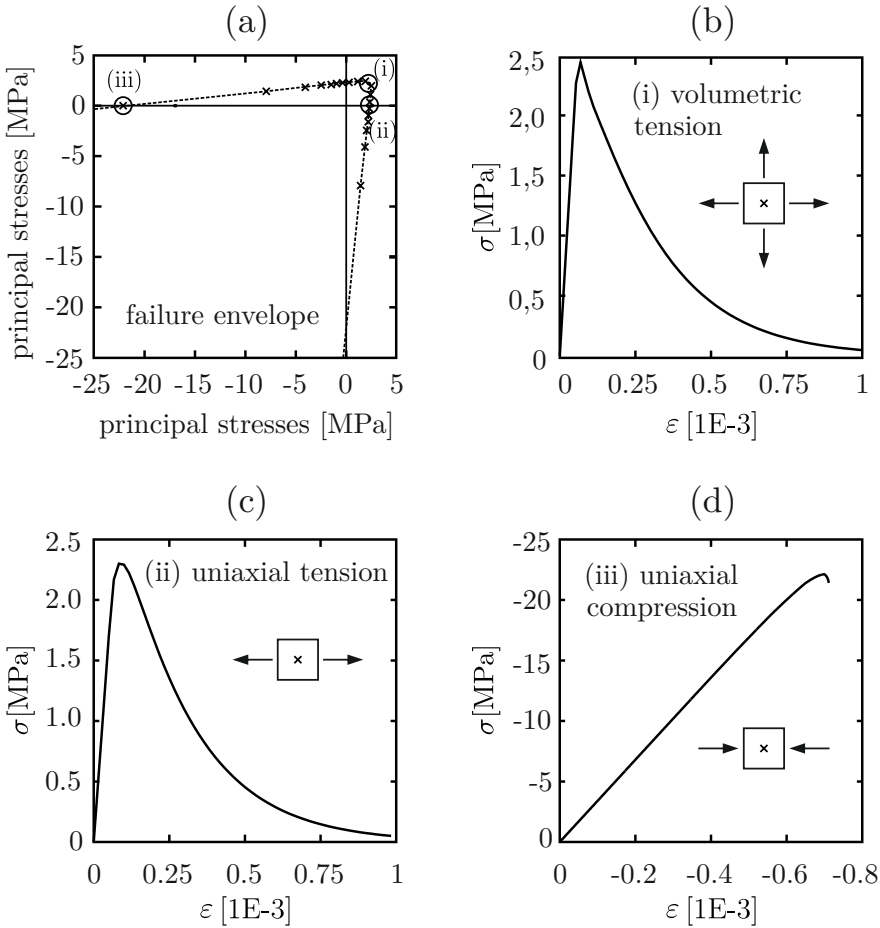


**Figure 11.9** Damage envelope calculated for the microplane-damage model.

mesh diagonals compared to the results obtained from Fig. 11.5. The load displacement curves of  $F - \delta$  are shown in Fig. 11.11. Apparently, a better match between the predicted and calculated crack geometries has been achieved as compared to the concrete damage plasticity model described in Sec. 11.1.1.

In order to shed some light onto the large number of model formulations and to provide better understanding about the validity of individual models provided in commercial codes we discuss the tests focusing on the combined tensile and shear loading. On the one hand elementary verification tests, that can discover pathological behavior of models are available. On the other hand, validation tests provide the information on to what extent can the model predict the real behavior of a structure.

## 11.2 Elementary tests of material models for concrete cracking

The present example with mixed-mode crack development indicates the difficulty to describe an inelastic behavior leading to crack localization for highly non-proportional loading paths with rotating principal stress axes. The classical tensorial models of plasticity type fail to correctly predict the behavior for such loading scenarios.

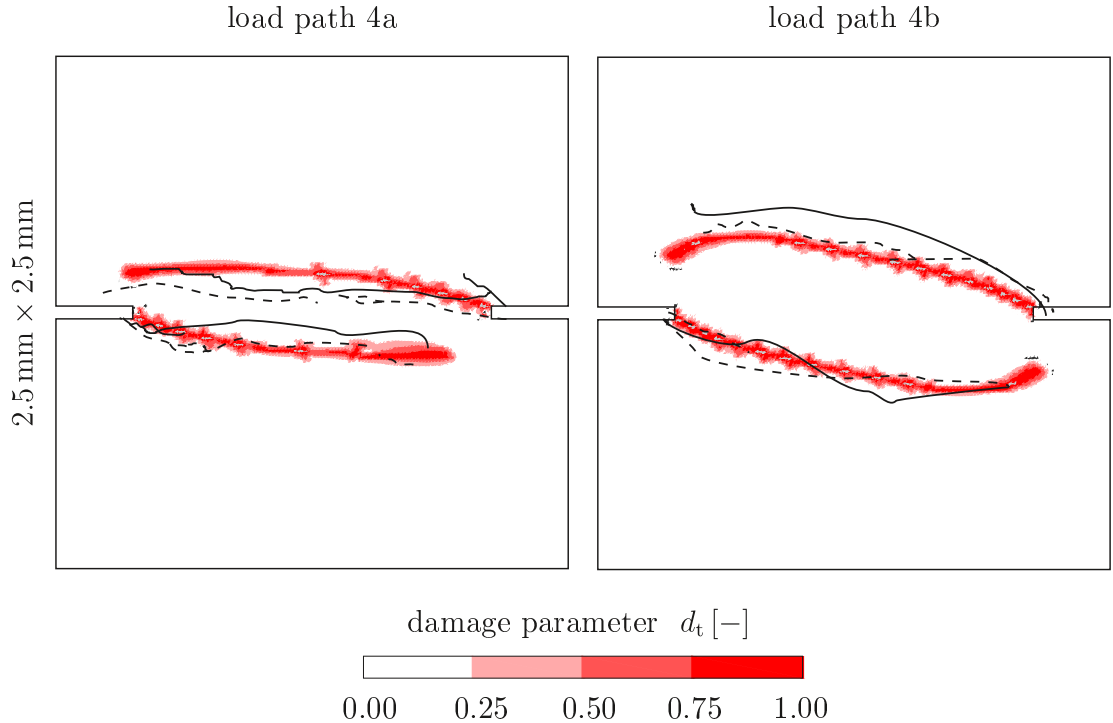


**Figure 11.10** Load-displacement curves of the Nooru-Mohamed test from test and finite element simulation using *microplane damage model* (a) load path 4a; (b) load path 4b

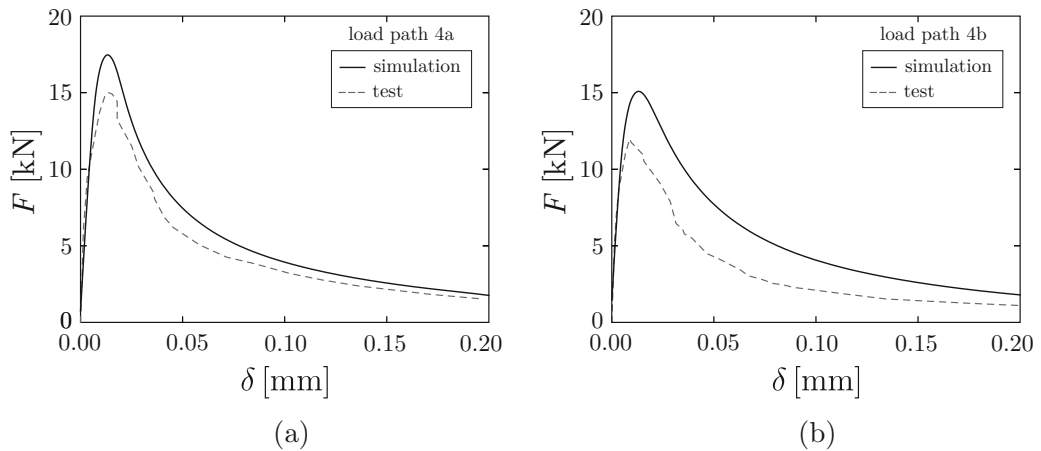


**Figure 11.11** Load-displacement curves of the Nooru-Mohamed test from test and finite element simulation using *microplane damage model* (a) load path 4a; (b) load path 4b

To illuminate the effect and to provide a general test for quality assessment of the developed models, elementary numerical tests have been proposed in the past. An combining tensile loading with subsequent shear has been proposed Willam test [[willam1989fundamental](#)] combining tensile loading with subsequent shear. This test illuminates the core of the problem for tensorial material models formulated in the framework of plasticity and softening. Another example is a vertex test combining a compressive loading with a subsequent loading traveling parallel to the yield surface. In both these cases, principal strain or stress axes rotate against the material [[caner2002vertex](#)].

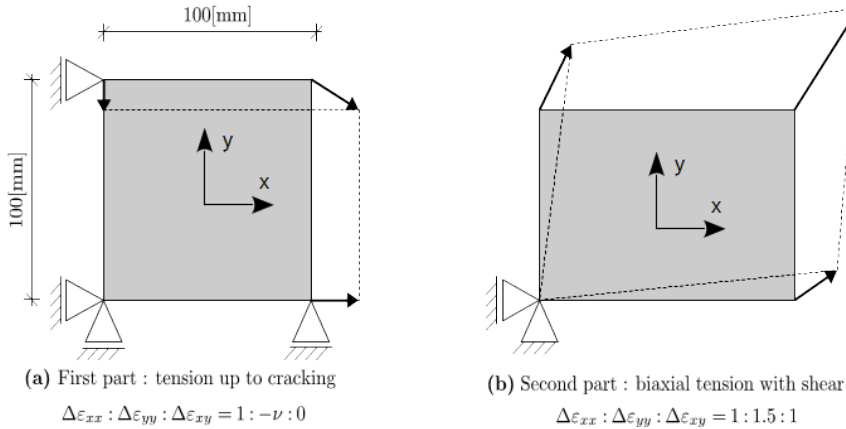
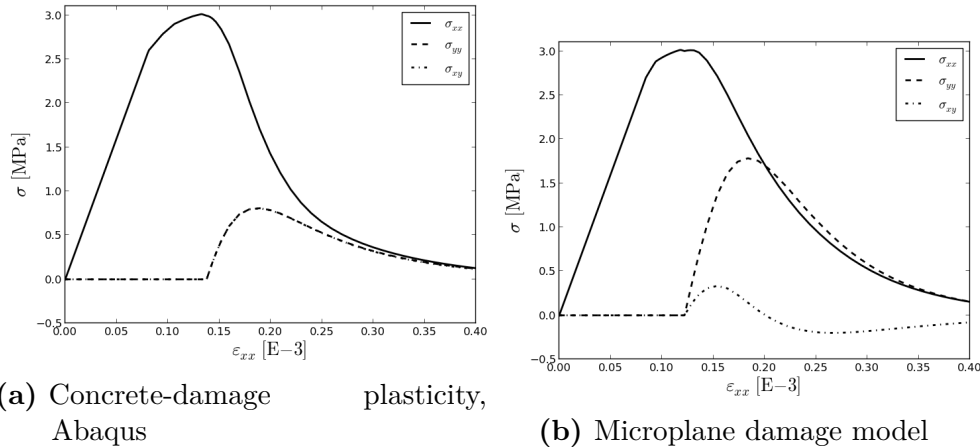


Figure 11.12 Willam test illustration


 Figure 11.13 Willam-test,  $\sigma_{xx}, \sigma_{yy}, \sigma_{xy}$  versus  $\epsilon_{xx}$ 

Let us examine the behavior of the two models considered in this lecture for combined tension and shear.

### 11.2.1 Willam test

The loading history of Willam's test is characterized by uniform tensile loading followed by shear loading leading to a rotation of principal strains. Basically, Willam's test is passed when

- the maximum principal stress is always lower than or equal to the uniaxial tensile strength  $f_u$  of concrete and
- all stress components tend to zero.

## 11.3 Examples

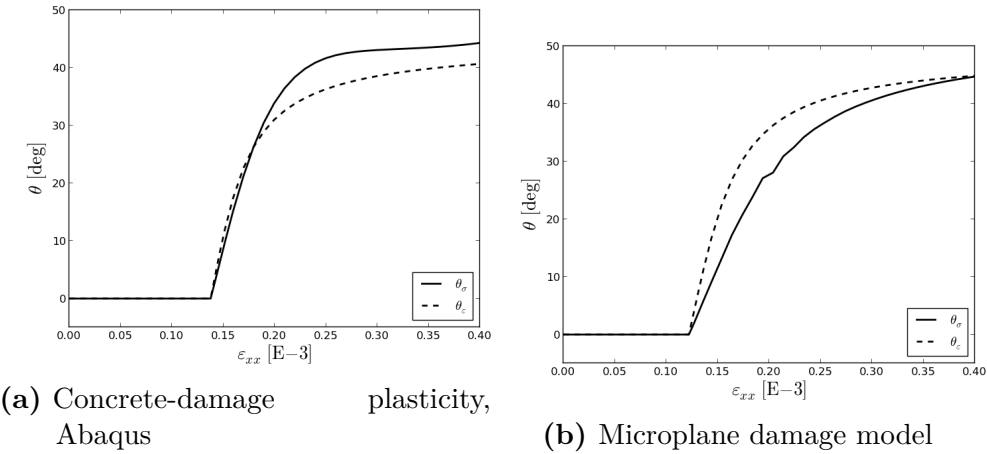


**Figure 11.14** Willam-test, evolution of directions of principal stress  $\sigma_{11}$  and strains  $\varepsilon_{11}$

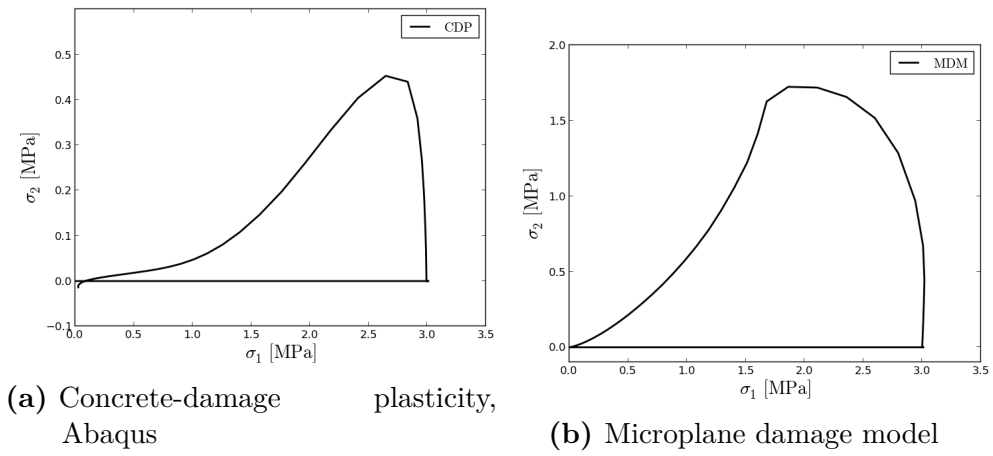


**Figure 11.15** Willam-test, evolution of principal stresses

---

## **Part III**

### **Cracking & Debonding**

## 12 Tensile response of brittle-matrix composites

The appearance of disintegration mechanisms introduced in the previous lectures was describing the material and structural behavior in view of the damage and failure mechanisms. In the present chapter, however, we will focus on a phenomenon appearing in brittle-matrix composites that uses the interaction between emerging cracks and debonding of the reinforcement form the matrix to achieve a desired structural behavior. The concept of tension-stiffening is well known in steel-reinforced concrete. It can be further exploited when using non

### 12.1 Pseudo-ductility

Tensile response of a reinforced specimen can be regarded as dynamically evolving chain of crack bridges. Cracks emerging during the tensile loading of a reinforced concrete specimen act as starting points of debonding. The structural behavior of the system can be described by regarding two inelastic mechanisms - cracking and an adjacent debonding. To understand the principle concept how to achieve ductile behavior using purely elastic-brittle components, let us use a simple analytical description of the cracking and debonding process.

The response of fibrous composites to tensile loading depends on the material properties of both the matrix, and the fibers, and their interface [cox:52, marcoxeva:85, cur:93c]. The typical form of such a response includes an initial linear stage with the stiffness defined by the rule of mixtures as

$$E_c = E_f V_f + E_m (1 - V_f) \quad (12.1)$$

with  $E_f$  and  $E_m$  denoting the fiber and matrix moduli of elasticity, respectively, and  $V_f$  denoting the fiber volume fraction. With the inception of the first matrix crack marking the beginning of multiple cracking (matrix fragmentation), the stiffness starts to decrease. During the following phase of multiple cracking, stress redistributions both between and within the constituents take place. This second phase continues up to the state where all fibers are fully debonded so that the composite is saturated with cracks, which marks the start of the third phase – a linear response with stiffness equal to  $E_f V_f$ . The vertical offset between the composite stress in the third phase and an equivalent reinforcement response  $E_f V_f \varepsilon_c$ , with  $\varepsilon_c$  being the global strain, is due to the tensile stress accumulated in the matrix fragments (see Fig. 12.1).

Probabilistic approach to modeling of composites exhibiting fragmentation in one of the components has been applied by several authors in the past, e.g. [avekel:73, huiphoibn:95]. The class of methods generally referred to as “random strength approach” [casgellac:10] can be informally explained using the graphical representation of stress states at several selected load levels shown in Fig. 12.3. The matrix strength distribution

shown in all diagrams was simulated by a random field following the Weibull probability distribution.

The first diagram (Fig. 12.3a) shows the matrix stress along the specimen after the first crack has appeared at the location of minimum matrix strength. Upon further loading, the matrix stress is growing until the matrix strength has been reached at some other point of the specimen (Fig. 12.3b). New crack is then inserted into the numerical representation of the specimen by updating the stress profile (Fig. 12.3b) in accordance with the considered crack bridge model summarized in Fig. 12.2.

The crack bridge model delivers the local profile of the matrix stress in the vicinity of the crack. The stress profile depends on the underlying bond law describing the stress transfer between the reinforcement and the matrix and on the instantaneous crack spacing. In the shown example a simple crack bridge model with constant bond has been used. For this model, expressions for matrix stress ( $\sigma_m$ ), reinforcement strain ( $\varepsilon_f$ ), and of crack width  $w$  required by the crack-tracing algorithm are available in a closed form as summarized in Fig. 12.2.

$$\sigma_m = \begin{cases} \frac{TV_f}{1-V_f}|z| & : |z| < a \\ \frac{\sigma_c E_m}{E_m(1-V_f) + E_f V_f} & : |z| \geq a \end{cases} \quad (12.2)$$

where  $z$  is the local coordinate equal to zero at the crack bridge position,  $T$  is the bond intensity,  $V_f$  is fiber volume fraction,  $\sigma_c$  is the composite stress, and  $E_f$ ,  $E_m$  denote the stiffness of the reinforcement and of the matrix, respectively. The instantaneous debonded length  $a$  is given as the product of the remote stress and bond intensity  $a = T\sigma_c$ . The resulting linear matrix strain profiles  $\varepsilon_m = \sigma_m/E_m$  and  $\varepsilon_f = (\sigma_c - \sigma_m)/E_f$  in the vicinity of a crack bridge are depicted in Fig. 12.2b. The grey area represents the crack opening  $w = \int(\varepsilon_f - \varepsilon_m) dz$ .

This model has already been derived in Sec. 2.3 for one-sided pull-out for rigid matrix. An extension for elastic matrix using an additional kinematic equation has been provided in Sec. 2.3.2.

With the detected cracks, stress and strain profiles and values of crack openings at hand, the nominal composite strain can be evaluated. The process of crack detection, stress update and strain evaluation is repeated until the saturated crack state has been achieved. The simulation delivers the relation between the composite stress and strain as shown in Fig. 12.3e. At the same time, the matrix crack widths in all crack bridges is evaluated at individual levels of composite stress; see Fig. 12.3f. This detailed output allows the user to analyze the sensitivity of the composite behavior to the input parameters and their statistical variability. Parameters used for the present example are summarized in Fig. ??e. Although the matrix stress profiles show a 100 mm long composite, the stress-strain diagram and the crack widths were simulated for a composite with a length of 3000 mm.

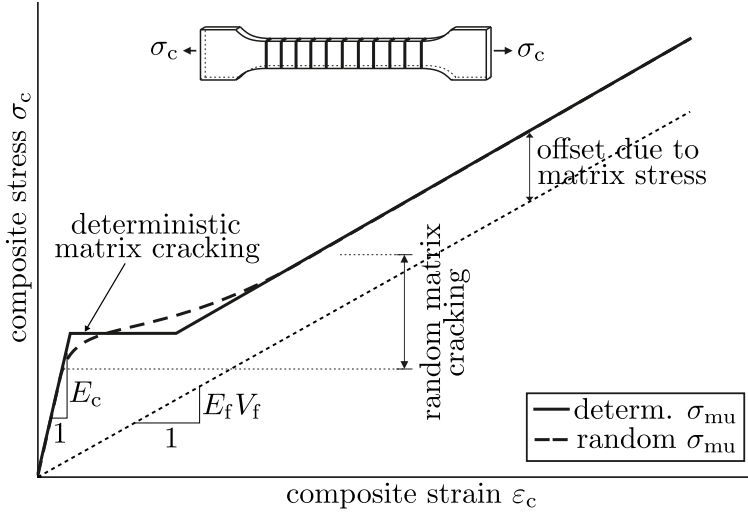


**Figure 12.1** Tensile response of a composite specimen, random, deterministic matrix

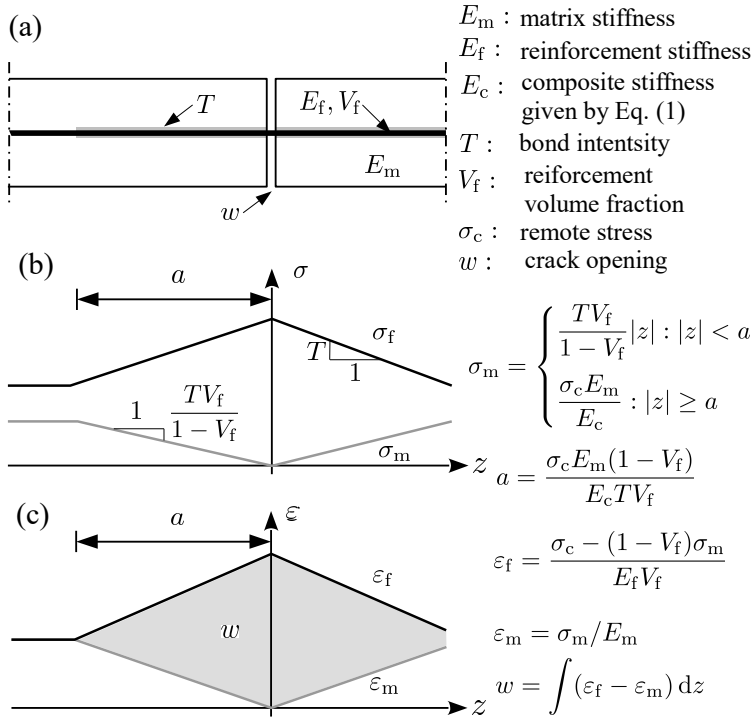


**Figure 12.2** Stress and strain state of a single crack bridge with constant bond

**Composite stress-strain curve** With the identified history of the matrix cracking states  $K = 1, 2, \dots, K_{\text{sat}}$  at hand, the composite strains  $\varepsilon_c$  corresponding to the load  $\sigma_c$  can be evaluated for the given crack positions  $\mathbf{X}^{(K)}$  as

$$\varepsilon_c^{(K)}(\sigma_c) = \frac{1}{L_c} \left[ \sum_{k=1}^K w_k^{(K)}(\sigma_c) + \frac{1}{E_m} \int_0^{L_c} \sigma_m^{(K)}(\sigma_c, x) dx \right]. \quad (12.3)$$

The matrix stress  $\sigma_m^{(K)}$  is prescribed by Eq. (??) and the  $K$  crack openings  $w_k^{(K)}$ ,  $k = 1, 2, \dots, K$  have to be provided by a crack bridge model.

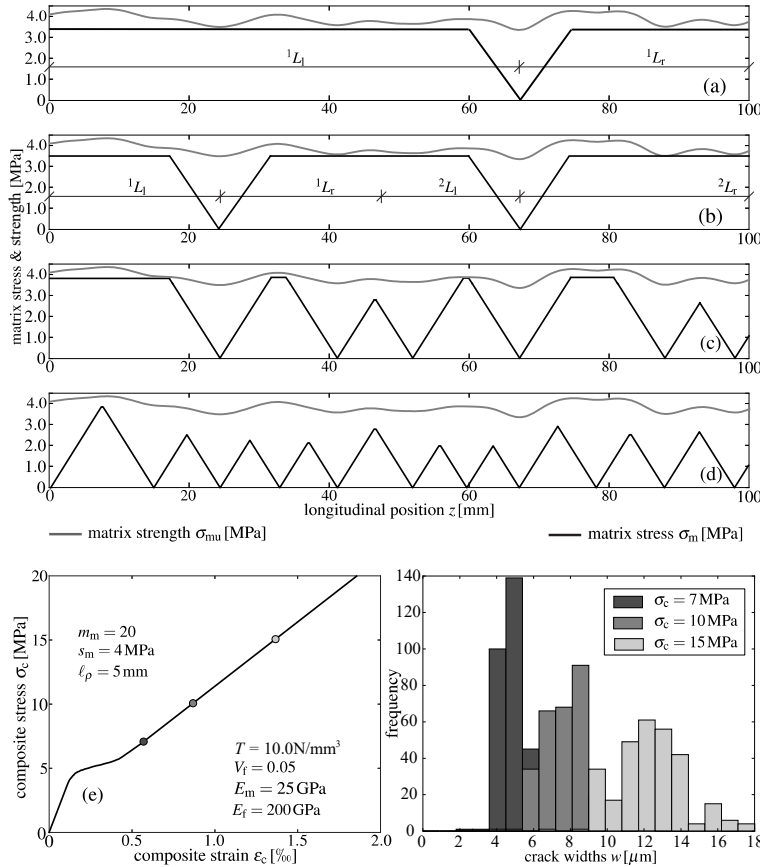


**Figure 12.3** Stress and strain state along the tensile specimen at increasing remote stress levels

### 12.1.1 Effect of reinforcement ratio

Given the strain hardening curve

(12.4)

- Crack as a starting point of delamination
- Multiple cracking, using finite elements? alternative approaches?
- Statistics – just a sugar?
- Characterization strategies
- Measurement techniques
- Modeling approaches

## **13 Influence of heterogeneity**

Seminars – with focus on application to

- Steel-reinforced concrete
- Textile-reinforced concrete
- Short-fiber concrete
- Ceramics composites

---

## **14 Shear loading**

Interaction of fibers and matrix. Layers

### **References**

**Figure A.1** Schematic picture of a typical pull-out test

**Figure A.2** A simplified mechanical model of the pull-out problem

## A Multilayer model

### A.1 Governing equations

In pull-out tests, the reinforcements are pulled out from the matrix as shown in Fig. A.1. The output of such tests is typically the relationship between the pull-out force  $P$  and the displacement  $w$ . Two coupled problems can be formulated based on the pull-out test, the direct pull-out problem and the inverse pull-out problem. In some cases, for example in order to verify the experimental results, one needs to numerically determine the pull-out force vs displacement relationship according to the known bond-slip law, which formulates the direct pull-out problem. More commonly, the purpose of pull-out tests is to determine the unknown bond-slip law according the test output, this kind of problems are named as the inverse pull-out problems.

Let us consider the following simple case for some insight into the mathematical background of the pull-out problems. For thin specimens made of cementitious composites, the shear deformation in matrix can generally be neglected, thus the problem can be simplified to a one dimensional problem as shown in Fig. A.2. The reinforcement and the matrix are coupled through the bond interface in which the shear stress  $\tau$  is characterized as a function of the slip  $s$ . The equilibrium of an infinitesimal segment of the reinforcement leads to

$$A_f \sigma_{f,x} - p\tau(s) = 0, \quad (\text{A.1})$$

where the index  $(.)_x$  denotes the derivative with respect to the spatial coordinate  $x$ ,  $A_f$  and  $p$  are the cross-sectional area and the perimeter of the reinforcement, respectively. Similarly, the equilibrium of the matrix can be expressed as

$$A_m \sigma_{m,x} + p\tau(s) = 0, \quad (\text{A.2})$$

in which  $A_m$  is the cross-sectional area of the matrix.

The slip in the bond interface is defined as  $s = u_f - u_m$ , where  $u_f$  and  $u_m$  are the reinforcement displacement and matrix displacement, respectively. The second order derivative of  $s$  can be written as

$$s_{,xx} = \varepsilon_{f,x} - \varepsilon_{m,x}, \quad (\text{A.3})$$

where  $\varepsilon_f$  is the reinforcement strain and  $\varepsilon_m$  is the matrix strain. The constitutive laws of the reinforcement and the matrix are given as

$$\sigma_f = D_f(\varepsilon_f) \quad (\text{A.4})$$

$$\sigma_m = D_m(\varepsilon_m). \quad (\text{A.5})$$

### A.1.1 Weak formulation of the multi-layer problem

In order to generalize the differential bond problem for multi-layer multi-dimensional plies let us rewrite the equilibrium equations defined in Eq. (A.4) with enumerated layers

$$\begin{aligned}\sigma(u_1)_{1,x} - \tau(u_2 - u_1) &= 0 \\ \tau(u_2 - u_1) + \sigma(u_2)_{2,x} &= 0\end{aligned}\quad (\text{A.6})$$

without distinguishing between matrix and fibers. By introducing a layer index  $c = [1, 2]$  we can rewrite the equations in an indicial notation as

$$\delta_{cd} A_c \sigma_{c,x} + \delta_{cd} (-1)^c p_c \tau = 0, \quad c, d = [1, 2] \quad (\text{A.7})$$

In order to provide a more general model of the pull-out problem defined by these differential equations we construct a weak form of the boundary value problem within the domain  $\Omega := [0, L]$  shown in Fig. A.2. The corresponding essential and natural boundary conditions are specified as

$$u_c = \bar{u}_c(\theta) \text{ on } \Gamma_{u_c} \quad \text{and} \quad \sigma_c A_c = \bar{t}_c(\theta) \text{ on } \Gamma_{t_c} \quad (\text{A.8})$$

Denoting the integration of the product of the terms  $u, v$  over  $V$  as  $(u, v)_V$ , the weak formulation can be expressed as

$$(v_d, \delta_{cd} A_c \sigma_{c,x} + \delta_{cd} (-1)^c p_c \tau)_\Omega + (v_c, u_c - \bar{u}_c(\theta))_{\Gamma_{u_c}} + (v_c, -A_c \sigma_c + \bar{t}_c(\theta))_{\Gamma_{t_c}} = 0 \quad (\text{A.9})$$

Since  $v_c = 0$  on  $\Gamma_{u_c}$ , the second and fifth terms in Eq. (A.9) vanish. Using integration by parts, the orders of the stress derivatives  $\sigma_{c,x}$  can be reduced as follows

$$(v_d, \delta_{cd} A_c \sigma_{c,x})_\Omega = - (v_{d,x}, \delta_{cd} A_c \sigma_c)_\Omega + (v_d, \delta_{cd} A_c \sigma_c)_\Gamma \quad (\text{A.10})$$

Finally, by substituting Eq. (A.10) for both matrix and fibers into Eq. (A.9), the following variational formulation of the pull-out problem is obtained

$$(v_{d,x}, \delta_{cd} A_c \sigma_c)_\Omega + (v_d (-1)^d, \delta_{cd} p_c \tau)_\Omega - (v_d, \delta_{cd} \bar{t}_c(\theta))_{\Gamma_{t_c}} = 0. \quad (\text{A.11})$$

Note that the term  $v_d (-1)^d = \delta(v_2 - v_1) = \delta s$  renders the virtual slip between the components.

### A.1.2 Finite element discretization

The displacement field of a material component  $c = 1 \dots N_c$  for  $N_c$  number of components is approximated using the shape functions

$$\begin{aligned}u_c &= N_I d_{cI} & u_{cE} &= N_i d_{cI[E,i]} \\ v_c &= N_I \tilde{d}_{cI} & v_{ce} &= N_i \tilde{d}_{cI[E,i]}\end{aligned}\quad (\text{A.12})$$

with index  $I = 1 \dots N_d$  representing a global node number. In the present case of the pull-out problem, index 1 represents the matrix m and index 2 the fibers f. The strain field in each material component is then expressed as

$$u_{c,x} = B_I d_{cI} \quad (\text{A.13})$$

$$v_{c,x} = B_I \tilde{d}_{cI} \quad (\text{A.14})$$

where  $B_I = N_{I,x} = N_{I,\xi} J(\xi)^{-1}$ . As a consequence, the slip field is approximated as

$$s = u_2 - u_1 = u_c (-1)^c = (-1)^c N_I d_{cI}. \quad (\text{A.15})$$

Eq. (A.11) can be rewritten as

$$\tilde{d}_{dI} (B_I, \delta_{cd} A_c \sigma_c)_\Omega + \tilde{d}_{dI} ((-1)^d N_I, \delta_{cd} p_c \tau)_\Omega - \tilde{d}_{dI} (N_I, \delta_{cd} \bar{t}_c(\theta))_{\Gamma_{t_c}} = 0, \quad (\text{A.16})$$

Since  $\tilde{d}_{dI}$  is arbitrary, and  $(N_I, \bar{t}_c)_{\Gamma_{t_c}}$  can be simplified to nodal loads as  $\bar{t}_{cI}$  Eq. (A.16) can be reduced to

$$R_{dI}(\theta) = \delta_{cd} \left[ (B_I, A_c \sigma_c)_\Omega + ((-1)^c N_I, p_c \tau)_\Omega - \bar{t}_{cI}(\theta) \right] = 0. \quad (\text{A.17})$$

### A.1.3 Iterative solution algorithm

In case of nonlinear material behavior assumed either for the matrix, reinforcement or bond, Eq. (A.17) must be prepared for iterative solution strategies by means of linearization i.e. by Taylor expansion neglecting quadratic and higher order terms. The expansion up to the linear term reads

$$R_{dI}^{(\theta)}(d_{cJ}^{(k)}) \approx R_{dI}^{(\theta)}(d_{cJ}^{(k-1)}) + \frac{\partial R_{dI}}{\partial d_{cJ}} \Big|_{d_{cJ}^{(k-1)}} \Delta d_{cJ}^{(k)}. \quad (\text{A.18})$$

Assuming nonlinear material behavior of the components  $c$ , the derivative of the residual  $R_{dI}$  with respect to  $d_{cI}$  reads

$$\frac{\partial \sigma_c}{\partial d_{cJ}} = \frac{\partial \sigma_c}{\partial \varepsilon_c} \frac{\partial \varepsilon_c}{\partial d_{cJ}} = \frac{\partial \sigma_c}{\partial \varepsilon_c} B_J \quad (\text{A.19})$$

Similarly, for nonlinear bond behavior, the derivative of shear flow with respect to

$$\frac{\partial \tau}{\partial d_{cJ}} = \frac{\partial \tau}{\partial s} \frac{\partial s}{\partial d_{cJ}} = \frac{\partial \tau}{\partial s} N_J (-1)^c \quad (\text{A.20})$$

The derivative of the residual then reads

$$\frac{\partial R_{dI}}{\partial d_{cJ}} \Big|_{d_{cJ}^{k-1}} = K_{dIcJ}^{(k-1)} = \delta_{cd} A_c \int_\Omega B_I B_J \frac{\partial \sigma_d}{\partial \varepsilon_c} \Big|_{d_{cJ}^{k-1}} dx \quad (\text{A.21})$$

$$+ (-1)^{c+d} p_c \int_\Omega N_I N_J \frac{\partial \tau}{\partial s} \Big|_{d_{cJ}^{k-1}} dx \quad (\text{A.22})$$

Assuming a linear elastic constitutive law of the components the derivatives of  $\sigma_c$  with respect to  $\varepsilon_d$  read

$$\delta_{cd} \frac{\partial \sigma_c}{\partial \varepsilon_c} = E_d \quad (\text{A.23})$$

and linear bond

$$\frac{\partial \tau}{\partial s} = G \quad (\text{A.24})$$

is the constitutive matrix. Finally, substituting Eqs. (A.26) and (A.23) into Eq. (A.18), the following incremental form of equilibrium is obtained,

$$K_{dIcJ}^{(k-1)} \Delta d_{cJ}^{(k)} = R_{dI}^{(\theta)}(d_{cJ}^{(k-1)}) \quad (\text{A.25})$$

By introducing index function  $I(e, i)$  mapping the finite element and node number to a global degree of freedom.

$$K_{dIcJ}^{(k-1)} = \left[ A_c B_{I(e,i)M(e,m)} B_{J(e,j)M(e,m)} \delta_{cd} \left. \frac{\partial \sigma_c}{\partial \varepsilon_c} \right|_{d_{cJ}^{k-1}} \right] \quad (\text{A.26})$$

$$+ \delta_{cd} (-1)^{c+d} p N_{I(e,i)M(e,m)} N_{J(e,j)M(e,m)} \left. \frac{\partial \tau}{\partial s} \right|_{d_{cJ}^{k-1}} w_{M(e,m)} |J|_{M(e,m)} \quad (\text{A.27})$$